Cell behaviors influencing the mode of cell division of retinal progenitors: a role for the Zebrafish Anillin protein

Alessio Paolini

2014

Dissertation
submitted to the
Combined Faculties for the Natural Sciences and for Mathematics
of the Ruperto-Carola University of Heidelberg, Germany
for the degree of
Doctor of Natural Sciences

Presented by
M.Sc. in Sciences and Biomolecular Technologies, Alessio Paolini
Born in: Livorno (Italy)
Oral-examination: 11.07.2014

Cell behaviors influencing the mode of cell division of retinal progenitors: a role for the Zebrafish Anillin protein

Referees
Prof. Dr. Joachim Wittbrodt
Dr. Lucia Poggi

Acknowledgments

First of all, I would like to thank my Parents… this wouldn't have been possible without you, thanks for your efforts and patience to make me who I am.

A special thank to Dr. Lucia Poggi for having giving me the chance to grow up in this cool scientific environment. Thanks for the plethora of suggestions you gave me during these years; they allowed me to overcome all the problematic situations. A huge thank to Prof. Jochen Wittbrodt, you have been a scientific model for me. Your words and attitude helped me to set my mind in a scientific way. I would like to thank my thesis Committee Prof. Dr. Jochen Wittbrodt, Prof. Dr. Thomas Holstein, Dr. Gislene Pereira and Dr. Lucia Poggi.

Another special thank to Dr. Shahad Albadri. It was a pleasure to grow up with you. I will never forget all your help and encouragements during this stressful adventure. My appreciation extends to my labmate and friend Anne-Laure, my collaborators from Paris, Vincenzo and Dr. Filippo Del Bene and from Uruguay, Prof. Flavio Zolessi.

Thanks to all the Wittbrodt Lab …. Micha, Burkhard, Rebecca, Daigo, Katha, Robert, Stephan K…. and all the others. Thanks to you, I was feeling home.

Finally a special thanks to all the 5th and 6th floor, in particular to Amaya, Mouli, Silvi, Ira, Christophe etc…

Another little thing ... just a really special thanks to Francesca: thanks for having sharing a part of your life with me. You have been the most important person in this period of my life.

Table of content

Summary

Understanding molecular and cellular events influencing the neural progenitor mode of cell division and fates of daughter cells is central to Developmental Biology. Members of the cytokinetic machinery have received increasing attention as possible molecular mediators of this event: their inheritance or retention appears to influence proliferation versus differentiation of daughter cells in cancer and stem cells. I therefore took under investigation the F-actin binding protein Anillin, shown to be essential for cytokinesis progression and completion in invertebrate model systems.

I found Anillin downregulation to be mediated by the bHLH transcription factor Atoh7, which is essential for the generation of Retinal Ganglion Cells (RGCs). I therefore first investigated the expression and *in vivo* dynamics of Anillin in the zebrafish neural retina. This analysis revealed that Anillin expression correlates with proliferative states of retinal progenitor and. Concomitantly, Anillin knock down promoted RGCs and early born retinal cell type generation at the expense of the late born ones, such as bipolar and muller glia cells. These effects on cell fate were due to change in mode of cell division promoted by Anillin knock-down – Anillin morpholino injected clones tend to undergo symmetric neurogenic division, generating two Atoh7 positive cells or two RGCs, while the control clones tend to undergo asymmetric division. These results reveal a role for Anillin in neurogenesis by affecting cell division outcomes.
I then asked if *anillin* knockdown effect on cell division outcome correlates with putative roles in cytokinesis. By developing a zebrafish transgenic line recapitulating Anillin-GFP epression in the *in vivo* developing embryo, I could analyze Anillin distribution at cellular level. Anillin protein highlights the progression of the cytokinetic furrow, as well as midbody formation and postmitotic inheritance in dividing retinal progenitor cells. Research in invertebrates and vertebrates suggests a colocalization of Anillin and its main interactor, F-actin, during cytokinesis progression. Accordingly, Anillin and F-actin co-localized at the cleavage furrow and midbody of cycling retinal progenitors. Midbody and F-actin spot remnant are both inherited by the daughter cell that differentiates as RGC, suggesting for the first time a correlation between apical F-actin/midbody distribution and fate. I further aimed at elucidating the effect of Anillin knockdown on F-actin dynamics during cytokinesis. Results show that symmetric outcome of cell division produced by Anillin knock down correlate with symmetric apical F-actin inheritance at the daughter cell's apical domain. These results indicate that Anillin links cytokinesis progression with apical F-actin distribution between the daughter cells. In addition to slowing down cytokinesis progression, Anillin appears to influence the basal to apical interkinetic nuclear migration of progenitor cells, which I found slowed down in Anillin morpholino-injected embryos, along with an increase in the progenitors cell cycle length. This results in an longer permanence of the nuclei close to the basal side of the neuroepithelium namely, far away from proliferative signal. Likewise, longer permanence of nuclei in this basal side of the neuroepithelium have been associated with symmetric neurogenic divisions of retinal progenitors.
Controversial studies showed how correlation between mode and orientation of cell division in vertebrates is not clear. In the present study I found that increase in symmetric fate outcome of daughter cells (in term of Atoh7 expression) correlates with a shift in the orientation of cell division from radial to circumferential. The biological significance of this switch remains to be investigated.

These functional studies combined with in vivo imaging provide evidences indicating that Anillin affects neurogenesis by maintaining the progenitor pool and influencing the mode of cell division. By directly assessing correlations between F-actin, midbody inheritance, orientation of cell division and daughter cell fate, our study also provides insight into the mechanism whereby this might operate *in vivo*.

Zusammenfassung

Der Modus der Zellteilung von neuralen Vorläuferzellen wird von molekularen und zellulären Faktoren beeinflusst, deren Verständnis einen zentralen Aspekt der Entwicklungsbiologie darstellt. In den Fokus rücken dabei zunehmend Teile des Zellteilungsapparats,, deren Weitergabe bzw. Rückhaltung während der Zellteilung die Proliferation und Differenzierung von Stamm- und Tumorzellen beeinflussen kann. In diesem Kontext habe ich das F-Aktin- bindende Protein Anillin untersucht, von dem in Invertebraten bereits gezeigt wurde, dass es für die Zellteilung notwendig ist.

In meiner Arbeit konnte ich zeigen, dass Anillin durch den bHLH Transkriptionsfaktor Atoh7 herunterreguliert wird, welcher für die Generierung von retinalen Ganglionzellen notwendig ist. Darüber hinaus korreliert die Expressionsdynamik von Anillin in der neuralen Retina von Zebrafischen mit Zellproliferation. Knockdown von Anillin führt zu einer erhöhten Produktion früh generierter retinaler Zelltypen (insbesondere von Ganglionzellen), bei gleichzeitig verminderter Generierung später auftretender Zelltypen wie Bipolare und Müller-Glia Zellen. Ich konnte dieses Ungleichgewicht auf eine Veränderung des Zellteilungsmodus zurückführen. Zellklone, die zuvor mit Anillin Morpholinos injiziert wurden, absolvieren überwiegend symmetrische neurogene Teilungen, aus denen zwei Atoh7-positive Zellen hervorgehen, die sich dann zu Ganglionzellen ausdifferenzieren. Vergleichbare uninjizierte Zellklone, die als Kontrolle dienen, teilen sich hingegen eher asymmetrisch. Diese Ergebnisse belegen eine Funktion von Anillin bei der Neurogenese durch die Beeinflussung des Zellteilungsmodus.
Ausgehend von diesen Ergebnissen habe ich untersucht, ob die beobachteten Effekte durch die Funktion von Anillin während der Zellteilung erklärt werden können. Die Etablierung von Anillin-GFP transgener Zebrafische, deren Transgenexpression die endogene Expression von Anillin rekapituliert, ermöglichte den Nachvollzug der Expressionsdynamik *in vivo* mit (sub-) zellulärer Auflösung. Anillin ist in der Zellteilungsfurche und Flemming-Körpern lokalisiert und kann asymmetrisch auf die Tochterzellen verteilt werden. Sowohl bei Invertebraten als auch bei Wirbeltieren wurde bereits vermutet, dass Anillin während der Zellteilung mit F-Aktin assoziiert. Tatsächlich kolokalisieren Anillin und F-Aktin in der Zellteilungsfurche und Flemming-Körpern von retinalen Vorläuferzellen. Interessanterweise werden Flemming-Körper und Überreste von sogenannten “F-Aktin-Spots” an die Tochterzelle weitergegeben, die sich zu einer Ganglionzelle differenziert. Diese Ergebnisse weisen erstmals auf einen Zusammenhang zwischen apikaler F-Aktin/Flemming-Körper Verteilung und Zelldifferenzierung auf. Ein weiteres Indiz ist, dass apikales F-Aktin nach Anillin-Knockdown symmetrisch auf die Tochterzellen verteilt wird, was mit dem ebenfalls beobachteten symmetrischen Zellteilungsmodus konsistent ist. Zusammengenommen belegen diese Ergebnisse einen durch Anillin hergestellten Zusammenhang zwischen Zellteilung und F-Aktin Verteilung.
Darüberhinaus konnte ich beobachten, dass Knockdown von Anillin die Zellteilung, sowie die intermitotische Kernwanderung in apikaler Richtung verlangsamt. Als Folge davon befinden sich die betroffenen Nuklei länger an der basalen Seite der Retina, und damit weiter entfernt von einem proliferationsfördernden Signal auf der entgegengesetzten apikalen Seite. Eine längere basale Verweildauer der Kerne wurde bereits vorher mit einem symmetrischen Zellteilungsmodus assoziiert, was mit meinen Ergebnissen konsistent ist.
Der Zusammenhang zwischen Orientierung und Modus von Zellteilungen in Wirbeltieren wird kontrovers diskutiert. In meiner Arbeit habe ich beobachtet, dass die Zunahme symmetrischer Teilungen (definiert durch Expression von Atoh7 in beiden Tochterzellen) mit einer Veränderung der Ausrichtung der Zellteilung von radial nach umlaufend korreliert. Die Bedeutung dieser Beobachtung ist jedoch noch nicht abschließend geklärt.

Die vorgestellten funktionellen Experimente in Kombination mit *in vivo* Mikroskopie, implizieren eine Rolle von Anillin in der Beibehaltung der Population neuronaler

Vorläuferzellen und der Einstellung des Zellteilungsmodus. Die direkte Korrelation der Verteilung von F-Aktin und Flemming-Körper auf die Tochterzellen, sowie der Ausrichtung der Zellteilung, erlaubt dabei Rückschlüsse auf die Mechanismen *in vivo*.

Introduction

How does a multipotent progenitor cell acquire the competence to differentiate into multiple cell types, each with specific morphology and function? Addressing this fundamental biological question is central to developmental biology as well as to medical research as it allows knowing how to reprogram a cell in case of a tissue-specific disease. The simple structure and accessibility of the vertebrate retina makes it an ideal model to study cell division and differentiation during neurogenesis. Moreover the use of the tropical freshwater fish *Danio rerio* (Zebrafish), with its external development and transparency at early embryonic stages, allows performing high-speed and cellular resolution microscopy. In combination with powerful genetic approaches, it is possible to study these processes as they happen *in vivo* in the developing animal. In the following thesis, I will raise outstanding questions regarding regulation of neural fate acquisition in relation to asymmetric cell division and describe how I addressed them using zebrafish as model system.

1. Neurogenesis in the vertebrate neural retina

The vertebrate retina as part of the central nervous system (CNS) arises as an optic primordia from the lateral walls of the diencephalon (Kimmel et al. 1995). The optic primordial invagination leads to the formation of a cup made of two cell mono-layers: the retinal pigment epithelium and the retinal neuroepithelium. At this stage both epithelia are proliferative, causing a rapid increase of the cup size. As such, the proliferative retinal neuroepithelium is composed of an array of adjacent elongated cells densely packed (reviewed in (Galli-Resta et al. 2008)), forming a pseudo-stratified mono-layer. These elongated cells remains attached to both sides of the epithelium *via* one apical and one basal process and move their nucleus along this axis in phase with the cell cycle (Murciano et al. 2002) – a characteristic movement named interkinetic nuclear migration (INM) (Sauer 1935). Apical to basal INM corresponds to the G1

and S phase of the cell cycle. This is followed by a basal to apical INM during G2 phase (Norden et al. 2009) (Leung et al. 2011). Mitosis always occurs at the most-apical side of the neural retinal epithelium (Figure 1 B).

Neurogenesis describes the process by which undifferentiated neural progenitor cells generate functional neurons and it starts in the retina after a short period in which symmetric proliferative divisions increase the pool of multipotent progenitors. In the vertebrate retina a neurogenesis wave progresses in a central to peripheral manner (Figure 1 A) and follows a histogenetic order that is conserved among different vertebrate species (Cepko et al. 1996). The mature retina comprises six main types of neurons and one type of glial cell which arise in the following order: retinal ganglion cells (RGC) differentiate first, followed in overlapping waves by amacrine cells (Ac), horizontal cells (Hc), cone photoreceptors (cPh), rod photoreceptors (rPh), bipolar cells (Bp) and, finally, Müller glia cells (Mc) (Figure 1 C). Neural fate specification depends on the competent state of the progenitor cell at the time of cell cycle exit. This competence state is defined by combinations of intrinsic and environmental cues ((Cepko et al. 1996) (Agathocleous & Harris 2009) (Cayouette et al. 2006)), regulated in synchrony with modes of cell division and INM ((Baye & Link 2007) (Baye & Link 2008)). For example, the precursor of an RGC migrates at more basal location before its last division. As a result this precursor becomes less exposed to apical proliferative extrinsic signals ((Baye & Link 2007) (Del Bene et al. 2008)), which leads to the up-regulation of the transcription factor Atonal homolog 7 (Atoh7) (Baye & Link 2007) (Poggi et al., 2005), setting the competence for the generation of a RGCs (W. Liu et al. 2001) (Kay et al. 2001) (Z. Yang et al. 2003) (Poggi et al., 2005) (Figure 1 B). Thus, RGCs genesis is coordinated by integrated regulation of INM, extrinsic signals, intrinsic cell fate determinants expression and mode of cell division. How such cellular and molecular processes are coordinated *in vivo* remains however poorly understood.

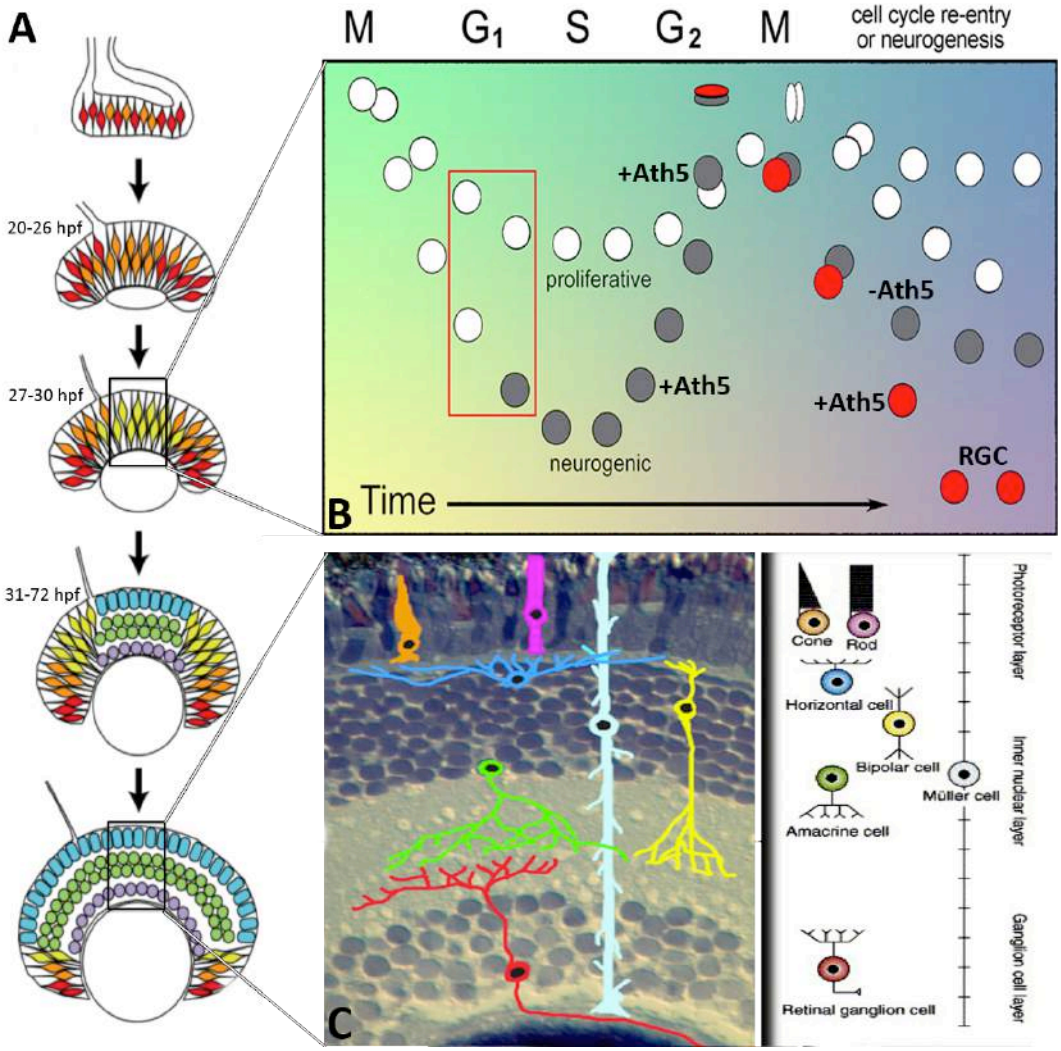

Figure 1. Neurogenesis in the vertebrate neural retina. (A) "neurogenesis wave" in the retina (Red cells: stem cells; Orange cells: multipotent proliferating progenitor; Yellow cells: neural committed precursor; Blue, green and purple cells: differentiated cells which occupy the three retinal layers) (Figure adapted from (Bilitou & Ohnuma 2010)). (B) Interkinetic Nuclear Migration (INM) and early neurogenesis in the neural retina (Figure adapted from (Baye & Link 2007)). (C) A fully differentiated vertebrate neural retina (Figure adapted from (Cayouette et al. 2006)).

2. Intrinsic influences on the competence state and subtype specification of Retinal Progenitor Cells (RPCs)

Transcription factors including members of the basic Helix-Loop-Helix (bHLH), Homeodomain and Forkhead families have emerged as key intrinsic regulators of retinal cell fate and RPCs competence states

(reviewed in (Bassett & Wallace 2012)). For instance, expression of the homeodomain containing repressor "Vsx2" determines the specification of RPCs into Müller glia and a specific subtype of bipolar cell (Vitorino et al. 2009). Before the beginning of neurogenesis in the Zebrafish retina, *vsx2* is expressed in all RPCs. As neurogenesis begins at 25 hours post-fertilization (hpf), *vsx2* expression becomes selectively down regulated, allowing for the generation of lineage-restricted RPCs (Vitorino et al. 2009). For example, down-regulation of *vsx2* in RPCs at 25 hpf allows for the expression of the bHLH transcription factor Atoh7 and the genesis of early born retinal cells, including RGCs (Vitorino et al. 2009).

Expression of *atoh7* has been shown to be required for the genesis of RGCs from zebrafish to primates (W. Liu et al. 2001) (Kay et al. 2001) (Brown et al. 2002) (Sun et al. 2003) (Z. Yang et al. 2003) (Matter-Sadzinski 2005) . Not all *atoh7*-expressing progenitors however become RGCs (Poggi et al., 2005). Previous work has shown that the developmental potential of *atoh7*-expressing RPCs is indeed restricted to the generation of RGCs, a specific subset of ACs, all HCs and PHs (Poggi et al., 2005) (Jusuf et al. 2012). Such studies have further shown that *atoh7* is up-regulated just before the last mitotic division (Figure 2). This division generates one RGC-daughter and another daughter cell that will give rise to other neuronal types (Poggi et al., 2005) (Figure 2). A study performed in our group further highlighted that, whilst determining the cell cycle exit of the RGC progenitor, Atoh7 indirectly controls the correct number and subtypes specification of ACs deriving from *atoh7*-expressing progenitors (Jusuf et al. 2012). *In vivo* time-lapse imaging of the lineage-origin of such ACs revealed that they derive from an asymmetric cell division of the RGC sister cell (Jusuf et al. 2012). In the zebrafish Atoh7 mutant (also called *lakritz*,(Kay et al. 2001)), both daughter cells undergo one further asymmetric cell division, thereby doubling the number of ACs subtypes (Jusuf et al. 2012)

The finding that Atoh7 turns on just before the last mitotic division and that it is required for the cell cycle exit of the RGC indicated that 1) Atoh7 down-regulates genes encoding for components of the cell division

machinery and 2) Atoh7 itself might be implicated in regulating modes of cell division.

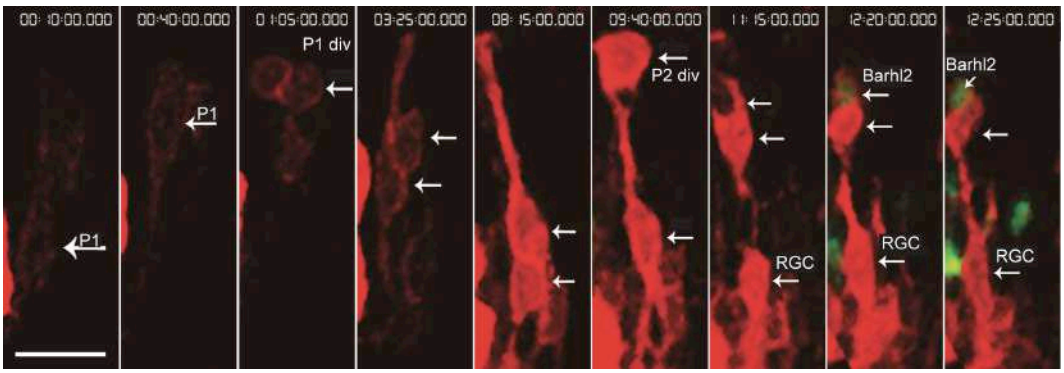

Figure 2. Competence restriction along the Atoh7-cell lineage. Time-lapse series shows the lineage of an Atoh7:gap43-RFP (red) progenitor (P1). After P1 division (P1 div), both daughter cells migrate basally (white arrows, t: 3h25 min). At t: 8h15 min, one daughter cell migrates apically, dividing at t: 9h40 min (P2 div), whereas the other daughter cell remains close to the basal surface, differentiating as a RGC. The diving daughter generates one Barhl2-positive cell (green), which specify a ACs subtype (Jusuf et al. 2012). Scale bar: 7µm. (Figure adapted from(Jusuf et al. 2012)).

3. Extrinsic influences on RPCs

With extrinsic factor or environmental cues we refer to all morphogenes, secreted factors and cell-cell signalling that are known to influence the RPCs developmental potential during neurogenesis. Extrinsic factors have been shown to influence the expression of intrinsic cell fate determinants. For example, the beginning of *atoh7* expression and the wave of neurogenesis appears to be influenced by the *fgf3 and fgf8* expressions from the optic stalk (Martinez-Morales et al. 2005). Sonic Hedgehog signalling ensures timely expression of *atoh7* along the differentiation wave (Kay et al. 2001). The most well studied extrinsic cue during neurogenesis is the Notch-Delta signalling pathway. Notch is a membrane receptor, which can be activated by its ligand Delta, another membrane protein strongly expressed in differentiating cells. Upon Delta-mediated activation, the Notch receptor is cleaved and the Notch intracellular domain can migrate in the

nucleus to inhibit the expression of genes activating neurogenesis (proneural genes). Cells with high levels of Delta and therefore with high proneural genes activity differentiate as neurons, whereas cells that retain high Notch activity go on to remain neuroepithelial cell and eventually become Müller glia (reviewed in (Agathocleous & Harris 2009)). In the absence of this signalling all RPCs exit the cell cycle at the same time and adopt similar fates (reviewed in (Agathocleous & Harris 2009)). Thus, orchestration of Notch-Delta signalling distribution within the retinal neuroepthelium guarantees the maintenance of RPCs heterogeneity during neurogenesis (reviewed in (Agathocleous & Harris 2009)).

A number of studies have analysed the Notch and Delta signalling distribution within the retinal neuroepithelium and with respect to RPCs INM and neurogenesis. Such studies have shown that the receptor Notch and the ligand Delta are expressed in a polarized fashion (Murciano et al. 2002) (H. Liu et al. 2003) (Masai 2005) (Del Bene et al. 2008) (Ohata et al. 2011). In particular, an apical-basal gradient of Notch-Delta signal have been defined in which Notch activity is located in the most apical positions in the retina neuroepithelium while Delta is expressed more basally (Figure 3).

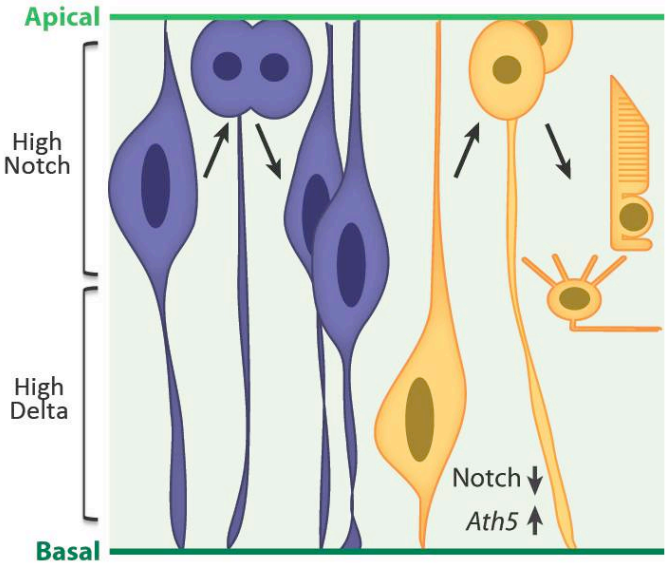

Figure 3. Influence of INM and Notch signalling on neurogenesis. The blue progenitor does not migrate at the most basal location during INM, remaining in an area with high Notch activity. The yellow progenitor migrates more basally, being exposed to low Notch signal. As a result, this progenitor up-regulates *atoh7* (*Ath5* in the figure) and becomes cell fate restricted. (Figure adapted from(Agathocleous & Harris 2009))

It has been proposed that INM can influence the exposure of progenitor nuclei to neurogenic *versus* Notch signals therefore affecting the balance between neurogenesis and proliferation (Murciano et al. 2002) (Cappello et al. 2006) (Baye & Link 2007) (Z. Xie et al. 2007) (Del Bene et al. 2008) (Latasa et al. 2009) (Schenk et al. 2009) (Ge et al. 2010) (Taverna & Huttner 2010) (Y.-T. Yang et al. 2012) (Figure 3).

What regulates INM? Recent research suggests that INM depends on cell cycle progression and its driving force is represented by cytoskeletal components (reviewed in (Lee & Norden 2013)). Which cytoskeletal components play major role in controlling INM in the retina *in vivo* remains a controversial question. While some studies suggest that the apical to basal nuclear movement during INM is stochastic and the basal to apical movement is active, mainly controlled by the actomyosin complex (Norden et al. 2009), other studies provide evidences for a direct role of microtubule components in driving the apical to basal movement (Del Bene 2011). Whether intrinsic cell fate determinants directly regulate such cytoskeletal components, thereby linking INM to environmental cues and neurogenesis, is not known.

4. Mechanisms of asymmetric cell division: spindle orientation and inheritance

Another important cellular aspect that has to be finely regulated during neurogenesis is the RPCs cell division mode. A cell division can be described as asymmetric when the two deriving daughter cells have different fates. A symmetric cell division in contrast gives rise to two daughter cells sharing the same fate, which can be proliferative or neurogenic. Unequal distribution of cell fate determinants during cell division could be the process by which two daughter cells can acquire different fate. In Drosophila and *C. elegans* the asymmetric segregation of cell fate determinants involves the Par3/6/αPKC complex (reviewed in

(Neumuller & Knoblich 2009)), which is contained in the neuroepithelial cells' apical domain (reviewed in (Siller & Doe 2009)). The apical polarity complex is evolutionary conserved in vertebrates and unequal distribution of such apically localized proteins has been correlated with asymmetric cell fate acquisition (Cayouette et al. 2001) (Kosodo et al. 2004) (Žigman et al. 2005) (Bultje et al. 2009) (Marthiens & ffrench-Constant 2009) (Alexandre et al. 2010) (Figure 4). For example, studies in the zebrafish neuroepithelium have shown that divisions that differentially partition the apically localized Par3 drive asymmetric fates, whereas divisions that equally segregate the Par3 containing apical domain result in symmetric fates (Alexandre et al. 2010). Likewise, divisions that unequally segregate apical adherens junctions components are asymmetric (Figure 4 A, (Kosodo et al. 2004)). Studies in fish and chick neuroepithelia have shown that cells that inherit the majority of the membrane apical domains tend to exit the cell cycle and become neurons (Alexandre et al. 2010) (R. M. Das & Storey 2012).

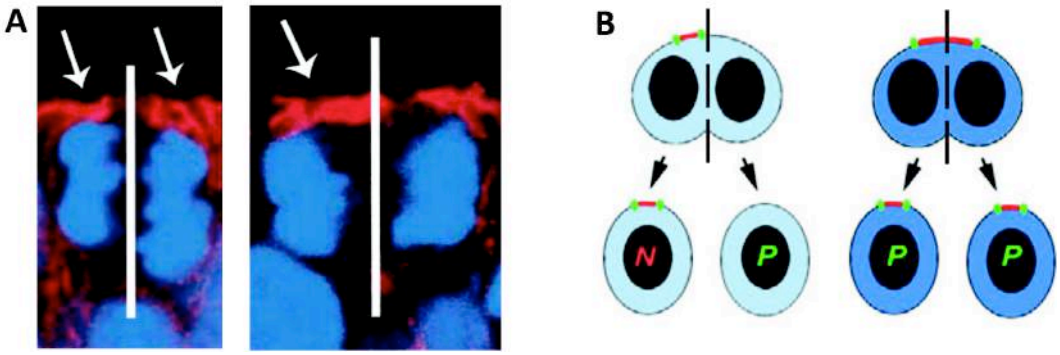

Figure 4. Asymmetric distribution of apical membrane during neural progenitor division. (A) Division of a progenitor (the blue highlights the newborn nuclei) in a mouse hindbrain showing symmetric (left) and asymmetric (right) distribution of the apical domain represented by cadherin protein (red) (picture adapted from (Kosodo et al. 2004). (B) Divisions that differentially partition the apical membrane drive asymmetric fates, whereas divisions that equally segregate the apical domain result in symmetric fates (picture adapted from (Clark et al. 2012)).

How is this unequal distribution regulated? In *Drosophila* neuroblasts the orientation of mitotic spindle has been shown to be essential for the

correct asymmetric segregation of the cell fate determinants Numb, Brat, and Prospero into only one of the two daughter cell, and for correctly specifying neuronal and neuroblast fates (reviewed in (Knoblich 2008)) (Figure 5 A).

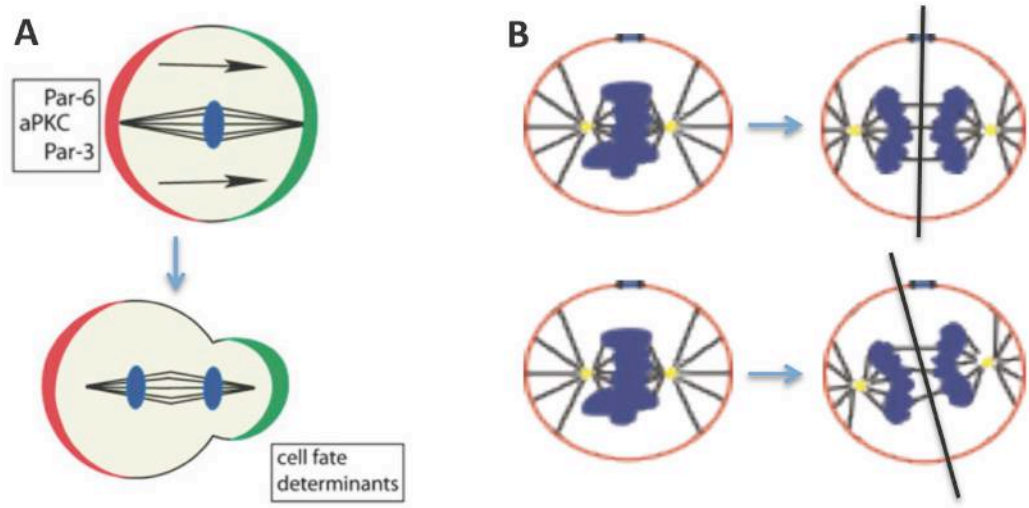

Figure 5. Asymmetric distribution of cell fate determinants in invertebrates and vertebrates neuronal progenitors. (A) Distribution of cell fate determinants during cell division in invertebrates depends on the orientation of the mitotic spindle and the position of polarity proteins. (Figure adapted from (Neumuller & Knoblich 2009)) (B) In vertebrates the role of mitotic spindle orientation in relation with the fate is controversial, but the changes of mitotic spindle orientation genetically or drug-induced can make two daughter cells genetically no longer equal (Figure adapted from (Fish et al. 2008).

In vertebrates, however, divisions with a cleavage plane parallel to the apical basal surface of the neuroepithelum (apico-basal) are somewhat rare under normal circumstances and can be induced to a greater extend upon genetic manipulation (Figure 5, B) (reviewed in (Lancaster & Knoblich 2012)), ultimately leading to a change of cell division outcome (Y. Xie et al. 2013). In many tissues with an epithelial organization, progenitors divide with a cleavage plane perpendicular to the apical surface (planar orientation of cell division) (reviewed in (Morin & Bellaïche 2011)). In vertebrates, it has been proposed that the spindle orientation impacts on cell fate in the cortex and retina so that planar divisions tend to generate two identical cells while vertical divisions (cleavage plane parallel to the apical surface)

generate two different daughter cells (Siller & Doe 2009). This proposed model is in contrast with the finding that the orientation of asymmetric cell division can also be planar (Siller & Doe 2009). Likewise, other studies have reported that cell division orientation along the apical-basal axis does not always predict daughter cell fate outcomes (T. Das et al. 2003) (Lyons 2003) (Kosodo et al. 2004) (Kosodo et al. 2008) (Kosodo & Huttner 2009) (Alexandre et al. 2010). Finally, no divisions were noticed with a cleavage plane parallel to the ventricular surface in the zebrafish retina – all the divisions observed were planar (T. Das et al. 2003) (Poggi et al., 2005). Such studies have suggested that orientation along the planar axis namely circumferential (90°, from the central-peripheral axis) and central-peripheral (radial) (0°) (T. Das et al. 2003) (Figure 6) might correlate with different modes of cell division (Poggi et al., 2005).

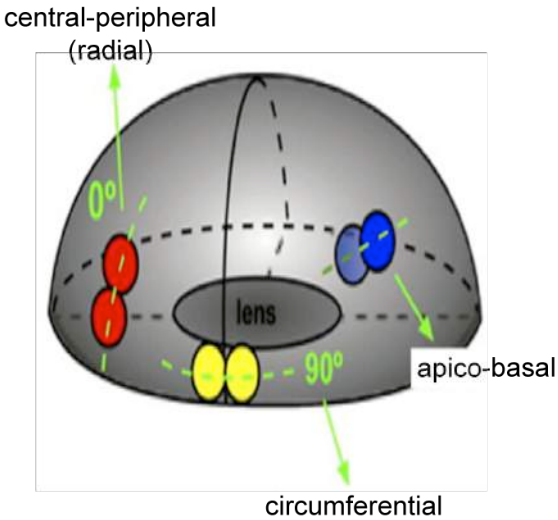

Figure 6. 3D representation of the zebrafish retina as an ellipsoid body, (adapted from (T. Das et al. 2003) (Poggi et al., 2005)).

While the role of mitotic spindle orientation in determining the mode of cell division remains elusive, recent evidences highlight cytokinesis components as attractive potential signalling source for instructing daughter cell fate (Dubreuil et al. 2007) (Ettinger et al. 2011) (Pollarolo et al. 2011) (reviewed in (Chen et al. 2013). During cytokinesis, the cleavage furrow ingression is driven by constriction of the actomyosin contractile ring (Figure 7). As cytokinesis proceeds, the furrow ingression compacts the central spindle to form a structure known as the midbody. The midbody constitutes a cytoplasmic bridge between the two nascent daughter cells and contains the remnants of the central spindle and the contractile ring (Mullins & Biesele 1977) (Mullins & McIntosh 1982) (Figure 7). After abscission, the post-mitotic midbody can be either released after a

secondary bridge-severing event or inherited by one of the two daughter cell (reviewed in (Chen et al. 2013) (Figure 7). This is consistent with the hypothesis that the midbody and its associated actomyosin contractile ring remnants have non-cytokinetic functions such as cell fate determination (reviewed in (Chen et al. 2013)).

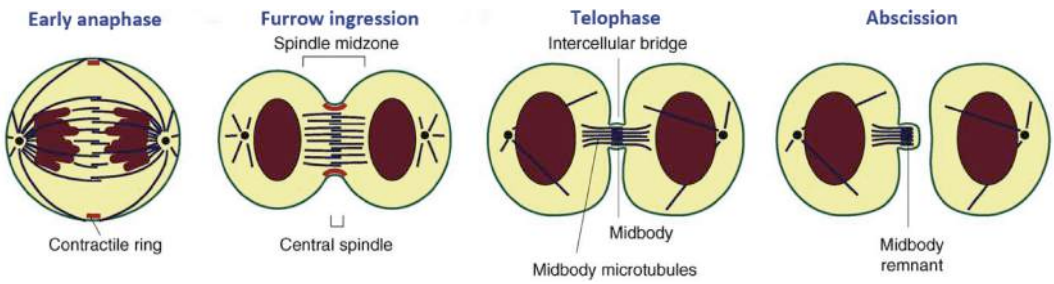

Figure 7. Cytokinesis stages and midbody inheritance (adapted from (Steigemann & Gerlich 2009)).

Differently from non-epithelial cells, cytokinesis of polarized epithelial cells have been shown to begin before anaphase, highlighted by the assembly of cytokinesis machinery components such as F-actin and the F-actin binding protein Anillin in the basal process of the RPCs (Kosodo et al. 2008) (Figure 8). From this point, the cleavage furrow progresses in a basal to apical direction, ending with the formation of a midbody at the most apical side of the RPC (Kosodo et al. 2008) (Figure 8).

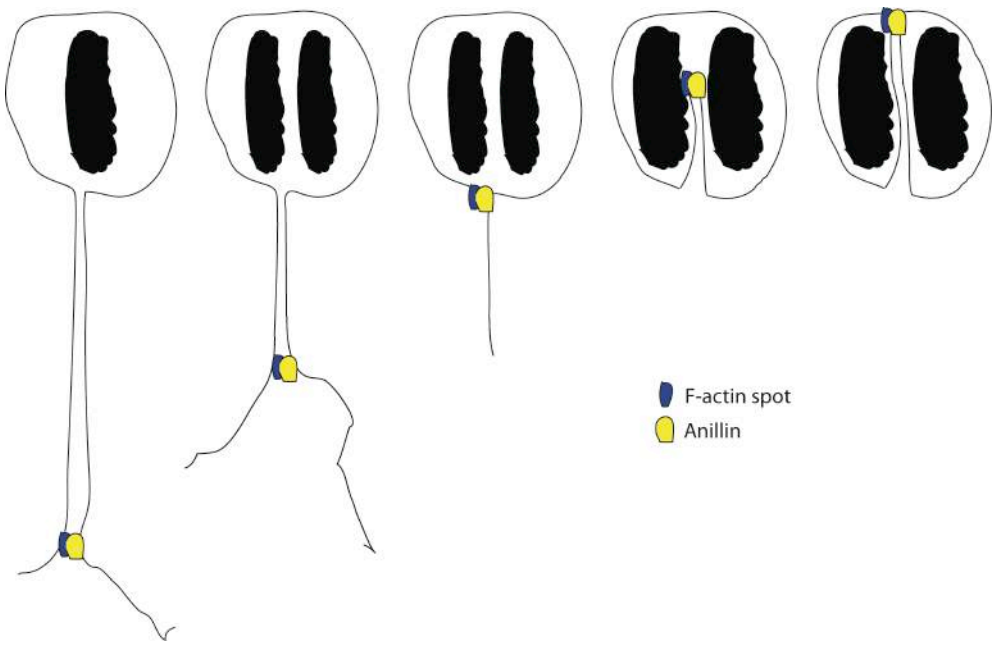

Figure 8. Scheme representing polarized epithelial cells cytokinesis. Anillin and F-actin highlight the cytokinesis progression, which starts before the cell goes through anaphase. Apical side of the neuroepithelium is up, whereas the basal is down. After the completion of cytokinesis, Anillin together with F-actin highlights the intercellular bridge remaining between the two newborn daughter cells (Kosodo et al. 2008) (Hesse et al. 2012), known as midbody, which persist until abscission and eventually retained by one of the two daughters (reviewed in (Chen et al. 2013).

Asymmetry in midbody inheritance or release upon division of RPCs could therefore make two daughter cells no longer equal in terms of developmental potential due to for instance an unequal distribution of membrane-associated and cytoskeletal components. Consistently studies in cell cultures, *C. elegans* and mouse neocortex have reported membranous and cytoplasmic components clustered at the midbody (Skop et al. 2004) (Janetopoulos & Devreotes 2006) (Dubreuil et al. 2007) (Steigemann & Gerlich 2009) (Sagona & Stenmark 2010). Tight association of activated signalling molecules with accumulated filamentous actin at the apical domain has been also observed in human endothelial cells (Galvagni et al. 2012). These observations, combined with the finding that the midbody works as a positional landmark to orient actin flow and polymerization in Drosophila epithelial cells and *C. elegans* blastomeres (Herszterg et al. 2013) (Singh & Pohl 2014), are enforcing this hypothesis.

5. Anillin as molecular link between cell fate determination factors, extrinsic cues and cell behaviours influencing neurogenesis

With the aim of unravelling possible links between cell division regulation and daughter fate outcome, data from comparative micro-array analysis of wild type and *lakritz* (*atoh7*$^{-/-}$) zebrafish retina have been used to search for Atoh7-down regulated factors that are implicated in the regulation of cell division. Such analysis raised interest in the actin-binding

protein Anillin. Anillin is a conserved multi-domain protein, known for its role in scaffolding and organizing the cytoskeleton as well as its regulators during cytokinesis (Figure 9). Anillin was originally isolated from *Drosophila* embryos (Field & Alberts 1995) and homologs were later found in vertebrates (Oegema et al. 2000) (Straight et al. 2005) and *C. elegans* (Maddox 2005). In *Drosophila* and human cultured cells Anillin has been implicated in the regulation of the actomyosin contractile ring ingression during cellularization and cytokinesis (Straight et al. 2005) (Zhao & Fang 2005) (Hickson & O'Farrell 2008) (Piekny & Glotzer 2008) (Goldbach et al. 2010) through the recruitment and binding of many cytokinesis proteins, including F-actin (Field & Alberts 1995) (Gregory et al. 2008) and myosin (Straight et al. 2005) (Figure 9). In human cell culture, induction of exogenous expression of *anillin* enhanced the migrating ability of the cells, potentially *via* induction of actin stress fibers (Suzuki et al. 2005). Accordingly, *anillin* expression levels correlate with the metastatic potential of tumors (Hall 2005). In Drosophila, Anillin is also required during asymmetric cell divisions to ensure the correct number of particular cell types populating the sensory organs of the larval peripheral nervous system, possibly *via* its asymmetric inheritance (O'Farrell & Kylsten 2008).

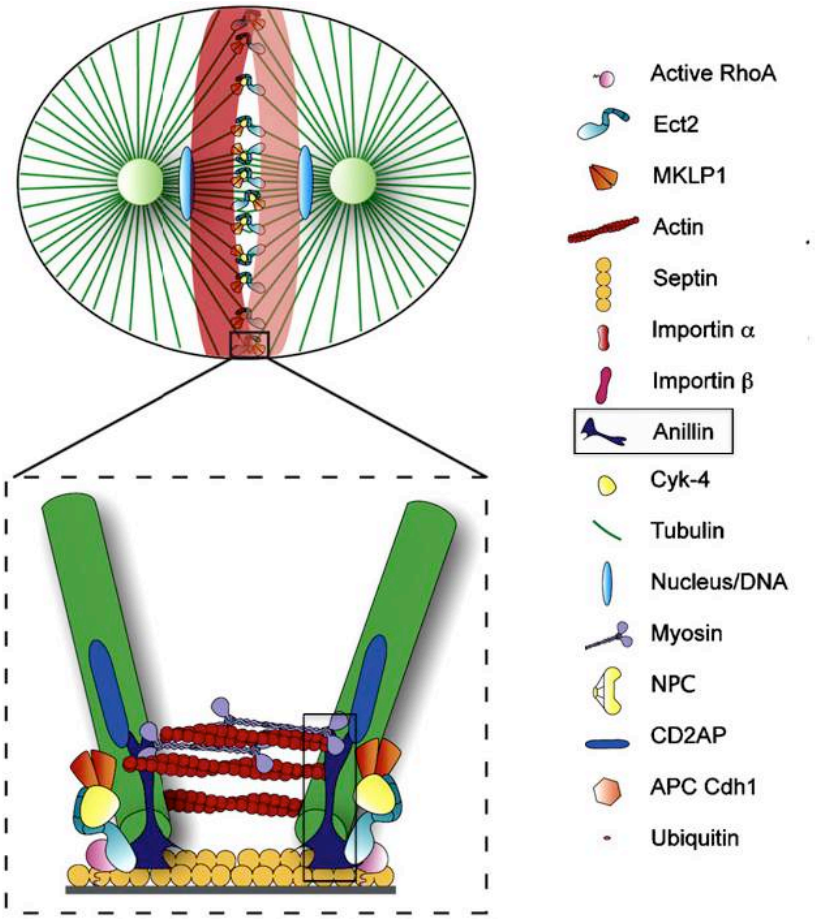

Figure 9. Anillin links to the most important cytokinetic elements. A schematic of a mammalian cell highlighting the main components of the cleavage furrow. Anillin can simultaneously bind to actin, myosin, the GTPase RhoA, the spindle microtubules and the cell cortex *via* Septin (Figure adapted from (Piekny & Maddox 2010)).

Among Anillin's interactors, F-actin is the most studied. Anillin is able to bundle F-actin (Field & Alberts 1995), a function that is conserved throughout vertebrates (Kinoshita et al. 2002). By regulating F-actin bundling, Anillin may increase the efficiency of actomyosin contractility and promote its polymerization in the contractile ring (Reviewed in (Piekny & Maddox 2010)), allowing for cytokinesis progression. Consistently, depletion of *Drosophila* or human cultured cells' Anillin perturbs the temporal and spatial stability of actin and myosin at the cell equator during cytokinesis. This in turn leads to the lateral oscillation of the cytokinetic furrow, and subsequent cytokinesis failure (Reviewed in (Piekny & Maddox 2010). On the other hand, Anillin knock-down in Drosophila epithelial cells was shown to provoke a reduction of the contractile ring constriction's rate

while the basal to apical ingression remains polarized (Guillot & Lecuit 2013). Thus, when a very low amount of Anillin protein is still present, the cleavage furrow ingression still occurs but at slower velocity. In this condition, actomyosin contractility can still occur, but cannot be accurately maintained at the division plane (Reviewed in (Piekny & Maddox 2010)). Recent studies in invertebrates also assigned to Anillin an important role in midbody biogenesis. At the end of cytokinesis, Anillin, F-actin, and other contractile ring components are retained in the midbody (Madaule et al. 1998) (Gai et al. 2011) (Hu et al. 2012) (Kechad et al. 2012).

Anillin expression in relation to the cell-cycle phases has been extensively studied in invertebrates, and also more recently in vertebrates. Studies in *Drosophila*, *S. pombe* and human cultured cells have shown that Anillin localizing primarily to the nucleus during interphase, and at the cell cortex following the breakdown of the nuclear envelope. During cytokinesis, Anillin is enriched at the contractile ring where it persists throughout furrow ingression. Just before abscission, Anillin localizes at the midbody (Reviewed in(Piekny & Maddox 2010)). Studies in human cultured cells and the Drosophila embryo have shown that upon completion of cytokinesis Anillin re-localizes to the nucleus and is targeted by the APCCdh1 for degradation to the proteasome (Field & Alberts 1995) (Zhao & Fang 2005) (Monzo et al. 2005). More recent studies reported of *anillin* expression in the mouse and chick neuroepithelium (Kosodo et al. 2008) (Hesse et al. 2012). Firstly, *anillin* expression has been reported as restricted to proliferative regions of the brain (Hesse et al. 2012). Second, analysis of Anillin cellular distribution and dynamics in proliferating RPCs suggests a conserved role in regulating cytokinesis and midbody formation in vertebrate neuroepithelia (Kosodo et al. 2008) (Hesse et al. 2012) (See figure 8)

Finally, a role of Anillin in orienting the division plane during cell division have been proposed, through interactions with the central spindle, anti-parallel bundled microtubules that form between segregating chromosomes in anaphase (reviewed in (Glotzer 2009)). The central spindle no longer extends to the cortex in Anillin depleted cells in *Drosophila* larval

brains, and often looks distorted and improperly positioned in human cells (reviewed in (Piekny & Maddox 2010).

Functional studies of Anillin in the vertebrate CNS are however still missing.

Aim of the thesis

The aim of this work was to understand the roles of Anillin in the vertebrate neuroepithelium. The implication of Anillin in scaffolding and organizing the actomyosin complex makes it a good candidate for the regulation of cellular processes such as cleavage furrow positioning and midbody inheritance during cytokinesis in the retinal neuroepithelium. This process might orchestrate reorganization of signaling molecules and cell fate determinants located in the daughter cell's apical membrane compartments, ultimately leading to different developmental fates.

To address these questions I firstly aimed at characterizing *anillin* expression in the zebrafish retinal neuroepithelium. In addition, I established a readout for the cellular distribution and dynamics of Anillin protein in the *in vivo* developing zebrafish retina and investigated the following aspects:

1. *Anillin* expression with respect to the retinal neurogenic wave.
2. *Anillin* expression with respect to *atoh7* and RGC genesis
3. *Anillin* expression with respect to the cell cycle and mitotic phases

I then asked what are the effect of Anillin down-regulation on neurogenesis and investigated the following aspects

4. What is the influence of Anillin knock-down on retinal neurogenesis?
5. Does Anillin knock-down affect mode of division of retinal progenitors?

I then analyzed Anillin function in relation to cytokinesis. To this end I used molecular tools to visualize *in vivo* both F-actin dynamics and daughter cell fate during divisions of Atoh7-positive RPCs. The addressed questions were:

6. How is Anillin related to cytokinesis progression and F-actin dynamics?
7. How are cytokinesis and F-actin dynamics affected by Anillin knock down?

8. Is there any pattern of inheritance that could be linked to symmetric *versus* asymmetric division outcome?
9. Is the orientation of cell division affected? Does this predict daughter cell fate outcome?

In addition to driving the constriction of the contractile ring during cytokinesis, actomyosin has been reported as the main driver of basal to apical INM *via* constriction of the basal process (Leung et al. 2011). I therefore investigated whether Anillin knock-down affects INM of RPCs.

All together, this work provides evidences indicating that Anillin is required for the maintenance of the RPC pool and demonstrate a molecular link between the cytokinesis machinery and cell fate determinants during symmetric and asymmetric cell division outcomes.

Results

1. *Anillin* expression correlates with proliferative states of retinal progenitors

Since the zebrafish *anillin* transcriptional dynamic has not been described so far, we firstly analysed its expression in the developing retina by *in situ* hybridisation. *Anillin* transcripts were found throughout the entire undifferentiated retinal neuroepithelium at 25 hpf (Figure 10 A, C, E). From 30 hpf and all the following stages analysed *atoh7* and *anillin* expression patterns remained mostly complementary (Figure 10 B, D, F, G) with *anillin* expression remaining stronger in proximity to the retinal marginal zone (Figure 10 B, G, green arrows in G'). Some degree of overlap could be seen in few cells at the boundary between *atoh7* and *anillin* expression domains (yellow arrowheads in Figure 10 F, G'), consistent with *atoh7*-expressing progenitors undergoing further rounds of cell division (Jusuf et al. 2012). No overlap of *anillin* with the early post-mitotic RGC marker *cxcr4b* (C-X-C chemokine receptor type 4b) was detected (Figure 12 I, I') (Chong et al. 2001), indicating that *anillin* is restricted to proliferating progenitors, consistent with what reported for *anillin* expression in other vertebrate neuroepithelia (Hesse et al. 2012). Detection of *anillin* transcripts in the proliferative area of the midbrain at 30 hpf (white arrows in Figure 10H) further supports this hypothesis. Thus *anillin* expression correlates with proliferative states of retinal progenitors. This is consistent with our microarray data suggesting that *anillin* is a down-regulated gene in the absence of Atoh7 (data not shown). To further corroborate these data, I analysed *anillin* expression in the *lakritz* mutant retina using the *cxcr4b* gene as marker for post-mitotic RGCs. In all analysed embryos (n = 23), the absence of *cxcr4b* was coincident with a strong increase of *anillin* expression in the central retina (Figure 10 J, J'), consistently with progenitors undergoing another round of cell division in the absence of *atoh7* (Jusuf et al. 2012). All these observations indicate that *anillin* expression is down-regulated in the daughter cell that up-regulate *atoh7* and becomes a RGC.

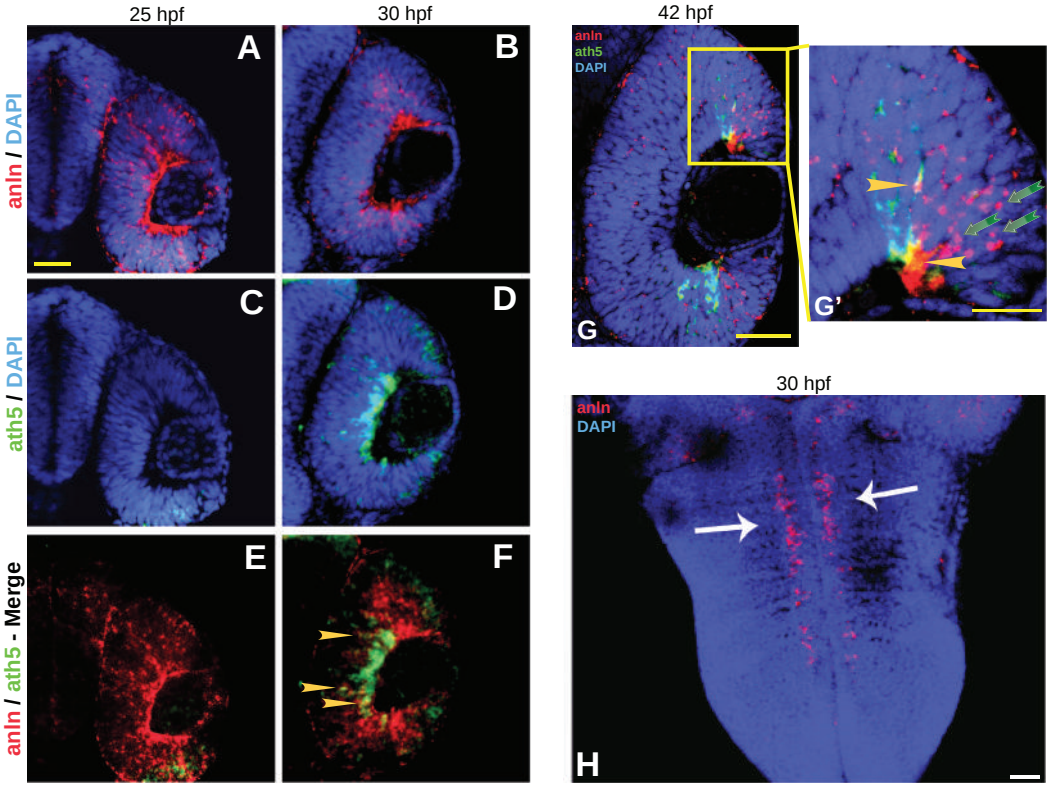

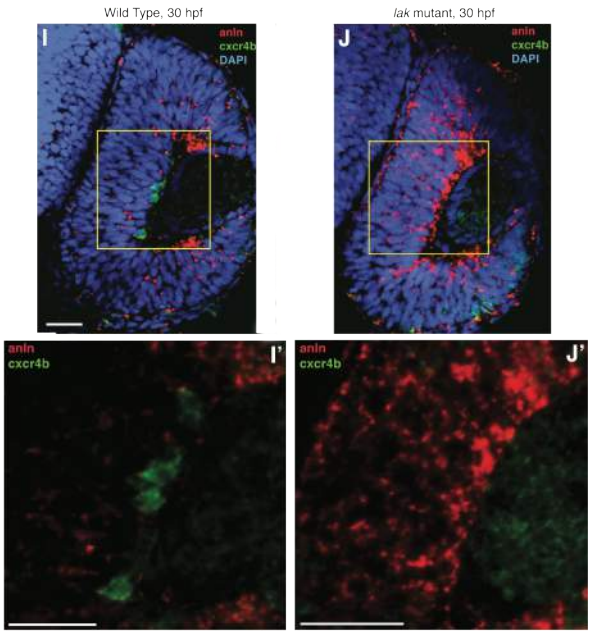

Figure 10. *Anillin* is expressed in proliferative areas of the central nervous system. (A-G') (I-J') Frontal confocal sections of the central retina from an embryo hybridised with *anillin*-Cy3 (red, A-B, E-G', I-J') *atoh7*-FITC (green, C-D, G-G') and *cxcr4b*-FITC (green, I-J') antisense RNA probes. Yellow arrowheads in (F) and (G') indicate overlap between *anillin* and *atoh7* transcripts in few cells at the boundary of the expression domains. Green arrows indicate cells close to the marginal zone only expressing *anillin*. (H) Dorsal confocal section of the midbrain from an embryo hybridised with *anillin*-Cy3 (red). White arrows indicate a*nillin* expression domain. The yellow rectangles in (I-J) indicate optical zooms on a central portion of the retina showing that there is no colocalization between *anillin* and *cxcr4b* transcripts in wild type (I'). When *cxcr4b* is absent (*lakritz*), there is an increase in *anillin* expression (J'). Nuclei were

counterstained with DAPI (in blue, A-B, G-H, I-J). Scale bars: (in A, G, G' and H) A – H, 42 μm, in (I, I' and J') I-J', 21 μm.

2. Anillin protein localizes to the nucleus, contractile ring and midbody of cycling RPCs.

To investigate Anillin dynamics in relation to the cell cycle and mitotic phases of RPCs, we tagged the zebrafish *anillin* to the green fluorescent protein (eGFP) coding sequence. Mosaic expression of the *anillin–eGFP* reporter from a bacterial artificial chromosome (BAC) containing *anillin* cis-regulatory sequences (*anillin:anillin-eGFP*) (made with the help of Dr. Shahad Albadri and Vincenzo Di Donato, Institut Curie, Paris) recapitulated the temporal and spatial *anillin* distribution in the developing retina (data not shown and Figure 11 A). *In vivo* imaging of 28 hpf developing retinas revealed localisation of Anillin-eGFP in the nuclei at interphase. At the end of prophase, during nuclear breakdown, Anillin localized in the cytoplasm and concentrated to the cortex at the basal tip of the cell and in the cleavage furrow during telophase (indicated by the yellow arrow in Figure 11 A). Finally, an Anillin-eGFP spot became apparent at the apical domain of the newly divided daughter cells, consistent with the formation of an apically localized midbody at the end of cytokinesis (Kosodo et al. 2004) (Wilcock et al. 2007) (Kosodo et al. 2008) (Hesse et al. 2012) (Figure 11 A). Using the Tg(*atoh7:gap43-RFP*) transgenic line, where membrane-tethered red fluorescent protein (gap43-RFP) is expressed under the control of the *atoh7* promoter, I could detect some dividing Atoh7-positive cells expressing *anillin* (Figure 11 B). Upon division, *anillin* expression was restricted to one of the two daughters (Figure 11 B), consistent with an asymmetric division generating one post-mitotic RGC and a self-renewing RPC.

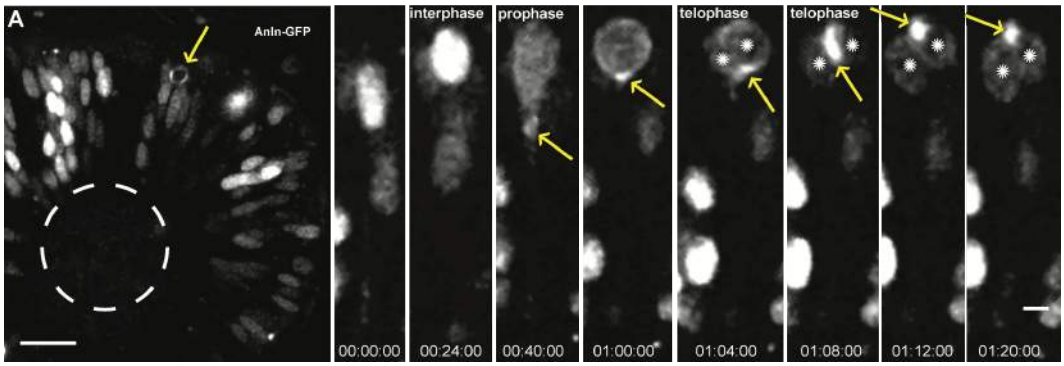

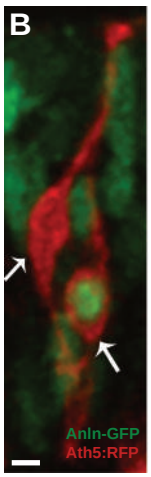

Figure 11. Anillin-eGFP dynamic in a dividing retinal progenitor highlights cytokinetic furrow progression and midbody formation. Maximal projection of confocal stacks from a time-lapse series showing localisation of Anillin-eGFP during the different mitotic phases. Time-lapse series of a single dividing progenitor starting at 28 hpf (t=0h00min). The yellow arrow points at Anillin-eGFP enrichment in the basal process (t=0h40), at the basal side of the cell body (t=01h00) in the contractile ring (t=01h04, t=01,08) and to the apical midbody (t=01,12, T=01,20). White asterisks indicate the two newborn daughter cells (B) Maximal projection of confocal stacks from a time-lapse series at 30 hpf showing two daughter cells (white arrows) of a progenitor expressing *atoh7-gap43-RFP*. One of the two daughters expresses *anillin:eGFP* in the nucleus.

Scale bars: In (A) A, 20 μ m; (in A last timepoint) A, 4 μ m; in (B) B, 3.5 μ m.

3. Anillin functional knock-down promotes neurogenesis

I then investigated the impact of Anillin on retinal neurogenesis *via* a morpholino approach. I designed a splicing morpholino targeting the first exon-intron boundary of the *anillin* gene and checked the effect on neurogenesis using the Tg(*atoh7:GFP*) transgenic line as readout for the production of early-born neurons at 72 hpf, when the differentiation in the central retina is complete. When compared to control, 48,4% (n = 31) of the analysed embryos showed an increase of the *atoh7*-expressing cells (Figure 12 A, B) as well as an increase in the ganglion cell layer's (GCL) size as highlighted by immunostaining against Zn5, an RGC membrane-localised marker (Figure 12 A', B'). A multipoint *in vivo* imaging of Tg(*atoh7:gap43-RFP*) control (Movie 1) and *anillin* splicing morpholino injected embryo

(Movie 2) showed the strong increase of Atoh7-positive cells generation over time. This kind of morpholino prevents the correct splicing of *anillin* pre-mRNA, leading to a retention of the intron 1, the generation of an in frame stop codon and the translation of a truncated protein. I assessed the functionality of Anillin splicing morpholino by RT-PCR of total mRNA from embryos injected with Anillin or control morpholino (Figure 12 C). I choose three different developmental stages covering the progenitors proliferative period and the beginning of the neurogenic wave coincidently with the peak of *atoh7* expression. There was a decrease of the correct spliced form of *anillin* mRNA at 20 hpf and 30 hpf in the injected embryos, while at 40 hpf a recovery of this form (Figure 12 D) can be seen. The retention of the first intron was verified for all of the three stages analysed (Figure 12 D).

To assess specificity and reproducibility of the Anillin knock-down phenotype I used an Anillin translational blocking morpholino. The morpholino injected retina showed a similar phenotype to the one observed after the injection of Anillin splicing morpholino, highlighted by an increase in the *atoh7*-expressing cells in 30 hpf (from 10.5% ± 1.6% SEM to 18.5% ± 1.2% SEM, p - value < 0.001, n = 15) (Figure 12E-G), 35 hpf (71%, n = 24) (Figure 12 H, I) and 72 hpf (Figure 12 J, K) embryos.

Collectively, these data indicate that the Anillin knock-down phenotype is consistent with a specific targeting of the endogenous *anillin* mRNA.

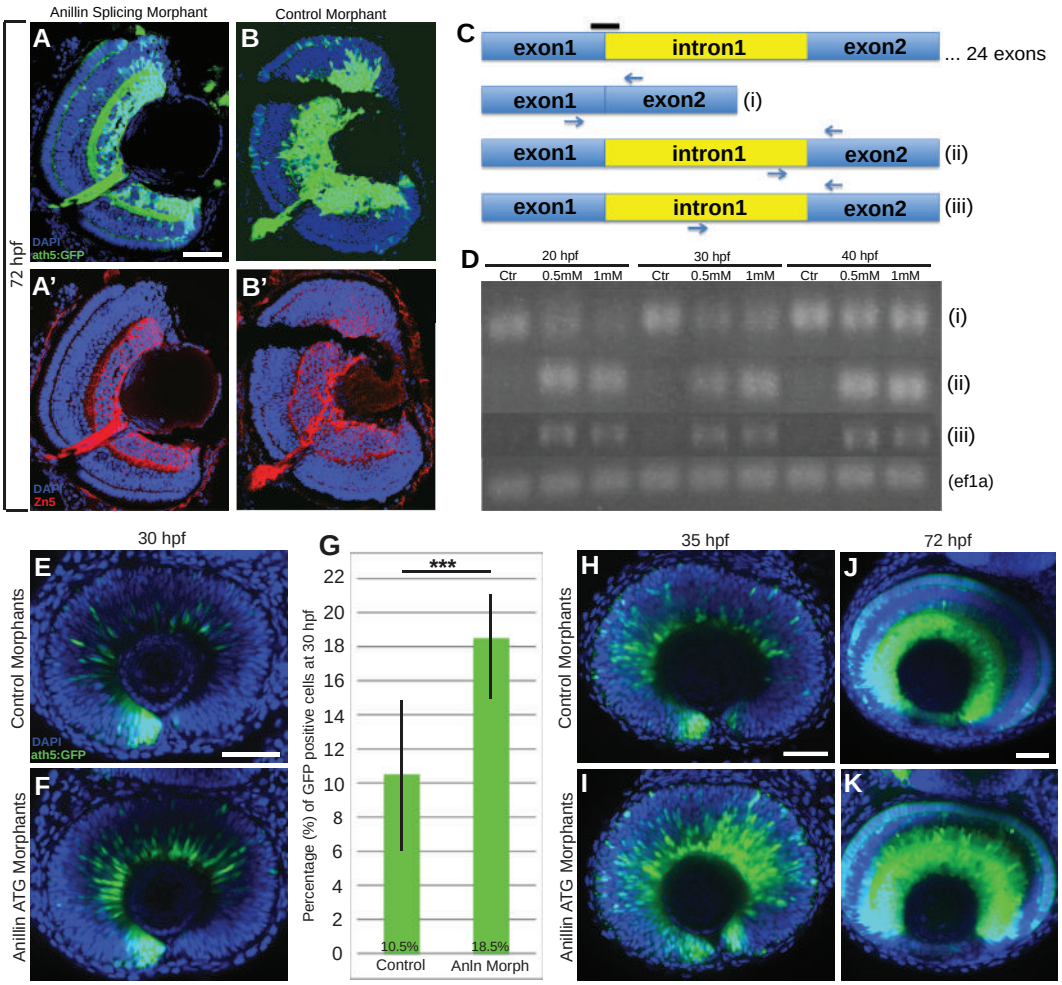

Figure 12. Anillin knock-down affects retinal neurogenesis. (A-B') Confocal section through the central retina of a Tg*(atoh7:GFP)* embryo injected with either control morpholino (A-A') or Anillin splicing morpholino (B-B') showing that Atoh7-GFP signal is increased at 72 hpf. Embryos in (A') and (B') are immunolabeled with Zn5, to highlight the ganglion cell layer. (C-D) Assessment of Anillin splicing morpholino efficiency. (C) (top) Schematic representation of the endogenous *anillin* pre-mRNA and the splice blocking morpholino target site (black bar); (i) expected length after *anillin* mRNA splicing, using the primer set indicated with blue arrows; (ii) and (iii) expected length amplified with two different primer sets (blue arrows) after intron 1 retention mediated by morpholino splice blocking. (D) Total mRNAs extracted from 20, 30 and 40 hpf morpholino-injected embryos were used to assess the efficiency of 0.5 and 1 mM morpholino concentrations. eF1 α was used as housekeeping gene for the RT-PCR validation. (E-F, H-K) Confocal section through the central retina of a Tg*(atoh7:GFP)* embryo injected with either control morpholino (E, H, J) or Anillin translation blocking morpholino (F, I, K) showing that Atoh7-GFP signal is increased at 30, 35 and 72 hpf. (G) Quantification of the ratio of GFP/DAPI cells in injected embryos shows increase in the number of GFP-positive cells in the translational morpholino-injected retinas at 30 hpf. Pictures in (A-B') show a frontal view (dorsal side to

the top) while pictures in (E-F) and (H-K) show a lateral view (dorsal side to the top). All represented retinas were counterstained with DAPI (in blue). Morphants, morpholino-injected embryos; (***), $p < 0.001$; the vertical black lines in (G) represent the standard deviations. Scale bars: (in A) A-B', (in E) E-F, (in H) H-I; (in J) J-K, 42 μ m.

4. The increase of early born retinal cell types occurs at the expense of the late born ones in the absence of Anillin protein

In addition to RGCs, *atoh7*-expressing progenitors differentiate into other early born cell types in the vertebrate retina. Among these are ACs and HCs (Poggi et al., 2005). It is therefore possible that these other cell types are also preferentially generated as a result of *anillin* down-regulation. To investigate this aspect I used the Tg(*atoh7:GFP/ptf1a:dsRed*) double transgenic line. Ptf1a:dsRed signal highlights all ACs and HCs in the retina (Jusuf et al. 2011). At 72 hpf Anillin morpholino-injected embryos showed an increase of Ptf1a:dsRed positive cells (from 22.2% ± 0.3% SEM to 26.7% ± 0.6% SEM, p - value < 0.0001, n = 16) (Figure 13 A-C). Most of the morpholino-injected embryos also show an increase in the GFP signal, as a confirmation of what was previously shown (Figure 13 A'', B''). Thus, Anillin knock-down increases early-born cell types. I then asked if this phenotype occurs at the expense of the late-born retinal cell types. To verify this I used the double transgenic line Tg(*vsx2:GFP/atoh7:RFP*). All Anillin morpholino-injected retinas showing an increase of RFP signal (n=11) also displayed a decrease in GFP expression (Figure 13 D-E''). To rule out that the observed decrease of Vsx2:GFP-positive cells was not due to apoptotic events induced by Anillin morpholino, I performed an activated Caspase 3 immunostaining on Tg(*vsx2:GFP*) Anillin morpholino-injected embryos at 30 hpf. This analysis showed no increase in apoptotic cells in the Anillin morpholino-injected retina (from 21.4% to 38.4%, p = 0.28 by the Chi-squared test; n = 43) (data not shown), indicating that the decrease in late born cell types is not due to apoptotic events.

If more Vsx2-positive proliferating RPCs become Atoh7-positive in the Anillin knock-down condition, then we would expect a decrease of the mitotic index in these RPCs. We assessed the mitotic index of 30 hpf retinas from Tg(*atoh7:GFP*) Anillin morpholino-injected embryos performing an immunostaining against phosphohistone H3 (PH3), a mitotic marker. Surprisingly, quantification of PH3-positive cells revealed no significant difference between control and Anillin morpholino-injected retinas (from 3.65% ± 0.3% SEM to 3.57% ± 0.3% SEM. p - value = 0.46) (Figure 13 F-H). Instead, the number of PH3-positive cells within the GFP-positive population was significantly lower after Anillin knock-down (from 5.1% ± 0.6% SEM to 3.3% ± 0.5% SEM, p - value < 0.05, n = 15) (Figure 13 F-G, I). This result supports the idea that *atoh7*-expressing progenitors are less likely to undergo further rounds of cell division in the Anillin morpholino-injected retinas.

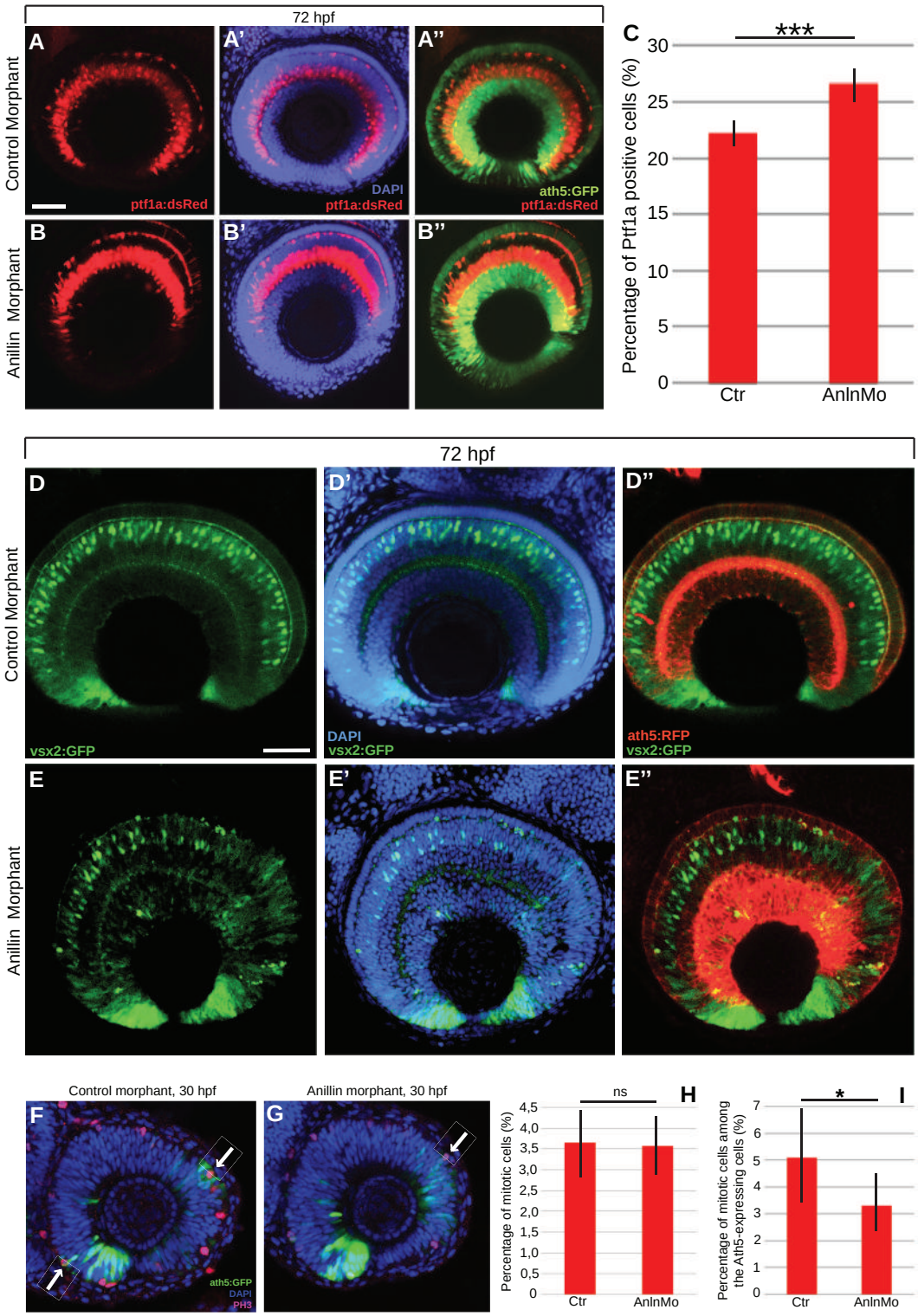

Figure 13. Increase of the early born retinal cell type at the expense of the late born retinal cell types. (A-B'', D-E'') Confocal section through the central retina of a Tg*(atoh7:GFP/ptf1a:dsRed)* (A-B'') or Tg(*atoh7:gap43-RFP/vsx2:GFP*) (D-E'') 72 hpf embryo injected with either control morpholino (A-A'', D-D'') or Anillin morpholino (B-B'', E-E''). (C) Quantification of the ratio of Ptf1a/DAPI cells in injected embryos shows increase in the number of Ptf1a-positive cells in the Anillin morpholino-injected retina at 72 hpf. (F-G) Confocal sections through the retina of a Tg(*atoh7:GFP*) embryo injected with either control

(F) or Anillin morpholino (G). These retinas were labelled with phosphohistone H3 (PH3) antibody to highlight mitotic cells. White arrows indicate GFP/PH3 positive cells. (H) Quantification of the ratio PH3/total DAPI positive cells shows that the overall number of mitotic nuclei is not affected after Anillin morpholino injection. (I) Quantification of the ratio of PH3 and GFP positive/total GFP positive cells shows a decrease of mitotic cells among the GFP positive population. All pictures show a lateral view (dorsal side to the top). Retinas in (A', B', D', E', F and G) were counterstained with DAPI. Morphants, morpholino-injected embryos; ns, not significant; (*), $p < 0.05$; (***), $p < 0.001$; the vertical black lines in (C, H, I) represent the standard deviations. Scale bars: (in A) A-B''; (in D) D-E''; (in F) F-G; (in h), 42 μ m.

5. Anillin knock-down affects RPCs mode of cell division

Since Atoh7-positive progenitors are less likely to divide, we wanted to investigate what divisions are affected in this cell population. To this aim we examined Anillin knock-down effect on the behaviour of individual RPCs *in vivo*. To perform this analysis at single-cell level, we used a transplantation approach to create mosaic embryos. Tg(*atoh7:GFP*) transgenic embryos were injected with *H2B-RFP* mRNA (to label nuclei of donor cells) and Anillin or control morpholino at the one-cell stage, and blastomeres were transplanted into unlabeled host embryos (Figure 14 A) Cell divisions were visualised by time-lapse confocal microscopy from 28 hpf for approximately 24 hours to assess daughter cell fate. I first followed the fate of *H2B-RFP* labelled siblings as they up-regulated *atoh7:GFP*. In the case of control morpholino-injected cells, 4/9 cell divisions (44%) produced two Atoh7:GFP-positive daughter cells, while the remaining 5/9 (56%) produced only one Atoh7:GFP-positive sibling (Figure 14 B, Movie 3). Strikingly, Anillin knock-down produced a significant increase in divisions where both siblings turned on *atoh7:GFP* (100%, n=9) (p = 0.03 by the Fisher's test) (Figure 14 C, Movie 4), consistent with the observed increase in Atoh7:GFP positive cells in these retinas. Thus, Anillin knock-down promotes symmetric divisions in which both daughter cells up-regulate

atoh7, thereby decreasing the progenitor pool available for later born cell types (i.e. *vsx2*-expressing progenitors).

We then examined divisions of GFP-positive progenitors. We found that 9/11 (82%) divisions in the control, GFP-positive progenitor cells generated progeny with asymmetric fate – namely, one RGC daughter and one self-renewing progenitor (Figure 14 D and Movie 5). In the remaining 2 cases (18%), both daughter cells remained as self-renewing progenitors (data not shown). By comparison, Anillin knock-down generated an increased number of symmetric/neurogenic divisions. Of the 7 divisions analysed, 4 generated two RGCs (Figure 14 E and Movie 6). Thus, after Anillin knock-down, *atoh7*-expressing progenitors are more likely to generate two post-mitotic daughters (p = 0.02 by the Fisher's test), consistent with the observed decrease in PH3-positive cells in the Atoh7:GFP population.

Collectively, these results indicate that Anillin knock-down affects the division outcome of retinal progenitors so that both daughters are more likely to up-regulate *atoh7*, become post-mitotic and adopt a neuronal (RGC) fate.

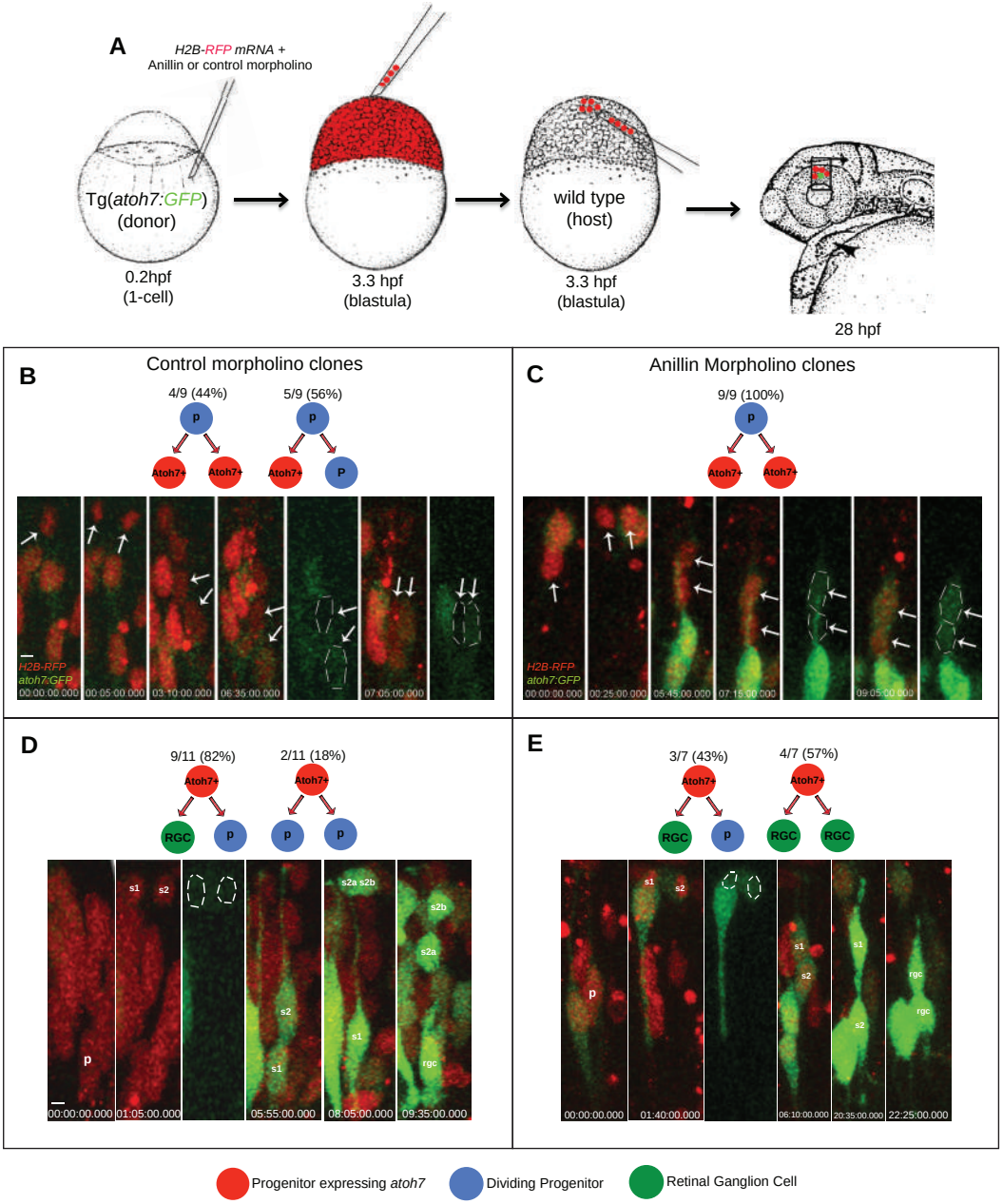

Figure 14. *Anillin* knock-down favours symmetric *versus* asymmetric mode of cell division. (A) Schematic representation of the transplantation experiments (adapted from (Kimmel et al. 1995)). (B-C) Proportions of H2B:RFP positive progenitors (P, in blue) divisions giving rise to either one or two Atoh7-GFP positive cells (Atoh7+ in red) in control morpholino (B) or Anillin morpholino (C) retinas. Selected frames from Movie 3 and Movie 4 are shown as example of a division generating one (B) or two (C) atoh7:GFP positive daughters (each time-frame represents a maximal projection). Divisions generating two Atoh7:GFP positive daughters are increased after Anillin knock-down. (D-E) proportions of Atoh7:GFP positive progenitors divisions generating one (D) or two (E) RGCs. Selected frames from Movie 5 and Movie 6 are shown as example of an asymmetric division (D) generating one RGC (s1) and one dividing progenitor (s2, giving rise to s2a and s2b) or (E)

two RGCs. Divisions generating two RGCs are increased after Anillin knock-down. Scale bars: (in B) B, C, 5 μ m; (in D) D, E, 3 μ m.

6. Anillin and F-actin co-localise at the cleavage furrow and midbody of cycling RPCs

The previous observations lead us to ask whether the Anillin knock-down effect on cell division outcome was related to its putative role in cytokinesis. To test this hypothesis, I firstly assessed F-actin distribution during cytokinesis progression in the differentiating retina. To this aim I expressed a *lifeact-venus* reporter as readout for F-actin dynamics *in vivo* (Riedl et al. 2008) and *H2B:RFP* to assess the basal to apical displacement of the F-actin spot, as indicative of cytokinesis progression during mitosis. I observed an F-actin (positive) spot appearing in the basal process at prophase and migrating in a basal to apical direction until it reached the basal side of the cell nucleus at metaphase where it remained until the end of anaphase (Figure 15 A, Movie 7). During telophase, F-actin highlighted the contractile ring constriction and then at the end of telophase, an F-actin enriched spot reappeared at the apical domain of daughter cells (Figure 15 A, Movie 7). I then assessed the Anillin and F-actin distributions during furrow progression and midbody formation in the differentiating retina. To this end, the anillin:anillin-eGFP reporter was injected in combination with another fluorescently labeled LifeAct construct (*lifeact-Ruby*). Confocal imaging on mosaically labelled retinas revealed evident concomitant enrichment of F-actin and Anillin in the basal process, as previously shown in mouse telencephalic neuroepithelium (Kosodo et al. 2008), just after the release of Anillin-eGFP into the cytoplasm during nuclear breakdown at prophase (Figure 15 B). As cytokinesis progressed, concurrent enrichment of F-actin and Anillin could be seen at the basal side of the cell body and in the contractile ring during telophase (Figure 15 B, B'). Interestingly, midbody formation at the end of cytokinesis coincided with a transient

accumulation of Lifeact-Ruby signal around the apically located Anillin-eGFP spot (Figure 15 B). This is strikingly similar to what was recently reported in Drosophila epithelia, where the midbody provides a positional cue for orienting apical actin accumulation (Herszterg et al. 2013) (Morais-de-Sá & Sunkel 2013).

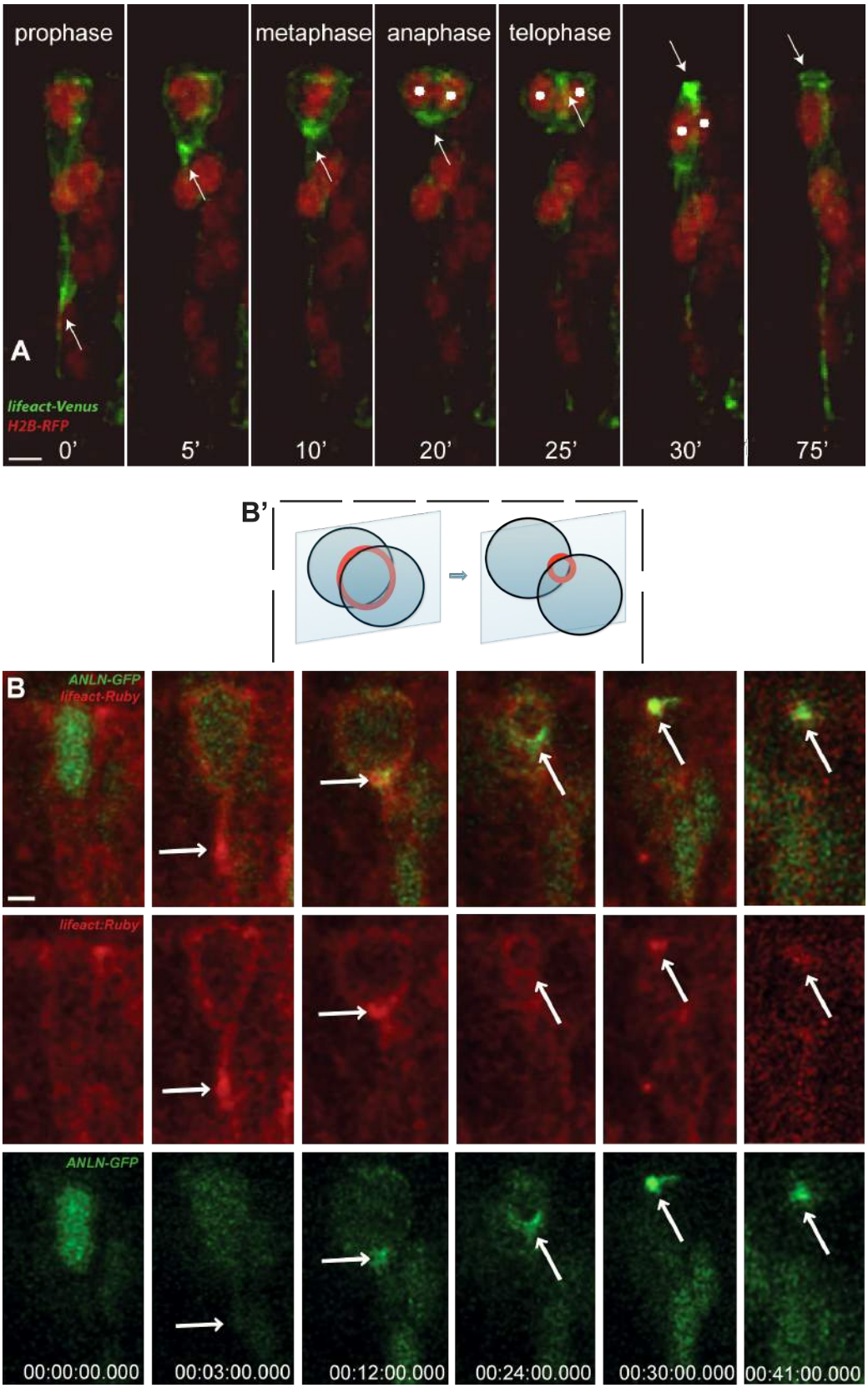

Figure 15. F-actin and Anillin colocalise highlighting the cytokinetic furrow. (A) Frames from a time-lapse sequence of a dividing progenitor from control morpholino injected embryos. The white arrow indicates the F-actin spot while the white dots indicates the two newborn nuclei after progenitor's division. (B) Maximal projection of confocal

stacks from a time-lapse series at 28 hpf showing a cell division. The white arrow (from left to right) highlights concomitant enrichment of Anillin-eGFP (green) and Lifeact-Ruby (red) in the basal process, basal side of the cell body, contractile ring and apical midbody. (B') Scheme illustrating the position of the two cells in (B) with respect to the contractile ring. Scale bars: (in A) A, 5.1 μm; (in B) B, 3.5 μm.

7. Correlation between inheritance of F-actin/midbody and cell fate

Since Anillin and F-actin co-segregate at the daughter cell's apical domain after cytokinesis, I went on to investigate 1) whether Anillin and F-actin become asymmetrically inherited by one daughter cell's apical domain; 2) whether asymmetric inheritance correlates with daughter cell fate (Experiments performed with the help of Anne-Laure Duchemin, Centre for Organismal Studies, Heidelberg, Germany). To this aim, I expressed *lifeact-venus* into Tg(*atoh7-gap43-RFP*) transgenic embryos to visualise concomitantly apical F-actin distribution and asymmetric daughter cell fate. Analysis of cells revealed 7 out of 8 (87%) divisions with an asymmetric distribution of F-actin at the daughter cells apical domain after cytokinesis (Movie 8). This proportion is consistent with the proportion of Atoh7-positive progenitors undergoing asymmetric cell division (Jusuf et al. 2012). In 3 of these divisions it was possible to follow the fate of the two daughter cells unambiguously. In all the cases, the daughter cell that inherited the apical F-actin enriched domain became a RGC whereas the other one divided again (Fig. 16 A, A'), suggesting a correlation between apical F-actin inheritance and asymmetric division outcome.

To investigate the inheritance of apical Anillin/midbody during asymmetric cell division, we imaged Anillin-eGFP while assessing daughter cell fate *in vivo*. At 28 hpf *atoh7*-expressing progenitor division give rise to one RGC and one progenitor. *In vivo* imaging of 28 hpf retinas revealed 4 out of 4 asymmetric divisions in which the apical Anillin-eGFP spot was inherited only by one gap43-RFP positive daughter (Figure 16 B-D', Movie 9

and Movie 10). This daughter then differentiated into a RGC (Figure 16 B, C and Movie 9). Notably, expression of *anillin* was reinitiated in the nucleus of the daughter cell that migrates back to the apical surface to divide (Figure 16 B and Movie 10). Interestingly, in one case we could follow a late division of one gap43-RFP positive progenitor that generated one dividing progenitor and one Ph cell inheriting the apical Anillin-eGFP spot (data not shown). These observations indicate that inheritance of the Anillin-eGFP/midbody and apical F-actin spot can predict asymmetric cell division and the post-mitotic daughter generally inherits it.

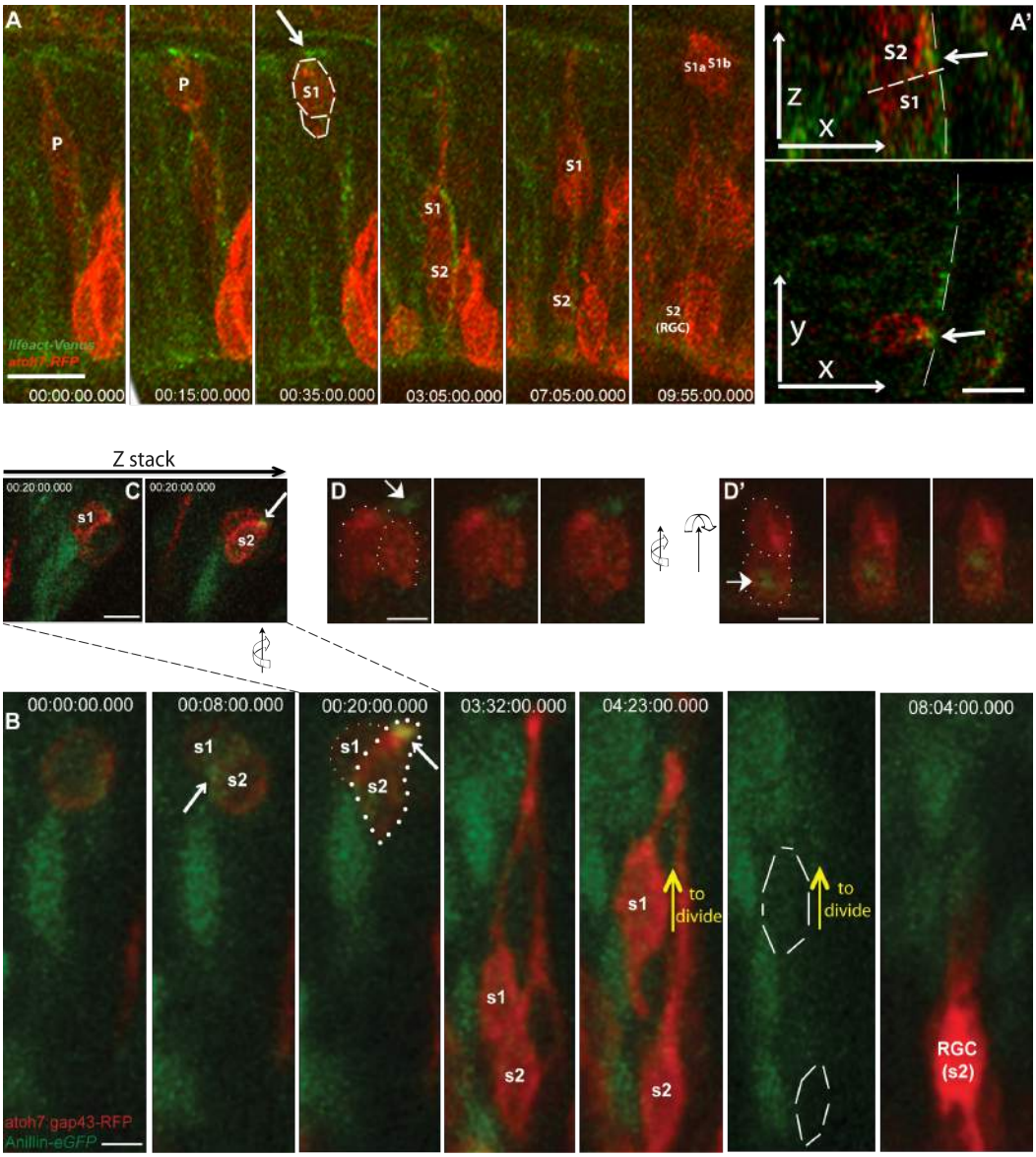

Figure 16. Asymmetric inheritance of apical F-actin and Anillin highlighting midbody correlates with asymmetric daughter fate. (A) Maximal projection of confocal stacks

from time-lapse series (starting at 28 hpf, t = 0h00min) of a division of a progenitor expressing *atoh7:gap43-RFP* and *lifeact-venus*. After division, the daughter s2 (behind s1, at t=0h35min) asymmetrically inherits the apical F-actin domain (indicated by the white arrow). White dashed line highlight both daughters. Single orthogonal planes (in A') (t=0h35min) are showing that the F-actin enriched apical domain indeed belongs to the daughter s2 (the white dashed line outlines the apical surface of the epithelium). This cell differentiates as RGC (t=09h55min) while the daughter (s1) divides again to generate cell s1a and s1b. (B) Maximal projection of confocal stacks from a time-lapse series (starting at 28 hpf, t=0h00min) showing the division of a progenitor expressing *atoh7-gap43-RFP* and *anillin:eGFP*. After cytokinesis (t=00h08) the daughter s2 inherits the Anillin-eGFP highlighted midbody (t=00h20). White dotted lines surround the two daughter cell bodies (s1 and s2). After division, s1 turns on *anillin-eGFP* in the nucleus (t04h23, green channel only) and goes back apically to divide (yellow arrow). The s2 daughter retracts the apical process and migrates to the basal surface differentiating into a RGC (t=08h04). (C) Two different Z-stack positions taken at t=0h20min show that the s2 daughter (in B) asymmetrically inherits the apical Anillin-eGFP spot (white arrow). (D, D') 3D reconstruction of an *atoh7:gap43-RFP*-expressing progenitor division. Rotations in 3 different angles and two directions highlight asymmetric inheritance of the Anln-eGFP spot (white arrow) (with the help of Anne-Laure Duchemin, see text). Scale bars: (in A, A') A, A', 10 μ m; (in B – D') B, C, D and D', 3.5 μ m.

8. Anillin down-regulation leads to a slowdown of the cleavage furrow ingression and affects apical F-actin distribution

In order to assess the effect of Anillin knock-down on cytokinesis progression and F-actin inheritance, I expressed a Lifeact-Venus reporter and H2B:RFP in Anillin morpholino-injected embryos and performed a blastomeres transplantation in wild-type embryos to check the behaviour of isolated clones. Anillin knock-down had no effect on the F-actin spot basal to apical displacement in relation to nuclei mitotic phases (Figure 17 A, C, Movie 11), as compared to Figure 15 A. Conversely, the cytokinesis progression highlighted by the basal to apical F-actin spot migration was significantly slower in the Anillin morpholino-injected clones (from 1.16 μ

m/min ± 0.07 μm/min SEM to 0.95 μm/min ± 0.05 μm/min SEM, p - value < 0.05, n = 57) (Figure 17 A-C, Movie 11). Anillin knock-down produced also a notable decrease in the rate of the F-actin displacement, with the newly forming basal F-actin spot consistently appearing at more apical distances from the basal surface of the neuroepithelium (from 21% (normalized position) ± 3% SEM to 31% ± 3.3% SEM, *p* - value < 0.05, n = 55) (Figure 17 D). This phenomenon was concurrent with a longer duration of mitosis (from 27.6 min ± 1.5 min SEM to 35.3 min ± 1.3 min SEM, p - value < 0.001, n = 36) (Figure 17 E, Movie 12), consistent with the unvaried F-actin spot displacement. These results are in favour of the hypothesis that Anillin controls furrow progression but not its direction in vertebrate neuroepithelium (Morais-de-Sá & Sunkel 2013) (Guillot & Lecuit 2013).

I next investigated the effect of Anillin knock-down on F-actin distribution at the daughter cell's apical domain. Time-lapse imaging on 28 hpf retina mosaically labelled with *lifeact-venus* and *H2B-RFP* revealed 14 out of 17 divisions (82%) showing an apical F-actin enrichment at one daughter's apical cell domain at the end of cytokinesis (Figure 17 F, H, Movie 13). The remaining 18% of the divisions showed no evident asymmetry of apical F-actin, but rather a duplication of the F-actin/apical domain, which remained associated with both the daughter cells. Anillin knock-down produced a significant increase in divisions with a duplication of the F-actin apical domain (43%, n = 14, p = 0.02 by the Chi-squared test) (Figure 17 G, H, Movie 14). These results are in line with the idea that symmetric outcome of cell division produced by Anillin knock-down is linked to the symmetric apical F-actin inheritance at the daughter cell's apical domain.

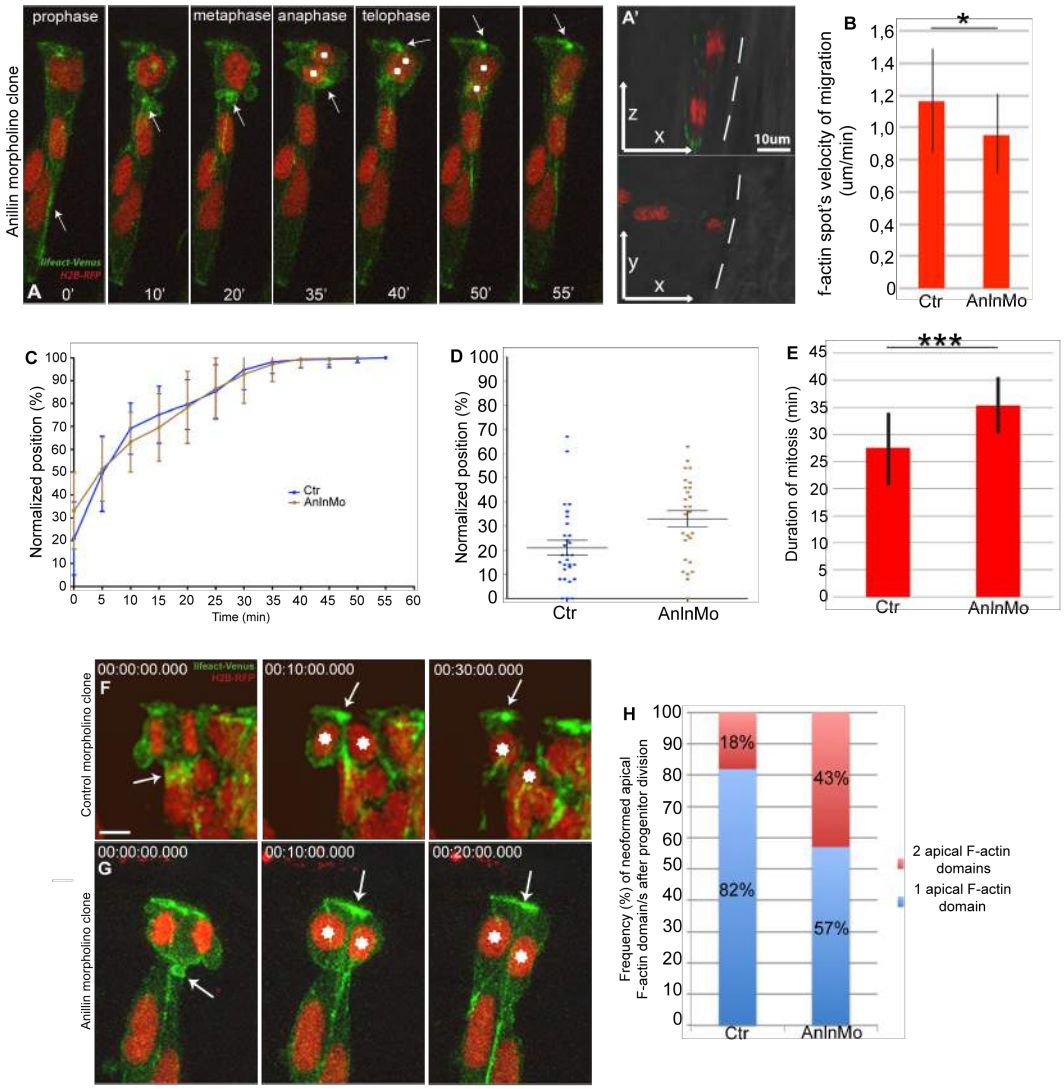

Figure 17. Anillin knock-down affects F-actin spot basal-to-apical displacement and inheritance. (A) Frames from a time-lapse sequence of a dividing progenitor from Anillin morpholino-injected embryos. The white arrow indicates the F-actin spot while the white dots indicate the two newborn nuclei after progenitor's division. The F-actin spot in relation to the nuclei (H2B-RFP) mitotic phases as compared to the Figure 7 A is unvaried. (A') Orthogonal view of the division (t=0h35) in (A) showing that this is parallel to the apical surface of the epithelium (highlighted with the white dashed line). (B) Quantification of the velocity of the basal to apical F-actin spot displacement reveals a significant slowdown of this movement after Anillin knock-down (C) Average position ('trend') of all F-actin spots analysed over time. (Ctr) Control morpholino-injected n=30; (AnlnMo) Anillin morphlino-injected, n=27. (D) Dot-plots illustrating the position of the newly appearing F-actin spot in the basal process for Ctr Mo, n=30 and Anln Mo n=27. This position is generally higher in Anln Mo. The middle line represents the average value of F-actin spots, the upper and lower lines indicate the edges of the standard error. (E) Quantification of mitosis length showed a significant slowdown after Anillin knock-down. (F, G) Maximal projections of confocal stacks from time-lapse series (at 28 hpf) of a progenitor H2B-RFP

and Lifeact-Venus -positive in control (F) or Anillin knock-down (G) conditions. The white stars highlight the two newborn nuclei while the white arrow indicates F-actin accumulation during cytokinesis. In (F), apical F-actin is asymmetrically distributed between the two daughter apical domains. In (G), apical F-actin is symmetrically distributed. (H) Divisions with symmetric apical F-actin inheritance are significantly increased in the Anillin knock-down condition deviation. The vertical black lines in (B, E) represent the standard deviations. (*) $p < 0.05$; (***) $p < 0.001$. Ctr, Control morpholino; AnlnMo, Anillin morpholino; min, minutes (‘). Scale bars: (in A) A, 5.1 μm; (in A’) A’, 10 μm; (in F) F, G, 5 μm.

9. Change in the orientation of RPCs cell division along the planar axis following Anillin knock-down

Since the orientation of cell division along the apical basal axis has been implicated in daughter fate outcome, I investigated on the possibility that changes in daughter cell fate upon Anillin knock-down correlate with changes in cell division orientation. Analysis of RPCs orientation of cell division along the apical-basal axis of the epithelium did not reveal any differences between control and anillin morphant retina. I detected only 5 out of 64 divisions in control and 6 out of 69 divisions in Anillin knock-down, which tended to be oblique, ($p = 0.86$ by the Chi-Square test, data not shown).

To see if Anillin knock-down can significantly influence orientation of cell division along planar axis, I measured the orientation of cell division of control and Anillin knocked-down clones from retinas around 30 hpf. I found that the average angle of cell division orientation is significantly different between control and Anillin morpholino-injected clones, being the control divisions oriented more preferentially towards the radial axis (from 37° in control to 51° in anillin morphants, $p = 0.012$ by the Kolmogorov-Smirnov test, n = 119) (Figure 18 B, C).

Subsequently I asked whether an association between these 2 orientations of cell division and fate outcome of the two daughter cells could

be present. The 5 progenitors analysed which gave rise to an Atoh7-positive and an Atoh7-negative daughters tended to divide along the central-peripheral axis (average 27°), while the 13 progenitors which gave rise to two Atoh7-positive daughters tended to significantly divide along the circumferential axis (average 56°, p - value < 0.05 by the t-test, n = 18) (data not shown). In conclusion, these observations support the hypothesis that Anillin knocked-down clones tend to divide more along the circumferential axis, and this kind orientation is more associated with symmetric fate of the two daughter cells in terms of *atoh7* expression.

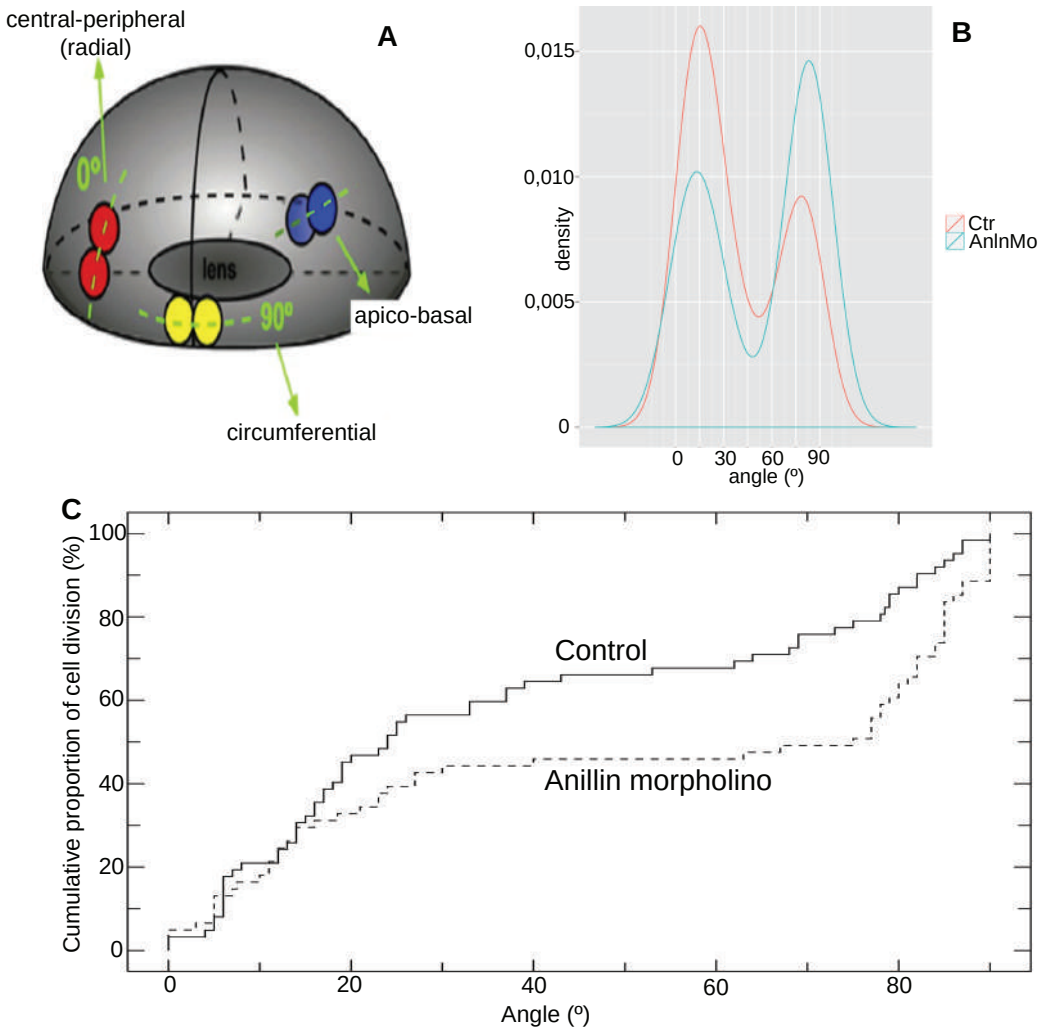

Figure 18. Anillin knock-down affects progenitors orientation of cell division along the planar axis. (A) 3D representation of the zebrafish retina as an ellipsoid body, adapted from (T. Das et al. 2003) (Poggi et al., 2005). (B) Graph showing the distribution of the angles of cell division among the control and Anillin knocked-down clones. (C) Cumulative distributions of the orientation of cell divisions found in control and Anillin knocked-down

clones. Both graphs in (B-C) show that the Anillin knocked-down clones preferentially divide along the circumferential axis.

10. Anillin knock-down affects the basal to apical nuclear migration and cell cycle length of RPCs.

Since acto-myosin components have been implicated in the basal to apical INM, we then addressed whether Anillin knock-down also affects this process. We performed a blastomere transplantation experiment in which Tg(*H2B:GFP*) or *H2B:RFP* mRNA-injected Anillin or control morpholino-injected embryos were used as donors. The wild-type acceptors were mosaic animals containing few isolated cells from either Anillin or control morphant clones. As expected, I observed an increase of the basal to apical velocity of Anillin morphant nuclear migration (from 0.59 μm/min ± 0.06 μm/min SEM to 0.2 μm/min ± 0.02 μm/min SEM, *p* - value < 0.0000001, n = 50) (Figure 19 A-C, Movie 15 and Movie 16). This indicates that even the longer permanence of the Anillin morphant nuclei far away from the apical proliferative signal could explain the change on mode of cell division towards an increase of early neurogenesis (Del Bene et al. 2008). An increase of the time the Anillin progenitors nuclei spent at the apical surface before to complete the anaphase were also detected (from 19.2 min ± 1.2 min SEM to 46.3 min ± 6.9 min SEM, *p* - value < 0.001, n = 50) (Figure 19 A, B, D, Movie 15 and Movie 16), confirming the previously shown data on the duration of mitosis. Since the basal to apical nuclear migration have been associated to the G2 phase of the cell cycle (Leung et al. 2011), I decided to monitor the cell cycle behaviour of Anillin knocked-down clones, at first evaluating the length of the cell cycle by measuring the time between two consecutive mitosis of a progenitor labelled with H2B-RFP, starting at 25 hpf. I detected an increase in the cell cycle duration of Anillin knocked-down progenitors (from 442 min ± 33 min SEM to 638 min ± 40 min SEM, *p* - value < 0.01, n = 17) (Figure 19 E, F). Looking at the Anillin knocked-down nuclei

dynamic during cell cycle/INM, I observed the basal to apical migration (G2) as stochastic as the apical to basal nuclear migration, which dynamic in general did not change from the control's one (Figure 19 E, F). This means that just the G2 phase seems affected by Anillin knock-down. To conclude, many evidences show that the lengthening of the cell cycle of a neural progenitor is associated with its commitment to differentiation (Takahashi et al. 1995) (Calegari 2003) (Calegari 2005) (Wilcock et al. 2007) (Chiodini et al. 2013) and this can partially explain also the impact on neurogenesis provoked by Anillin functional depletion.

Finally, time-lapse analysis of Atoh7:GFP positive or negative control cells from 8 control morpholino injected retinas revealed that the 71% of the analysed clones return apically to divide, while the remaining 29% stayed basally, up-regulating or further up-regulating Atoh7. Among the Anillin morpholino clones tracked in 5 different retinas, only the 54% of them return apically to divide ($p < 0.05$ from t-test, n=13) (data not shown). Looking at the overall phenotype induced by Anillin knock-down in Atoh7:GFP retina, this result is in line with previous research reporting that longer permanence of progenitors at the basal side are committing them to early-born lineages (Baye & Link 2007) (Del Bene et al. 2008).

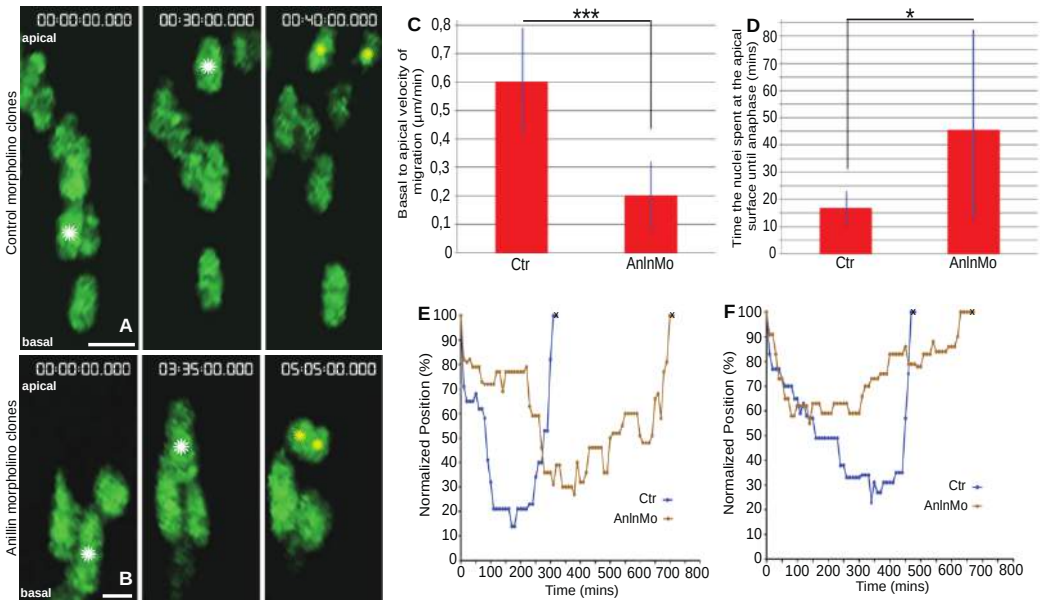

Figure 19. Anillin knock-down affect the basal to apical nuclear migration during progenitors cell cycle. (A, B) Maximal projections of confocal stacks from time-lapse series (at 28 hpf) of a progenitor H2B-GFP positive in control (A) or Anillin knock-down (B)

conditions. The white stars (in A-B) indicate the progenitors at the beginning and the end of their movement. The yellow stars (in A-B) indicate the two newborn nuclei after progenitor's division. (C) Quantification of the velocity of the basal to apical nuclear migration reveals a significant slowdown of this movement after Anillin knock-down. (D) Quantification of the time the nuclei spent at the apical surface until the completion of anaphase showed a significant slowdown of this time after Anillin knock-down. (E-F) Representative INM profiles from control and Anillin knocked-down cells showing that only the basal to apical nuclear movement is affected by Anillin knock-down. The black 'x' in (E-F) represents the moment in which the cell divides. The vertical blue lines in (C, D) represent the standard deviations. (*) $p < 0.05$; (***) $p < 0.001$. Scale bar: (in A), A, 7 μm; (in B), B, 4.5 μm.

Discussion

1. Cytokinesis progression affects inheritance of apical components and mode of cell division

It remains to be clarified how regulation of cytokinesis progression in progenitor cells is linked to asymmetric inheritance and fate outcome. It has been proposed that the early assembly of cytokinesis components in the basal process might serve as a signalling centre for the correct basal to apical cleavage furrow progression and inheritance of the apical plasma membrane (Kosodo et al. 2008) (Kosodo & Huttner 2009). A slow down of F-actin spot formation and apical migration in Anillin knock-down indeed leads to changes of F-actin distribution at the daughter cell's apical domain and correlates to different daughter cell fates (Figure 21). Thus a causal relationship between the early assembly of the cleavage furrow components and asymmetric cell division might exist *in vivo*.

This study further demonstrates that Anillin-associated midbody inheritance can be predictive of cell fate in asymmetric cell divisions – the RGC daughter generally inherits the Anillin spot that forms at the location of the apical midbody at the end of cytokinesis (Figure 20). This is consistent with recent studies reporting that the daughter of a neural progenitor that inherits cytokinetic remnants and/or apical footprint is more likely to become a neuron and suggests that midbody-associated cytokinesis remnants could instruct neuronal fate (Alexandre et al. 2010) (Pollarolo et al. 2011). Recent studies additionally suggest that the midbody may be retained by one daughter cell or released into the extracellular space and that this inheritance is associated with a particular cell fate acquisition (reviewed in (Chen et al. 2013)). It is however yet to be determined how midbody formation, inheritance and release is related to apical F-actin enrichment and segregation of cell fate determinants to one daughter's apical domain. For example, the midbody could guide F-actin accumulation during the establishment of new adherent junctions at the interface of the daughter cells (Herszterg et al. 2013) (Morais-de-Sá & Sunkel 2013) with

consequent redistribution of signalling and polarity molecules between daughter cell apical domains (Galvagni et al. 2012).

What might be the signalling or polarity molecules instructive for daughter cell fate? In the cortex asymmetric divisions of neural progenitors give rise to daughter cells with variable Notch levels. Cells with greater Notch activity tend to remain proliferating while those with lower Notch activity tend to become neurons (Reviewed in (Lancaster & Knoblich 2012)). In the zebrafish brain, the apical polarity complex protein Par3 has been shown to restrict Notch activity to the proliferating daughter through segregation of the ubiquitin ligase Mib (essential for the activation of Notch by Delta in the signal sending daughter (Itoh et al. 2003)) to the differentiating daughter cell (Dong et al. 2012). It remains to be determined whether Anillin plays a role in the asymmetric distribution of Par3 and Mib. Another study proposes that Numb, an inhibitor of Notch signalling, interacts with internalized Spdo-Notch oligomers at sorting endosomes to inhibit the recycling of Notch during cytokinesis of sensory organ precursor cells in Drosophila (Couturier et al. 2013). This interaction creates an asymmetry in Notch distribution at the interface between the daughter cells (Couturier et al. 2013). A possible role of Anillin in the establishment of Notch asymmetric distribution *via* the apical membrane domains at cytokinesis would enforce the implication of this gene as molecular link between cell fate determination factors and extrinsic cues.

2. Pleiotropy of Anillin protein

As suggested by (Willardsen & Link 2011), challenges arise from the functional pleiotropy of the molecules and signalling pathways that affect multiple cellular behaviours implicated in neurogenesis. Consistently our results show that the cell division and distribution of apical components are not the only cell behaviours affected by Anillin knock-down, but the neural

progenitors basal to apical nuclear migration during INM and cell cycle length are also affected (Figure 20 and 21).

Experiments in cell culture previously showed that a failure in properly regulating the Actin remodeler Esp8 levels in G2 prolongs its localization at the cell cortex and markedly delays cell rounding and pro-metaphase duration (Werner et al. 2013). Therefore, roles of Anillin in controlling Actin localization could underlie the observed slow down of these processes in Anillin knock-down conditions. Additionally, studies in the zebrafish retina proposed that a basal actomyosin activation/contraction squeezes the basal process to send the nucleus towards the apical side of the neuroepithelium during the S/G2 transition (Leung et al. 2011). By regulating actomyosin, Anillin could also mediate this contraction, explaining the observed slow down of the progenitor nucleus' apical movement (Figure 21). Many studies reported that cell cycle progression and INM of RPCs are tightly coupled processes (Karfunkel, 1972) (Messier 1978) (Webster and Langman, 1978) (Murciano et al. 2002) (Gambello et al. 2003) (Ueno et al. 2006) (Baye & Link 2008). For instance, in *Drosophila* the basal to apical INM and G2/M progression is influenced by the Hippo pathway (Reviewed in (Hergovich & Hemmings 2012)) through regulation of Rho signalling, which is essential for cytokinesis progression (Gregory et al. 2008). Rho kinase is also an upstream activator of actomyosin contractility during INM (Meyer et al. 2011) (reviewed in (Lee & Norden 2013)). Since Rho can bind myosin through interaction with Anillin at the actomyosin contractile ring (Piekny & Glotzer 2008), Anillin might regulate actomyosin contraction through regulation of Rho function. Finally, studies in fission yeast highlighted a role of the Anillin-like protein Mid1p in the nucleus where it targets the promoter of genes involved in M-phase progression, allowing the cell to go through mitosis and cytokinesis (Agarwal et al. 2010). We therefore cannot exclude that Anillin nuclear localization might have an additional biological function during this process.

The lengthening of the cell cycle observed upon Anillin knock-down (Figure 21) suggests alternative or additional mechanisms whereby Anillin might link intrinsic cell fate determinants (such as Atoh7) to environmental

cues to affect daughter cell fate. In the zebrafish retina, increase in cell-cycle length has been linked to the increase in symmetrical differentiative divisions (He et al. 2012). In the chick retina, a slow down of the cell-cycle has been proposed to allow the reaching of high levels of *atoh7* expression and RGC commitment (Chiodini et al. 2013). Along this line, a study on the zebrafish retina has shown that prolonged permanence of the RPC nuclei at the basal most side of the retinal neuroepithelium keep them away from higher Notch signalling activation (Del Bene et al. 2008). As a consequence, the time window for *atoh7* expression and the production of RGCs is extended at the expense of later-born Müller glia and bipolar cells (Del Bene et al. 2008). Therefore, a slow down of the basal to apical INM and cell cycle length in Anillin morpholino injected embryos could establish conditions favouring *atoh7* up-regulation in both daughter cells, hence symmetric cell fate outcome (Figure 21)

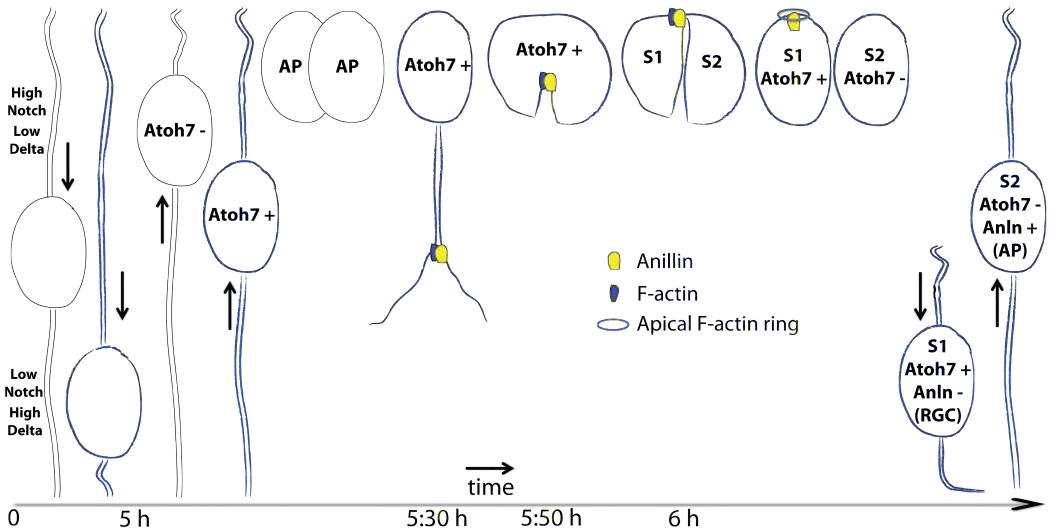

Figure 20. Model of a wild type neural retina showing INM, cell division and apical components inheritance of an *atoh7*-expressing progenitor. From left to the right, this model shows two sister cells undergoing INM. The one highlighted in blue migrates at more basal location, being less exposed to high level of Notch. This cell then up-regulates *atoh7* (Poggi et al., 2005) (Baye & Link 2007) during its apical to basal movement, divides and undergoes cytokinesis. At the end of cytokinesis, the midbody highlighted by Anillin and associated with the remnant of the F-actin spot is inherited by one of the two daughter cells (S1). Midbody could work as a positional landmark to orient the Actin flow and polymerization as already suggested in lower organisms (Herszterg et al. 2013) (Singh & Pohl 2014), to generate the apical F-actin ring. The daughter cells inheriting both the

midbody and the apical F-actin ring (S1) down-regulates Anillin and differentiate as RGC, while the other one (S2) up-regulates Anillin undergoing division. The apical side is up, whereas the basal side is down. Atoh7-: cell not expressing *atoh7*; Atoh7 +: cell up-regulating *atoh7*; AP: Apical Progenitor; S1: *atoh7*-expressing progenitor's daughter 1; S2: *atoh7*-expressing progenitor's daughter 2. Anln -: cell down-regulating Anillin. Anln +: cell up-regulating Anillin.

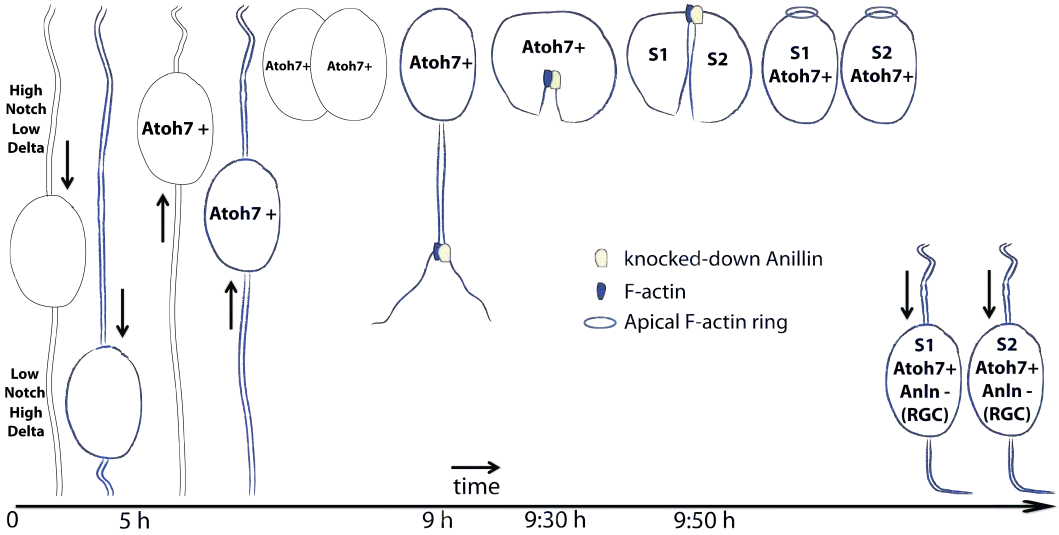

Figure 21. Model of a wild type neural retina showing INM, cell division and apical components inheritance of Anillin morpholino injected progenitors. From left to the right, this model show two Anillin morpholino-injected sister cells undergo INM. Both of the 2 cells slow down their basal to apical movement, being less exposed to Notch signalling. As a consequence both of the cells up-regulate *atoh7* undergoing symmetric division. The cell highlighted in blue shows a slower cell division and cytokinesis progression with respect to a wild type clone. At the end of cytokinesis, the F-actin apical ring duplicates and both of the new daughter cells inherit it. Both of the two daughter cells (S1 and S2) down-regulate Anillin and differentiate as RGCs. The apical side is up, whereas the basal side is down. Atoh7 +: cell up-regulating *atoh7*; AP: Apical Progenitor; S1: *atoh7*-expressing progenitor's daughter 1; S2: *atoh7*-expressing progenitor's daughter 2. Anln -: cell down-regulating Anillin.

3. Anillin might influence the orientation of cell division within the plane of the neuroepithelium

Discussion

The data here presented provide compelling evidence supporting the idea that cleavage furrow components contribute to the establishment of the asymmetry of cell division irrespective of spindle orientation along the apical-basal axis of the epithelium. In the zebrafish retina changes in the orientation of cell division can occur mainly along the planar axis (T. Das et al. 2003) (Poggi et al., 2005). In agreement with these previous findings, this study revealed that only a small percentage of progenitors divide obliquely with respect to the apical-basal axis. Here, a switch of cell division orientation from central-peripheral (radial) to circumferential was significant in Anillin morpholino injected retinas. In this study, however, increase of circumferential divisions following Anillin knock-down is rather associated with an increase in symmetric divisions generating two RPCs expressing *atoh7*. This is in conflict with what has been previously hypothesised. A careful correlation between orientation and fate of daughter cells is still needed. However, the present results suggest that oriented cell divisions along the plane might be uncoupled to daughter cell fate.

How can Anillin be related to oriented divisions along the plane? No evidences for a direct role of Anillin in controlling the orientation of cell division have been shown so far. In fission yeast, the export of the Anillin-like protein Mid1p from the nucleus couples the position of the division plane to the position of the nucleus itself (Paoletti & Chang 2000) (Almonacid et al. 2009). Moreover, the conserved C-terminal domain of Anillin binds RhoA, which has been implicated in several critical steps during cell division, including the positioning of the cleavage furrow (reviewed in (Piekny et al. 2005)). In fact, the expression of a dominant negative form of RhoA results in random spindle orientation in the chick neuroepithelium (Roszko et al. 2006). RhoA is linked to the contractile ring components Actin and myosin through its binding with Anillin (Piekny & Glotzer 2008). These data raise the possibility that Anillin, together with RhoA, may have a role in controlling cleavage plane orientation (reviewed in (Kosodo & Huttner 2009)). Anillin might also influence the orientation of cell division through regulation of midbody formation. A study in *C. elegans* has shown that during the first cell division, midbody remnants direct cell

division orientation *via* an indirect interaction with the polarity protein PAR-2 (Singh & Pohl 2014). Therefore in vertebrates, Anillin regulation of midbody inheritance and Par-2 distribution could potentially regulate orientation of cell division along the plane of the neuroepithelium. Whether these changes in division orientation play a direct instructive role on daughter cell fate remain unknown.

4. Interplay between Atoh7 and Anillin in influencing progenitors division

How does *atoh7* expression and function relate to the asymmetric expression of Anillin and daughter cell fate outcome? The presented results are in line with the hypothesis that Atoh7 directly represses *anillin* expression allowing for the cell cycle exit of the RGC. Analysis of the spatial-temporal and cellular Anillin-GFP distribution shows that *anillin* expression is restricted to cycling RPCs of the retinal neuroepithelium, before onset of neurogenesis and in the dividing sibling daughter upon asymmetric cell division of Atoh7-positive progenitors. Thus Anillin might be required in the dividing daughter for cell renewal and expansion of the *atoh7*-expressing progenitor pool. Consistently, the *anillin:Anillin-GFP* transgene is no longer expressed in the RGC daughter, suggesting that Anillin is not required in the post-mitotic RGC. *Atoh7* expression starts before the last mitotic division of the RGC progenitor (Poggi et al., 2005). Previous research in chick retina showed how the *atoh7*-expression increases during the temporal window of RGC genesis – a low level of Atoh7 initially allows for the expansion of RPC pools; later on, higher levels of ATOH7 protein up-regulate its own expression (Del Bene et al. 2007) to promote the transcription of genes involved in RGC differentiation (Matter-Sadzinski 2005) (Chiodini et al. 2013). The observed concomitant expression of *anillin* and *atoh7* in some RPCs suggests that high concentrations of Atoh7 are needed to down-regulate Anillin, further indicating that Atoh7 normally down-regulates

anillin only after mitosis in the RGC daughter. Accordingly, down-regulation of *anillin* leads to an increase of symmetric neurogenic division in which both daughter cells turn into RGCs, while in the *lakritz* mutant retina, such divisions give rise to two dividing RPC daughters (Jusuf et al. 2012).

Experimental procedures

1. Materials

a. Instrument

Instrument	Company
AccuJet Pro Pipetting Unit	Brand
Balance	Scaltec
Centrifuges 54130R, 5412C	Eppendorf
Centrifuge Mini	NeoLab
Confocal Laser Scanning Microscope TCS SP5	Leica
Confocal Laser Scanning Microscope TCS SPE	Leica
Digital Camera DFC 500	Leica
DNA Engine Dyad	BioRad
Electroporator GenePulser Xcell	BioRad
Electroporator MicroPulser	BioRad
Fluorescence Lamp XCite series	Olympus
Fluorescence Stereo Microscope MVX10	Olympus
Freezer Comfort (-20°C)	Liebherr
Freezer (-80°C)	Thermo Scientific
Fridge ProfiLine (4°C)	Liebherr
Geldetector	PeqLab
Geldetector printer P93	Mitsubishi
Gel electrophoresis chamber	PeqLab
Gel electrophoresis power supply Power Pac 300	BioRad
Incubator Rumed (28 °C; 32 °C)	Rubarth Apparate
Incubator (37 °C)	Binder
Shaking Bacterial Incubator (37 °C)	New Brunswick Scientific
Magnetic stirrer with heating plate	Heidolph
Mastercycler Pro	Eppendorf
Microwave	Sharp
Nanodrop Spectrophotometer ND-2000c	Nanodrop Technologies
pH-meter φ32	Beckmann

Thermal Cycler PTC-200 Multicycler DNA engine	MJ Research Peltier
Thermomixer compact	Eppendorf
Vortex (Genie, 2 Mixer)	Scientific Industries
Water bath WBT12	Medingen

b. Injection and transplantation material

i. Common

Needle puller: Sutter Instrument, Model P-97

Microinjector 5242 Eppendorf

InjectMan NI2 Eppendorf

Olympus Binocular SZX7, ACH1X

Grip head 0 for universal capillaryholder, Eppendorf

Universal capillaryholder, Eppendorf

O-rings, Eppendorf

Grip heads extraction tool, Eppendorf

ii. Injection material

Injection needles: Clark borosilicate glass capillaries with filament GC100F-10, Harvard Apparatus

Graticule S1 Stage MIC (10mm/0.1mm DIV), Pyser-SGI Limited

Petri Dishes (10 cm), Sarstedt

Microinjection 20 µL tips, Eppendorf

iii. Transplantation material

Transplantation set-up: CellTram Oil, eppendorf

Transplantation needles: Borosilicate Standard Wall without Filament Clark Capillary Glass, OD 1.0 mm, ID 0.58 mm, Harvard Apparatus,

Petri dishes (3 cm), Sarstedt

Filling tube with Luer Lock connection, female, Eppendorf

Disposable syringe with Luer Lock connection, male, Eppendorf

c. Chemicals

Chemicals were supplied by Sigma-Aldrich (Steinheim, Germany) and Merck (Darmstadt, Germany) and otherwise stated in the table below.

Chemicals	Providers
Agarose	Gibco
Ampicillin	Sigma
Bacto-agar	BD Bioscencies
Bacto-tryptone	BD Bioscencies
Bacto-yeast	BD Bioscencies
BSA	Fermentas
Chloramphenicol	Serva
Chlorophorm	Merck
D-Glucose	Sigma
4,6-diamidino-2-phenylindole (DAPI)	Sigma
Deoxynucleoside-5"-triphosphate (dNTPs) for PCR	Roche
DMSO (Dimethylsulfoxide)	Merck
EDTA	Sigma
Ethanol (70%)	Merck
Ethanol (100%)	Merck
Ethidium bromide	Sigma
Formamide	Sigma
Glycerol	J.T.Baker
Hydrogen peroxide	Sigma
Kanamycine Sulfate	Serva
L-Arabinose	Sigma
Lithium Chloride	Sigma
Methanol	Merck
MS222 (Tricaine methanesulfonate)	Sigma
Mineral Oil	Sigma
1-phenylazo-2-naphtol-6,8-disulfonic acid disodium	Sigma

salt (Orange G)	
Paraformaldehyde (PFA)	Sigma
pH-calibration solutions (pH9; pH9.5)	Buddeberg/VWR
Pronase	Roche
2-propanol	Merck
Proteinase K	Roche
PTU (0.0045% 1-phenyl-2-thiourea)	Sigma
Sodium acetate	Ambion
Sodium chloride	Merck
Sodium dodecyl sulfate	Sigma
Sodium hydroxyde	Merck
Tetracycline Hydrochloride	Calbiochem
Trypsin/EDTA (0.25%)	Life Technologies
TRIzol	Invitrogen
Triton-X-100 detergent	Sigma
Tween 20 detergent	Sigma

d. Media, solutions and buffers

Media were sterilized by autoclaving at 121°C for 20 minutes. Deionized water (dH2O, Millipore) was used for the preparation of the media and buffers.

Solutions	**Buffers Components**
Zebrafish fish medium	300 mg red sea salt H2O up to 1 L
Lysogeny broth (LB) medium	10 g Trypton Peptone 5 g Bacto-yeast extract 10 g NaCl H_2O up to 1L
LB plates	10 g Trypton Peptone

	5 g Bacto-yeast extract 10 g NaCl 15 g Agar-Agar H2O up to 1L
LB + Ampicillin medium	After LB autoclaving: 2 mL 500x Ampicillin (100 µg.mL^{-1} final concentration) pH 7.5
LB + Ampicillin plate	After cooling off to 50 °C: 2 mL 500x Ampicillin 100 µg.mL^{-1} final concentration
LB + Chloramphenicol (Cm)	Stock Cm: 34 mg.mL^{-1} in 100% ethanol After LB autoclaving: 1: 3000 dilution, final concentration 11.3 µg.mL^{-1}
LB + Chloramphenicol (Cm) and Tetracyclin (Tet)	Stock Cm: 34 mg.mL^{-1} in 100% ethanol Stock Tet: 10 mg.mL^{-1} in 50% ethanol /50% ddH2O (protect from light) 1:3000 dilution, final concentration 3.3 µg.mL^{-1}
LB + Chloramphenicol (Cm), Tetracyclin (Tet) and Ampicillin (Amp)	Stock Cm: mg.mL^{-1} in 100% ethanol Stock Tet: mg.mL^{-1} in 50% ethanol /50% ddH2O (protect from light) Stock Amp: 50 mg.mL^{-1} in ddH2O 1:3000 dilution, final concentration 16.7 µg.mL^{-1})
LB + Chloramphenicol (Cm), Tetracyclin (Tet) and Kanamycin (Kan)	Stock Cm: mg.mL^{-1} in 100% ethanol Stock Tet: mg.mL^{-1} in 50% ethanol /50% ddH2O (protect from light)

	Stock Kan: 50 mg.mL^{-1} in ddH2O 1:3000 dilution, final concentration 16.7 µg.mL^{-1}
LB recovery medium	2 ml 1M Glucose (9g D-glucose in 50ml of ddH_2O) in 98 ml of LB medium without antibiotics
1% Agarose for electrophoresis	1% Agarose (weight/volume) in 1x TAE buffer
1% Agarose for injection plates	1% Agarose (weight/volume) in H_2O
10% w/v arabinose	10g L-arabinose in 100 mL of ddH_2O
50x TAE	2 M Tris/ice cold acetic acid, pH 7.7 5 mM EDTA in H_2O
5x DNA Orange Loading Dye	50% (volume/volume) Glycerol 5x TAE-buffer 1% (weight/volume) Orange G.
6x DNA Blue Loading Dye	30% (volume/volume) glycerol 0.25% (weight/volume) bromophenol blue 0.25% (weight/volume) xylene cyanol FF
Fixing solution: 4% Paraformaldehyde	125 µL 16% Paraformaldehyde 375 µL PTW
In situ hybridization buffer	50% Formamide 750 mM NaCl 75 mM Na_3citrate 150 g.mL^{-1} Heparin 5 g.L^{-1} Torula RNA 0.1% Tween
Hepes (1 M, pH 7.3)	700 mL ddH_2O 238.3 g Hepes NaOH to pH 7.3
Morpholinos (GeneTools, LLC)	For 1mM stock solution: 300 nmol

	in 300 µL of H_2O
P1 buffer (Miniprep)	50 mM Tris 10 mM EDTA 100 µg.mL^{-1} RNase A pH 8.0
P2 buffer (Miniprep)	200 mM NaOH 1% SDS (weight/volume)
P3 buffer (Miniprep)	3 M Potassium acetate pH 5.5
PBS (Phosphate-buffered saline), 1x	137 mM NaCl 2.7 mM KCl 10 mM Na_2HPO_4 2 mM KH_2PO_4 pH 7.3
PTW	1x PBS 0.1% Tween-20
SSC 20x	3 M NaCl
	300 mM $Na_3CitrateX_2H_2O$
TAE buffer	40 mM Tris 1 mM EDTA 5 mM Acetic acid pH=7,8
TNT buffer	100 mM Tris 0.15 M NaCl, 0.2%Tween pH7.5
TNB buffer	2% DIG Blocking reagent in TNT buffer
Goat Serum (1 and 10%)	1% or 10% Donkey serum 0.8% TritonX-100 1X BSA

Buffers not specifically listed in the following table were prepared according to standard protocols (Sambrook et al. 1989).

e. Kits and *miscellaneous* materials

Material	Company
1 kb Ladder	Fermentas
1 kb plus Ladder	Fermentas
Ambion mMessage machine SP6/T3 Kit	Ambion
Digoxigenin RNA Labeling Mix	Roche
Fisher finest premium glass cover slips (24x60 mm and 22x22 mm)	Fisher Scientific
Fluorescein RNA Labeling Mix	Roche
Forceps (110 mm, straight)	NeoLab
HiPure Midi prep kit	Invitrogen
innuPREP PCRpure Kit	Analytik Jena
Microinjection tips Microloader	Eppendorf
Microscope glass slides (76x26 mm)	Menzel Glaeser
MinElute PCR Purification Kit	Qiagen
One step RT-PCR kit	Qiagen
Parafilm	Pechiney
PCR tubes (0.5 ml, thin walled)	Eppendorf
PCR tubes (0.2 ml, thin walled)	Eppendorf
Phusion High-Fidelity polymerase	Finnzymes
QIAfilter Plasmid Maxi Kit	Qiagen
QIAprep Spin Midiprep Kit	Qiagen
QIAprep Spin Miniprep Kit	Qiagen
QIAquick Gel Extraction Kit	Qiagen
QiaQuick nucleotide removal kit	Qiagen
QIaQuick PCR Purification Kit	Qiagen
RNAse Inhibitors	Invitrogen

RNA Loading Dye (2x)	Ambion
RNeasy Mini Kit	Qiagen
Safe-Lock Tubes 1.5 ml	Eppendorf
Safe-Lock Tubes 2.0 ml	Eppendorf
tRNA (yeast)	Sigma
TSA plus Fluorescein Kits	Perkin Elmer

f. Enzymes

Restriction enzymes were supplied either by MBI Fermentas (St.Leon-Roth, Germany) or *New England Biolabs* (Frankfurt, Germany). Protein kinase were purchased from Roche (Mannheim, Germany). Standard Taq DNA polymerase was provided by *New England Biolabs*, Phusion High-Fidelity DNA polymerase
Phusion was provided by Thermo Fisher Scientific (Karlsruhe, Germany), Axon Taq DNA Polymerase was provided by Axon Labortechnick (Kaiserslautern, Germany). RNA polymerases (T3 and T7) were purchased from Roche (Mannheim, Germany).

g. Antibodies

Antibodies	**Species**	**Dilution**	**Company**
anti-Zn8 (Zn5) (primary)	Mouse	1:300	Zebrafish International Resource Center
anti-Phospho Histone H3 (primary)	Rabbit	1:300	Millipore, 06-570
anti-Caspase 3 (primary)	Mouse	1:300	Abcam, ab13847

Secondary antibodies were goat or donkey anti-mouse or anti-rabbit IgG conjugated to Alexa Fluor 546, 647 or Cy5 fluorophores (1:500; Invitrogen).

h. Oligonucleotides

Primers were supplied either by Sigma-Aldrich or Eurofins MGW Operon as desalted or HLPC purified oligonucleotides.

i. Vectors

pCS2+:H2B-RFP (Jusuf et al. 2012), *pCS2+:lifeact-Venus* and *pDestTol2/CMVSP6:lifeact-Ruby* were used as templates for the mRNAs used in this study*; pCS2+:lifeact-Venus* (kindly provided by Prof. R. Köster) contains an *EcoRI/SalI*-flanked *lifeact* coding sequence from *lifeact-GFP* (Riedl et al. 2008) cloned in frame with a *Venus* sequence using *SalI*/*XbaI* restriction sites. *pDestTol2/CMVSP6:lifeact-Ruby* vector was generated by I. Weisswange through and LR reaction using *pDestTol2*, *CMVSP6*, *PolyA* and *lifeact-Ruby* and *attB* as cloning sites. This vector was kindly provided by Prof. J. Wittbrodt:

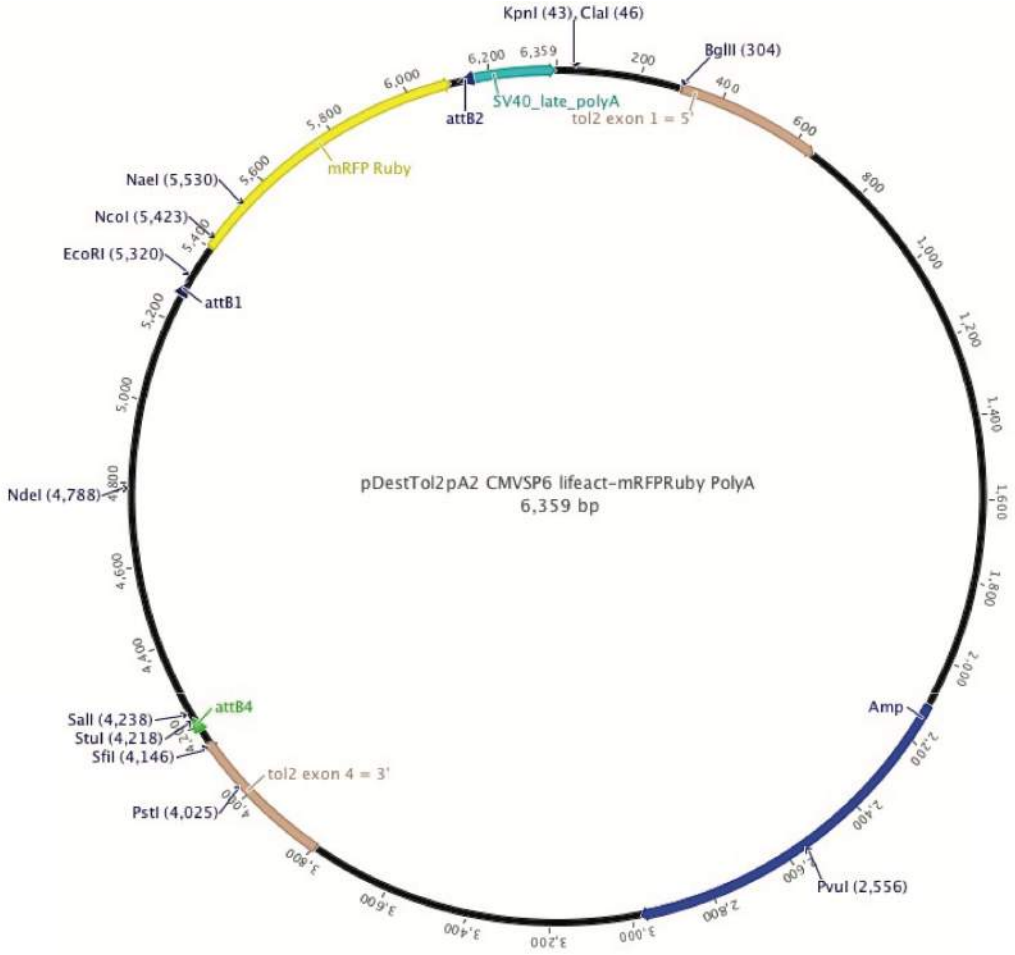

The previously homemade designed plasmid pBSKII-Atoh7-pA containing *atoh7* cDNA sequence was used for probe preparation:

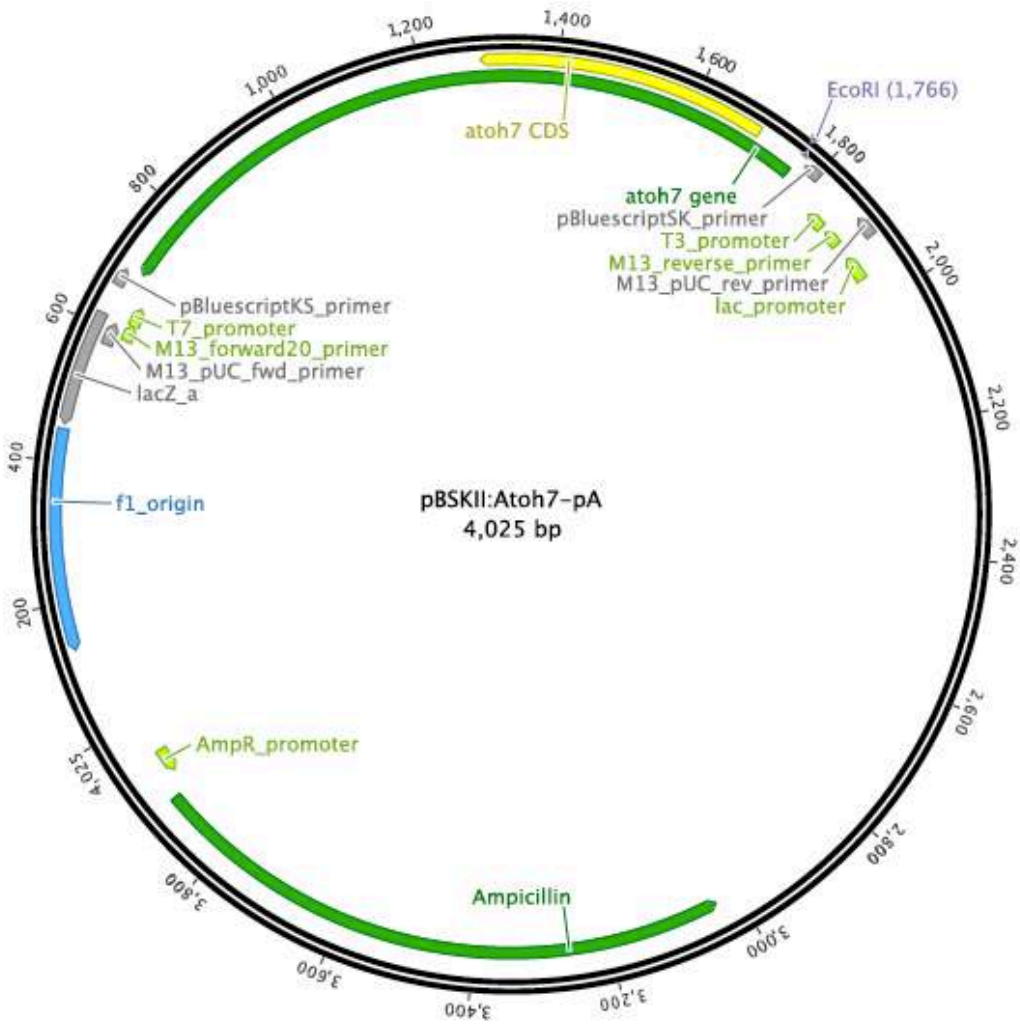

The *pCMVSPORT6.1-Anillin* vector was obtained from ImaGenes (IMAGE: 7063887; IRBOp991H0391D) and used for probe preparation.

The resistance of all the vectors listed so far is Ampicillin.

pRedET: Plasmid containing *red* functions, from Quick and Easy BAC recombination kit (GeneBridges), used for BAC recombineering. The resistance of this vector is Tetracyclin

j. Sanger sequencing

Sequencing of PCR products and plasmids was carried out by GATC Biotech AG (Konstanz, Germany) and Eurofins MWG Operon (Ebersberg, Germany).

k. Animals

i. Bacterial strains

The bacterial stains used in this study were *Escherichia coli* (*E.coli*) DH5# strains electro-competent (homemade) and Mach1-T1 chemically competent (homemade).

ii. Fish strains and ethics statements

Wild type WIK/AB and AB/AB were the strains used for zebrafish embryos, used and for medaka embryos, the Cab inbred wild-type strain was used.
Zebrafish (*Danio rerio*) breeding/raising was done following standard protocols. Adult fish were maintained at 26.5°C and embryos raised at 28.5°C or 32°C and staged as previously described (Kimmel et al. 1995). Fish were housed in the Fish facility of our German laboratory (built in accordance to Tierschutzgesetz 111, Abs. 1, Nr. 1 and with European Union animal welfare guidelines), which is under supervision of and in accordance with local animal welfare agencies. Embryos of either sex were used exclusively before freefeeding stages. Embryos used for whole-mount confocal imaging were treated with 0.0045% 1-phenyl-2-thiourea (Sigma) to delay pigment formation.

iii. Fish lines

Five transgenic lines were used in this study: *Tg(H2B:GFP)* (Köster & Fraser 2001); *Tg(atoh7:gap43-RFP)cu2*, a membrane tagged RFP under the control of *atoh7* promoter (Zolessi et al. 2006); *Tg(atoh7:GFP)rw021*, a cytoplasmic-GFP under the control of *atoh7* promoter (Masai 2003); *Tg(vsx2:GFP)*, a cytoplasmic-GFP under the control of *vsx2* promoter (Kimura 2006) (Vitorino et al. 2009); *Tg(5.5ptf1a:DsRed)ia6* (Jusuf et al., 2012), where a plasmid containing 5.5 kb of the 5' region of the *ptf1a* gene cloned upstream of *DsRed2* in pT2AL200R150G vector (Kawakami 2004) was generated and injected into wild type fish for making the line, provided by the Argenton research group (University of Padua, Italy). Double transgenic lines were generated *via* out-crossing.

2. Methods

a. Statistical validation and analysis

Statistical tests were performed using Microsoft Excel 14.0 and Prism 5.0 softwares, and $p < 0.05$ used as criterion level for significance. Tests used for Anillin knock-down experiments were: Unpaired homoscedastic two-tailed t-test (quantification of Atoh7:GFP positive cells, quantification of Ptf1a:dsRed positive cells, quantification of phosphohistone H3 (PH3) positive cells, velocity and position of the F-actin spot during progenitors cytokinesis, velocity of basal to apical nuclear migration, time the nuclei spent at the apical surface until anaphase, length of mitosis and cell cycle of retinal progenitors), two-tailed Chi-square test (orientation of cell division along apico-basal axis, inheritance of the F-actin apical accumulation), two-tailed Fisher's exact test (lineage studies), two-tailed Kolmogorov-Smirnov test (orientation of cell division along the planar axis). Unpaired homoscedastic two-tailed t-test was also used for assessing the significance of the correlation between orientation of cell division along the planar axis and fate of the two daughter cells.

The quantification of Ptf1a:dsRed positive cells was performed in the central retina where relatively mature neurons are present. The central retina region was delimitated by drawing a straight line through the center of the lens and two other lines forming a 45° angle around the first drawn line excluding the ciliary marginal zone as described previously (Holt et al. 1988). The quantification of Atoh7:GFP positive cells and PH3 positive cells was performed in all the retina. For each retina, a Z-projection of 14 µm corresponding to the centre of the retina was taken. Ratio of PH3 or Atoh7:GFP positive cells to the number of cells in each retina (DAPI staining) was assessed every 2 µm. We performed 8 countings (Z-stacks) per retina and average them. The same method was applied to calculate the ratio of PH3 to Atoh7:GFP positive cells.

b. Imaging

i. Mounting.

For live imaging, two to four dechorionated embryos were put into liquid agarose medium previously prepared and kept at 38°C. The mounting mix was containing the following:

Live imaging mounting mix	Amount
1% agarose (low-melting, diluted in Zebrafish fish medium)	800 µL
HEPES (pH 7.3)	100 µL
Tricaine 0.4%	100 µL

The anesthetized embryos were then transferred into a 35 mm Glass-bottom Microwell dish (P35G-1.5-10-C, MatTek) where they were embedded. Using femtoloader tips (Eppendorf) the embryos were carefully oriented until the agarose had polymerized completely. After allowing embryos to settle for at least two minutes and total solidification of the agarose, 3 mL of fish medium containing PTU and 100 µL of Tricaine 0.4% was added. For imaging of fixed whole-mount samples, embryos were mounted in 1% low-melting agarose (diluted in water).

ii. Image acquisition.

Photomicrography of whole-mount eyes or sections was performed with a laser scanning confocal microscope Leica SpE using a Leica 40X, 1.15 NA oil-immersion objectives and Leica Application Suite (LAS) software. Optical sections (<100 µm for fixed embryos) of 1 – 2 µm thickness were taken and Kalmann averaged 2 or 3 times (Jusuf et al., 2013). For confocal imaging, excitation was performed using the following laser lines:

Laser wavelength	Fluorophore excitation
405 nm	DAPI
488 nm	eGFP, FITC, Venus
561 nm	RFP, dsRed, Ruby, Alexa Fluor 546, Cy3
635 nm	Cy5

All the images were processed and analyzed using Fiji (NIH, USA) and Volocity Analysis version 5.3 (PerkinElmer). Brightness and contrast were adjusted with Fiji and Adobe Photoshop CS4.

iii. Time-lapse processing

Time-lapses were performed with a laser scanning confocal microscope Leica Sp5 using a Leica 63X, 1.2 NA water-immersion objectives and a Leica Application Suite (LAS) software. Images were taken every 5 minutes for 20 to 30 hours. Optical sections of 1 µm thickness were taken. Motorised XY stage was used to image multiple embryos. Laser power was minimised to avoid bleaching and phototoxicity. All the time-lapses were post-elaborated using Volocity 5.3 (PerkinElmer), Fiji and Adobe Photoshop CS3-Extended. The 3D reconstructions in Fig. 16 D, D' were done using Fiji software (3D projection) and applying the Gaussian 3D blur filter.

1. Cell tracking. All cell tracking were performed manually, using the Volocity classification module (PerkinElmer). For the assessment of daughter cell fate shown in Figure 16 A, 16 B, 14 B-E mosaic clones were randomly selected and cell fate tracked manually in 4D (timeframes and Z-positions). For divisions in Figure 14 B-E, RGCs or Atoh7-GFP positive cells were tracked back in time to assess the fate of the siblings. For nuclei tracking in Figure_19 A-B, clones were randomly selected. For cell cycle length quantification shown in Figure 19 E-F, randomly selected progenitor were tracked during the period in between two consecutive divisions. For the assessment of F-actin and Anillin apical inheritance in relation to cell fate in Figure 16A and 16B, each sibling cell has been tracked forward in time after division. In all cases, assignment of RGC identity was given based on

the observation of retraction of the basal process and cell body migration towards the basal surface (Poggi et al., 2005) (Zolessi et al. 2006). A dividing progenitor would always migrate back to the apical surface, round up and divide within the next 5 to 10 minutes. In the single case of the photoreceptor cell, a division and rounding up did not follow migration towards the apical side.

2. F-actin and nuclear velocity of migration. The velocity of the F-actin spot basal-to-apical migration was assessed as follow: the coordinates (X, Y, Z) of the spot at its initial appearance in the basal process and its appearance at the apical most surface at cytokinesis completion were recorded and the distance covered was calculated using these two measured points. The ratio of the distance covered to the time the spot spent to perform the translocation was calculated to obtain the velocity of the F-actin spot. The velocity of the nucleus basal to apical migration was assessed by recording the coordinates of the center of the nucleus as it starts moving from its basal location until migration stops at the apical surface of neuroepithelium. The ratio of the distance covered to the time the nucleus spent to perform the translocation was calculated to obtain the velocity of the nucleus itself.
3. Mitosis Length. I consider the starting of mitosis the moment when the chromosomes condensate (Prophase), which is visible thanks to H2B:RFP highlighting the nucleus as it forms a round shape. I consider the end of mitosis the moment the F-actin spot reaches the apical most surface (end of cytokinesis). I then measured the time the progenitor needed to go from Prophase to the end of cytokinesis.
4. Cell division orientation. The assessment of cell division orientation along the apical-basal (planar *vs.* oblique) and the planar (circumferential *vs.* radial) was performed as described in (Das et al. 2003) using orthogonal projections with Fiji software (NIH, USA). Through a Fiji plugin the angle between three points were measured. These three points were assigned as following: the best orthogonal projection (xy, xz or yz) where two nuclei right after division could

be clearly distinguished from time-lapse series was selected. I then identified the midpoint of the "spindle axis" of the two nuclei right after division and trace a line from this point to the center of the lens. In the center of the lens the first point was assigned. The second and the third point in the middle of the two nuclei respectively were thereafter added. The employed plugin then calculated the angle between the imaginary line traced from the spindle axis midpoint to the center of the lens and the imaginary line traced between the second and the third point. The value of the angle finally depends on the orthogonal plane I used to calculate it: an orientation of 0° would be measured for a division which can be perfectly seen on a single stack of an xz orthogonal projection and 90° a division which can be perfectly seen on a single stack of an xy orthogonal projection.

c. Experimental methodology

i. RNA extraction and cDNA preparation.

Embryos of specific stages were instantly frozen in 1 ml of TRIzol reagent (Invitrogen)_using liquid nitrogen. Tissue homogenization was performed mechanically by grinding_the embryos in TRIzol with plastic pestles. Grinded tissues were then incubated for 5_minutes at room temperature. After addition of 200 µL Chloroform, the mix was_shaken rigorously for 15 seconds and incubated for 3 minutes at room temperature. The mix was then centrifuged at 10,000 rpm for 15 minutes at 4°C. The upper phase, containing the RNA, was transferred into a new tube, mixed with 500 µL of isopropanol and incubated for 10 minutes at room temperature. The RNA pellet was obtained by centrifugation at 10,000 rpm for 10 minutes at 4°C, washed with 70% Ethanol and centrifuged for 5 more minutes at 8,000 rpm at 4°C. The pellet was then dried at room temperature for 5 minutes and re-suspended in 20 µL RNase free water by carefully pipetting up and down few times. The solution was incubated for 5-10 minutes at 57,5°C in case the re-suspension of the pellet would not have

been complete. The concentration of the total RNA was determined using a Spectrophotometer (NanoDrop 2000, Thermo Scientific). Before performing the reverse transcription, all traces of genomic DNA were removed using DNase I (2 U.μl^{-1}, Ambion) according to the manufacturer's protocol. Reverse transcription to generate full-length cDNA and PCR reaction directly on that was performed using the one step RT-PCR Qiagen kit following the users instruction manual.

ii. Genomic DNA extraction.

Plasmid DNA was isolated from bacterial cultures based on the alkali-lysis method (Sambrook et al. 1989). Single bacterial colonies were picked and used to inoculate 5 mL LB medium containing the appropriate antibiotic(s). Suspended cultures were grown for at least 8 hours at 37°C and harvested by centrifugation (15 minutes at 14,500 rpm). Pellets were re- suspended in 300 µL of cold P1 buffer, lysed by adding 300 µL of room temperature P2 buffer and incubated in additionally added 300 µL of P3 buffer. Lysed bacterias were then centrifuged for 10 minutes at 13,000 rpm and supernatants transferred into new tubes. Plasmid DNA was precipitated by adding 500 µL Isopropanol, incubated for 15 minutes at room temperature, followed by a centrifugation for 10 minutes at maximum speed. After washing with 500 µL of 70% Ethanol and centrifuging for 3 minutes, the pellet was dried and re-suspended in 30 µL of ultrapure H2O. DNA concentrations were measure by photometric measurement at OD260 using a Spectrophotometer (NanoDrop 2000, Thermo Scientific). For higher yield of plasmid DNA, bigger bacterial cultures were set up. Single colonies were picked and inoculated in 5 mL of LB medium containing the appropriate antibiotic(s). Suspended cultures were grown for 8 hours at 37°C. 1 mL of the suspended cultures were inoculated into liquid cultures of 200 mL of LB medium supplemented with the appropriate antibiotic(s), which were put to grow over night at 37°C. The bacterial pellet was then obtained by centrifugation (30 minutes, 4,000 rpm at 4°C). The plasmid DNA was purified using the QIAgen Midiprep Kit (QIAgen) following the manufacturer's instructions. DNA pellet was resolved in 100 µL of ultrapure

H2O and the concentration was measured using a Spectrophotometer (NanoDrop 2000, Thermo Scientific).

iii. DNA amplification by polymerase chain reaction (PCR).

Most polymerase chain reactions (PCRs) were performed using Phusion polymerase with proofreading activity (*New England Biolabs*) with the exception of *lakritz* mutant genotyping for which a separate protocol was followed (see below). The amplification of sequences of interest was achieved using either zebrafish genomic DNA, IMAGE clones (BioScience UK limited), plasmid contructs provided from other laboratories or total cDNA from zebrafish embryos or medaka embryos as PCR templates. To every reaction, the annealing temperature was adjusted according to the used primers and the elongation time according to the size of the fragments of interest. All PCRs were performed in a MJ Research and Mastercycler pro (Eppendorf) Thermocycler. Conditions used are listed in the tables below:

PCR components	Amount
DNA template (10 – 50 ng.µL^{-1} plasmid; 100 ng.µL^{-1} genomic DNA)	x µL
Buffer (HF, 5x)	1x
dNTPs (2.5 mM)	200 µM
Primers (10 µM)	0.5 µM each
Polymerase (Phusion)	0.02 U.µL^{-1}

PCR reaction	Cycles	Temperature	Time
Initial denaturation	1	98°C	30 seconds
Denaturation	25-38	98°C	30 seconds
Annealing	25-38	Tm – 3°C	x seconds
Extention	25-38	72°C	30 seconds / kb
Final extention	1	72°C	5 - 10 minutes

Quality, and size of the amplified DNA products were monitored by agarose gel electrophoresis. If the amplification reaction generated an expected

single band at the right size, the DNA was then purified using a PCR purification kit (QIAgen). If multiple bands could be obtained out of the PCR reaction, the band with the expected size was then cut from an agarose gel and gel purified.

iv. DNA purification after PCR amplification and/or enzymatic manipulation.

Purification of PCR products and other DNA fragments was performed using the QIAquick PCR Purification Kit (Qiagen) as described in the users instruction manual. To 1 volume of reaction mix, 5 volumes of supplied PB buffer were added, applied to a purification column and centrifuged for 1 minute at 13.000 rpm. The flow-through was discarded and the column washed with 750 µL of supplied PE buffer. After centrifugation (1 minute, 13.000 rpm) the flow-through was discarded and the column was centrifuged for an additional 2 minutes at 13.000 rpm, eliminating residual ethanol content. The column was then transferred into a new collecting tube where the DNA was eluted with an appropriate volume of sterile water.

v. Restriction digest of DNA.

Digestion of DNA was achieved using restriction endonucleases enzymes according to supplier's instructions. Generally, DNA was digested with the appropriate restriction enzymes and buffers at a concentration of 10 U of enzyme per µg of DNA, taking care that the total amount of enzyme wouldn't have overcome the 10% of the total preparation, because of the presence of glycerol in the enzyme stock solution. All digestions were carried out in a 37°C incubator or thermal block at the recommended temperature for the respective restriction enzyme for minimum 2 hours. Double digests were performed in a suitable buffer according to the manufacturer's specifications.

vi. Agarose gel electrophoresis.

Agarose gel electrophoresis was performed to separate DNA fragments, to check the quality and size of PCR products and DNA fragments

after restriction digestions. Generally, 1% agarose gels in TAE buffer were used to separate fragments of a size between 1-10 kb, 1.5% agarose gels for DNA smaller than 1 kb and 0.8% agarose gels for fragments bigger than 10 kb. Electrophoresis was carried out in TAE buffer with an electrical potential difference of 90 to 120V. Before loading onto the gel, DNA samples were mixed with Orange G loading dye. Based on the size of the considered fragment, the appropriate DNA-ladder (0,1µg.µl^{-1}, Fermentas) was used as reference for size and estimation the samples DNA yield. After running the gel, DNA bands were stained for 25 minutes in an aqueous TAE ethidium bromide solution (2 µg.mL^{-1}), which intercalates with DNA making it visible upon ultraviolet (UV) irradiation. Using an UV trans-illuminator and gels were imaged in a gel analysis chamber (Bioblock Scientific) connected with a CCD camera and a printer (Sony UP – 890CE) for documentation.

vii. Gel extraction.

Expected DNA bands were cut out the gel with a sharp scalpel, weighed and extracted from the gels using the QIAquick Gel Extraction Kit (Qiagen) following the users manual instructions. Three volumes of QG Buffer were added to 1 volume of gel weight and incubated at 50°C for an average of 10 minutes until the gel was completely dissolved. Isopropanol (1 volume) was added and mixed by inverting the tube several times. The sample was applied to a MinElute Column and centrifuged for 1 minute at 13.000 rpm. The supernatant was discarded, and the column washed with 500 µL of Buffer QG and 750 µL of Buffer PE with intermediate centrifugation steps for 1 minute at 13.000 rpm. The flow-through was then discarded and the tube was centrifuged for one more minute. Finally, the DNA was eluted with 20-50 µL of water and the concentration obtained was measured by spectrophotometer (NanoDrop 2000, Thermo Scientific).

viii. Transformation of *E.coli* Mach1-T1 chemically competent cells.

Plasmids were transformed into homemade (*E.coli* MachT1) competent cells. 50 µL of competent cells were thawed on ice and mixed with 2.5 – 10 ng of plasmid DNA. Cells were then incubated with the plasmid

for 5 minutes on ice, heat shocked at 42°C for 90 seconds and immediately incubated back on ice for 1 minute. 500 µL of LB medium was then added to the mix, after which it was incubated for 45 minutes to one hour in a 37ºC shaker. The transformed cells were finally plated on selective LB-agar plates containing the appropriate antibiotic(s) and incubated at 37°C over night. Single colonies were then picked for inoculation in selective LB medium for plasmid preparation.

ix. Transformation of DH5α strains electro-competent cells.

Homemade electro-competent cells (*E.coli* DH5α) were used. Generally 40 µL cells were transformed with 4 µL of a ligation mix or 2.5 – 10 ng plasmid DNA. Electroporation was performed in pre-cooled cuvettes at 1800V using a MicroPulser (BioRad). The transformed cells were immediately incubated in 500 µL LB medium and placed to shake at 37ºC for 1 hour. The cells were then plated on LB plates containing the correct antibiotic(s) for selection. After incubation over night at 37 ºC, grown colonies were picked for inoculation in selective LB medium for plasmid preparation.

x. *Lakritz* mutant genotyping.

Heterozygote *lakritz* carrier fish were identified by genotyping. After anesthetizing the fish in fish water containing 0.12% of Tricaine solution, part of the caudal fin was cut off using sterile scissors. The fish was then returned into a separate mouse cage until the genotyping results were obtained. The cut tissue was placed in an empty sterile 1.5 mL Epperdorf tube containing 100 µL of the following DNA extraction mix:

DNA extraction mix (Total 50 mL)	**Amount**
Tris pH 8.0 (2 M)	10 mL
EDTA pH 8.0 (0.5 M)	0.5 mL
NaCl (5 M)	1.5 mL
20% SDS	0.25 mL

H2O ultrapure	37.75 mL

1 mg/ml of Proteinase K was added and the cut tissue was incubated in the DNA extraction mix over night at 65°C. The morning after, 200 µL of ultrapure H2O was added to the mix which was inverted several times. The Proteinase K was then heat-inactivated for 10 minutes at 90°C. Using 2 µL of the obtained extracted DNA, the following subsequent PCR and restriction digestion reaction were set up:

PCR components (Total 50 µL)	**Amount**
DNA mix	2 µL
Buffer (F101, 10x)	3 µL
$MgCl_2$ (25mM)	0.75 µL
DMSO	0.5 µL
dNTPs (2.5 mM)	0.5 µL
Primer forward (10 µM): 5'-CCGGAATTACATCCCAAGAAC-3'	0.5 µL
Primer reverse (10 µM): 5'-GGCCATGATGAGCTCAGAG-3'	0.5 µL
Taq Polymerase (Axon)	0.25 µL
H_2O	22 µL

PCR reaction	**Cycles**	**Temperature**	**Time**
Initial denaturation	1	95°C	5 minutes
Denaturation	37	95°C	45 seconds
Annealing	37	56°C	45 seconds
Extention	37	72°C	45 seconds
Final extention	1	72°C	5 minutes

Restriction digestion reaction (Total 35 mL)	**Amount**
DNA (from the previous PCR reaction)	30 µL
StuI (Fermentas)	0.3 µL

Buffer B (SureCut)	3.5 µL
H_2O	1.2 µL

Digestion was performed for 3 hours at 37°, after which 30 µL of digested DNA was loaded on a 2% agarose gel for migration. Homozygote mutant DNA remains uncut, generating a band of 293 bp, while wild type DNA digestion generates two bands. Carrier fish's DNA, heterozygote for the mutation, can be identified by the presence of all the three bands. The carrier fish identified were then put back into the glass system for recovery and set up for crosses only 2 or more weeks after the procedure.

xi. BAC engineering

For BAC manipulation, bacteria containing a BAC clone spanning the *anillin* genomic locus (ANL-BAC / CH211-197N10, BACPAC Resources Center) were used. Transformation through electroporation of the pRedET plasmid was performed as described in (Bussmann & Schulte-Merker 2011). The BAC clone was inoculated in 1 mL of LB containing Cm for over night growth at 37°C. 40 µl of the o/n culture was transferred to 2 ml of fresh LB medium containing Cm and cultured for 3 hrs at 37°C. The o/n culture was also used to generate a glycerol stock: 500 µL of 50% glycerol were added to 500 µL of bacterial culture, transferred to a sterile tube and stored at -80°C.
The 2 mL culture was transferred to a 2 mL microcentrifuge tube and spinned down at 11000 rpm for 30 seconds. The supernatant was removed and a 1ml of icecold ddH2O was added. The bacteria was resuspended by pipetting up and down twice and everything was spinned down at 11000 rpm for 5 min. This step was repeated one more time. After the last centrifugation, about 50 µl was kept of the resuspension and 1 µl of 10 ng/µl pRedET plasmid was added. Everything was transferred to a pre-chilled 1 mm electroporation cuvette on ice and electroporated using standard *E.coli* settings (1800 V, 25 µF, 200 Ω, time constant of 4.8-5.2 ms). 1 ml of LB medium without antibiotics and containing 20mM D-glucose was quickly added. Everything was transferred to a fresh culture tube and culture at 37°C for 60 minutes. The cells were plated on LB plates containing Cm and

Tet and incubate at 30°C o/n. A single colony was picked up and transferred to fresh LB medium containing Cm and Tet and incubated at 30°C o/n (max. 16 hr). For Tol2 transposon-mediated BAC transgenesis, the iTol2-amp cassette (Bussmann & Schulte-Merker 2011) was amplified by PCR with the primer pair pTarBAC_HA1_iTol2_fw (5'- gcg taa gcg ggg cac att tca tta cct ctt tct ccg cac ccg aca tag atC CCT GCT CGA GCC GGG CCC AAG TG – 3') and pTarBAC_HA1_iTol2_rev (5' – gcg ggg cat gac tat tgg cgc gcc gga tcg atc ctt aat taa gtc tac taA TTA TGA TCC TCT AGA TCA GCT C – 3'), where the lower and upper cases indicate the pTarBAC2.1 sequences for homologous recombination and the iTol2-amp annealing sequences, respectively. The following PCR reaction were set up:

PCR components (Total 100 µL)	Amount
Plasmid template (5ng.µl^{-1})	1 µl
Phusion HF Buffer (5x)	20 µl
dNTPs (10 mM)	2 µl
Primer forward (10 µM)	2.5 µl
Primer reverse (10 µM)	2.5 µl
Phusion DNA polymerase	1 µl
ddH2O	71 µl

PCR reaction	Cycles	Temperature	Time
Initial denaturation	1	98°C	30 seconds
Denaturation	30	98°C	10 seconds
Annealing	30	58°C	20 seconds
Extension	30	72°C	1 minute
Final extension	1	72°C	5 minutes

1 µl Orange G loading buffer was added to 3 µl of PCR product and loaded on a 1% agarose gel and the proper migration of the iTol2_amp_iTol2 construct was checked (1516 bp)

2 µl (20 units) of DpnI were directly added to the PCR reactions and incubated at 37°C o/n. 5 µl 5M LiCl and 300 µl 100% ethanol were added at the reaction, which was incubated at -20°C for 30 minute and spinned down at maximal speed for 30 min at 4°C. The supernatant was discarded, the pellet washed with 70% ethanol and spinned down for 5 minutes at 4°C. The supernatant was discarded and the pellet was dryied at room temperature for 5-10 minutes and resuspended in 21 µl ddH2O. 1 µl was used to measure the DNA concentration. ddH2O was then added to a final concentration of 500 ng/µl.

Subsequently, the amplified iTol2-amp cassette was introduced into the backbone (pTarBAC2.1) of the ANLN-BAC. 150 µl of the Anln-BAC-pRedET o/n culture was transferred to a culture tube containing 1.8 ml of fresh LB medium with Cm and Tet and cultured for 2.5 hrs at 30°C. 67 µl 10% of w/v L-(+) Arabinose were added to the suspension and cultured for 1 hr at 37oC. The o/n culture was also used to generate a glycerol stock: 500 µL of 50% glycerol were added to 500 µL of bacterial culture, transferred to a sterile tube and stored at -80°C.

The 2 mL culture was transferred to a 2 mL microcentrifuge tube and spinned down at 11000 rpm for 30 seconds. The supernatant was removed and a 1ml of icecold ddH2O was added. The bacteria was resuspend by pipetting up and down twice and everything was spinned down at 11000 rpm for 5 min. This step was repeated one more time. After the last centrifugation, about 50 µl was left and 1 µl of 500ng/µl iTol2 amp targeting PCR product was added. The suspension was transferred to a 1mm electroporation cuvette and electroporated as previously indicated. 1 ml of LB medium without antibiotics and containing 20mM D-(+)-glucose was added to the electroporated bacteria and incubated at 37°C for 45 min. The cells were plated on LB plates containing Cm, Tet and Amp and incubated at 30°C o/n.

To confirm the iTol2 insertions, 5 single colonies were picked and resuspended in 50 µl ddH2O. 1 µl was used for PCR to identify BACs containing the correct iTol2 insertions. Per colony, 2 PCR reactions were performed, one for each homology arm with the following primer pairs:

pTarBAC_HA1_control_fw (5' – CTG TCA AAC ATG AGA ATT GGT C - 3') and amp_HA1_control_rev (5' – ACA TTT CCC CGA AAA GTG G - 3'); amp_HA2_control_fw (5' – CTG AGA TAG GTG CCT CAC TG - 3') and pTarBAC_HA2_control_rev (5' – GAG AGC CTT CAA CCC AGT C - 3'). The following PCR reaction were set up:

PCR components (Total 18 µL)	**Amount**
Suspended bacterial colony	1 µl
10x PCR buffer	2 µl
dNTPs (10 mM)	0.4 µl
Primer forward (10 µM)	0.4 µl
Primer reverse (10 µM)	0.4 µl
Taq polymerase	0.1 µl
ddH_2O	13.7 µl

PCR Reaction	**Cycles**	**Temperature**	**Time**
Initial denaturatio	1	95°C	5 minutes
Denaturation	30	94°C	30 seconds
Annealing	30	58°C	30 seconds
Extension	30	72°C	30 seconds
Final extension	1	72°C	5 minutes

5 µl of Orange G loading dye were added to the reaction and loaded on a 2% Agarose gel. The gel was run and carefully checked if product sizes were as predicted (pTarBAC_HA1_control_fw + amp_HA1_control_rev: 405 bp; pTarBAC_HA2_control_rev + amp_HA2_control_fw: 317 bp). Only colonies in which both arms are correctly integrated can be used. All the remaining suspended bacterial colony were added to 1 ml of LBmedium containing Cm, Tet and Amp and cultured o/n at 30°C (max. 16 hrs).

In order to obtain a C-terminal fusion of the eGFP protein to the Anillin protein, the *pGFPFRT-Kan-FRT* cassette (Abe et al. 2011) was amplified by PCR from the plasmid pBSK--*eGFP-pAFRT-Kan-FRT* using the primer pair ANL_StopMut_linker_GFP_fw (5' – tgg tgg acc tgc gca tgt ggc agc

cgg att cct gct aca gac cca tgt cag gtg gat ctg gtg gaa gcG CCA CCA TGG TGA GCA AGG GCG AGG AGC TG – 3') and ANL_frt_kan_frt_rev (5' - ctg tga tgc cgc att gca ctt cca aat cag aca tat agt cag tgt aaa agC CGC GTG TAG GCT GGA GCT GCT TC – 3') where the lower and upper cases indicate the CH211-197N10 sequences for homologous recombination and the *pGFP-FRT-Kan-FRT* annealing sequences, respectively; the underlined sequence in the ANL_StopMut_linker_GFP_fw primer codes for a linker peptide following a mutated stop codon. The following PCR reaction were set up:

PCR components (Total 100 µL)	Amount
Plasmid template (10ng.µl^{-1})	1 µl
Phusion HF Buffer (5x)	20 µl
dNTPs (10 mM)	2 µl
Primer forward (50 µM)	2 µl
Primer reverse (50 µM)	2 µl
Phusion DNA polymerase	1 µl
DMSO	3 µl
ddH2O	69 µl

PCR Reaction	Cycles	Temperature	Time
Initial denaturatio	1	94°C	2 minutes
Denaturation	5	94°C	30 seconds
Annealing	5	50°C	30 seconds
Extension	5	72°C	160 seconds
Denaturation	35	94°C	30 seconds
Annealing	35	58°C	30 seconds
Extension	35	72°C	160 seconds
Final extension	1	72°C	5 minutes

1 µl Orange G loading buffer was added to 3 µl of PCR product and loaded on a 1% agarose gel and the proper migration of the *pGFP-FRT-Kan-FRT*

cassette was checked (≈ 2500 bp). 2 µl (20 units) of DpnI were directly added to the PCR reactions and incubated at 37°C o/n. The purification steps are the same indicated for iTol2_amp_iTol2. After purification, ddH2O was then added to a final concentration of 500 ng/µl.

Subsequently, the amplified *pGFP-FRT-Kan-FRT* cassette was introduced into the backbone (pTarBAC2.1-iTol2-amp) of the ANLN-BAC. 150 µl of the Anln-BAC-iTol2-Amp o/n culture was transferred to a culture tube containing 1.8 ml of fresh LB medium with Cm, Tet and Amp and cultured for 2.5 hrs at 30°C. 67 µl 10% of w/v L-(+) Arabinose were added to the suspension and cultured for 1 hr at 37°C. The o/n culture was also used to generate a glycerol stock: 500 µL of 50% glycerol were added to 500 µL of bacterial culture, transferred to a sterile tube and stored at -80°C.
The 2 mL culture was transferred to a 2 mL microcentrifuge tube and spinned down at 11000 rpm for 30 seconds. The supernatant was removed and a 1ml of icecold ddH2O was added. The bacteria was resuspend by pipetting up and down twice and everything was spinned down at 11000 rpm for 5 min. This step was repeated one more time. After the last centrifugation, about 50 µl was left and 1 µl of 500ng/µl *pGFP-FRT-Kan-FRT* targeting PCR product was added. The suspension was transferred to a 1mm electroporation cuvette and electroporated as previously indicated. 1 ml of LB medium without antibiotics and containing 20mM D-(+)-glucose was added to the electroporated bacteria and incubated at 37°C for 45 min. The cells were plated on LB plates containing Cm, Amp and Kan and incubated at 37°C o/n.

5 single colonies were picked and resuspended in 50 µl ddH2O. 1 µl of the suspension was taken for, PCR to identify BACs containing the correct *pGFP-FRT-Kan-FRT* insertions. A pair of primer targeting around the integration site at the 3' of Anillin coding sequence were designed: Forward (5' - TTG ACA TCG GTC AAA ATT CG - 3'), Reverse (5' - AAG TAA GAG CCC GTC AGC AA - 3'). The PCR reaction conditions were the same indicated for the confirmation of iTol2-amp insertion. 5 µl of Orange G loading dye were added to the reaction and loaded on a 2% Agarose gel. The gel was run and carefully checked if product sizes were as predicted (≈ 2500 bp). All the

remaining suspended bacterial of the positive colony was added to 1 ml of LB medium containing Cm, Amp and Kan and cultured for 4-5hrs at 37°C. The suspension was then transferred in 100 ml of LB medium containing Cm, Amp and Kan and culture o/n at 37°C (max. 16 hrs). 500 µL of the o/n culture was used to generate a glycerol stock: 500 µL of 50% glycerol were added to 500 µL of bacterial culture, transferred to a sterile tube and stored at -80°C.

The BAC DNA preparation was done using the HiPure Midiprep kit (Invitrogen), with modifications for BAC DNA isolation as described by the manufacturer.

xii. Riboprobe preparation

Atoh7 probe was generated as described previously (Jusuf et al. 2012). *Anillin* antisense probe was generated from a zebrafish IMAGE clone (IMAGE: 7063887; IRBOp991H0391D, source ImaGenes) where *anillin* full-length coding sequence was cloned into *pCMVSPORT6.1* vector, which was linearized with *RsrII* (New England Biolabs) and transcribed with T7 Polymerase. *Cxcr4b* antisense probe was generated from30 hpf zebrafish embryos after total mRNA extraction. A region of *cxcr4b* coding region was amplified using the following primers forward (5' – ACT CCG GTT CTG GGG ACT AT - 3') and reverse: 5'- CCA AGC TTC att aac cct cac taa agg gag aCA GCA TAG TCA AAG CGT CCA - 3' (containing the recognition site of the T3 Polymerase indicated in lower-case letters). The generated PCR product was then used for *cxcr4b* antisense probe synthesis. Adding the components in this specific order, the riboprobes were synthesized:

Transcription mix	**Amount**
Linearized or PCR DNA template (1 µg. µL^{-1})	1 µL
DTT (100 mM)	2 µL
NTP-mix (much A, C, G, few U)	1.3 µL
10 mM Dig-UTP (*anillin*) or Fluorescein-UTP (*cxcr4b, atoh7*)	0.7 µL
RNAguard	0.5 µL

10x Transcription buffer	2 µL
RNA polymerase T7 (*anillin*) or T3 (*cxcr4b, atoh7*)	2 µL
H2O (RNase free, Sigma)	10.5 µL

The transcription mix was incubated for 3 hours at 37°C. DNAse treatment was then performed, adding 1 µL of TURBO DNAse (Ambion) and incubating the reaction for 15 minutes at 37°C. Using the Qiagen RNEasy kit (Qiagen), riboprobes were purified and elution was done in RNAse free water (Sigma). For quality and synthesis control, 2 µL of riboprobe was run in a 1% agarose gel after denaturation at 80°C for 10 minutes. The purified and eluted riboprobe was finally supplemented with 100 µL of hybridization mix and stored at -20°C.

xiii. mRNA *in vitro* synthesis

pCS2+:H2B-RFP and *pCS2+:lifeact-Venus* were linearized with *NotI*, *pDestTol2/CMVSP6:lifeact-Ruby* was linearized with *KpnI*. *Tol2* transposase mRNA was prepared from *Xba*I-linearized *pDB600* (Balciunas et al. 2006). The linearized vectors were purified using the QIAquick PCR Purification Kit (Qiagen). All the mRNA were *in vitro* synthesized using the Sp6 (*pCS2+:H2B-RFP, pCS2+:lifeact-Venus* and *pDestTol2/CMVSP6:lifeact-Ruby*) and the T3 (*pDB600*) mMessage mMachine kit (Ambion). The reaction components were added in the following order:

Transcription mix	**Amount**
Nuclease-free Water	5 µL
NTP/CAP (2X)	10 µL
Reaction Buffer (10X)	2 µL
Linear template DNA (1 µg. μL^{-1})	1 µL
Enzyme Mix (Sp6 or T3 RNA Polymerase)	2 µL

The reaction was incubated at 37°C for 2 hours. 1 µL of TURBO DNase was added and the reaction incubated for 15 minutes at 37°C. The mRNA was

purified using the RNeasy purification kit (Qiagen), and the pre-DNase mRNA together with the final purified product were run in 1% Agarose gel to test the quality and the efficacy of the DNase treatment. The purified mRNA was diluted to a final concentration of 100 ng/µl.

xiv. Efficiency test of the Anillin Splicing Morpholino

The efficiency of the SpMO was tested by carrying out RT-PCR reactions on total RNA (OneStep RTPCR Kit, Qiagen, manufacture instructions were followed) extracted from zebrafish embryos at the stages of interest. PCR primers used were: Forward 1 (5' - CGT GGC GAG TGT GTG TAT GT - 3'), targeting inside the *anillin* exon 1; Forward 2 (5' - GGT TTG GGA ACC CCT GTT AT - 3'), targeting inside the *anillin* intron 1; Forward 3 (5' - ACA ATG ATA GGG TCG CTT GG - 3', targeting inside the anillin intron 1; Reverse 1-2-3 (5' - CTC TCC GCC ATC TTC TTC TG - 3'), targeting inside the exon 2. As housekeeping gene, *ef1α* was used with the following primer: Forward (5' – CAT ACA TCA AGA AGA TCG GCT ACA ACC – 3'), Reverse (5' – GTA GTA CCG CTA GCA TTA CCC TCC TTG – 3') .The following RT-PCR reaction and condition were set up:

RT-PCR components (Total 25 µL)	**Amount**
RNA template (40ng.µl^{-1})	1 µl
Q Buffer (5x)	5 µl
dNTPs (10 mM)	1 µl
Primer forward (10 µM)	1.5 µl
Primer reverse (10 µM)	1.5 µl
Enxyme mix	1 µl
RNase Inhibitor	0.5 µl
ddH2O	13.5 µl

PCR reaction	**Cycles**	**Temperature**	**Time**
Initial denaturatio	1	98°C	2 minutes

Denaturation	30 (*anillin*) 27 (*ef1α*)	98°C	30 seconds
Annealing	30 (*anillin*) 27 (*ef1α*)	54°C	30 seconds
Extension	30 (*anillin*) 27 (*ef1α*)	72°C	1 minute
Final extension	1	72°C	5 minutes

d. Experimental embryology

i. Blastomere transplantation

This technique was performed in all experiments assessing the cell-autonomous role of Anillin. Embryos were dechorionated in zebrafish fish medium containing Pen/Strep (1 mL every 300 mL of fish medium) and 0.75 $mg.mL^{-1}$ of pronase for 5 minutes. Embryos were removed from pronase and embedded in 2.5% methylcellulose on a coverslip. 10 to 20 cells were withdrawn from the top of the animal pole (Figure 14 A) of *(atoh7:GFP)*$_{rw021}$, (*H2B:GFP*) or wild-type blastula stage donors (previously injected at 1 to 2 cell-stage with *H2B-RFP* and/or *lifeactVenus* mRNAs). These regions contain blastomeres, which will give rise to the retina and the forebrain (Woo & Fraser 1995). These cells were then distributed into the animal poles of up to four blastula-staged wild-type host embryos with a glass micropipette, penetrating the embryo from its lateral side to deliver the cell at the top-most region of the animal pole (Figure 14 A) as previously reported (Jusuf et al., 2013). This method prevents the lost of the transplanted blastomeres. Transplanted embryos were then incubated in zebrafish fish medium containing Pen/Strep until the desired stage as described at 28°C. Donor embryos were kept apart when necessary.

ii. Microinjections

Microinjection was used to deliver DNA, mRNA or morpholino to

embryos in the one-cell stage. Fertilized eggs were collected in zebrafish fish medium and sorted into prepared 1% agarose (diluted in water) injection moulds. For injection a pressure injector (FemtoJet microinjector, Eppendorf) was used with borosilicate glass capillaries (GC100TF10, Clark Electromedical Instruments). For the injection of BAC *anillin:anillin-eGFP* DNA, wild type embryos (from Ab/Ab strain) were injected in the cytoplasm of one cell stage with a mix where the final concentration was 250 ng/µL for BAC purified DNA and 250 ng/µL for *tol2* transposase mRNA. Injected embryos were then screened for mosaic fluorescence in the retina.

For *H2B-RFP, lifeact-Venus* and *lifeact-Ruby* mRNA injections, 50-100 pg of mRNA were injected in the yolk of each embryos at one-cell stage.

For Anillin ATG, Anillin Splicing and standard control morpholino injection, 1 mM of morpholino was injected in the yolk of each embryos at one-cell stage.

Anillin translation blocking (AtgMO) and splice blocking (SpMO) morpholino oligonucleotides were obtained from Gene Tools, LLC and were reconstituted as 1 mM stock solutions in water. The AtgMO (5' - GTA CGC TAC AAG CTG AAA GTA AAG T - 3') was designed to target a region 6 bp upstream of the *anillin* translational starting site. The SpMO (5' – TTT CAC AAA AAG CTC TCA CCT CGG T - 3') was designed to target the region containing the splicing donor site at the boundary between the exon 1 and the intron 1 of the *anillin* pre-mRNA (6 bp of the exon 1 + 19 bp of the intron 1). The retention of the intron 1 generates a truncated protein (non-functional), due to a premature stop codon in intron 1. The working amount for each morpholino was 1mM/embryo. As control, a standard control morpholino (5' - CCT CTT ACC TCA GTT ACA ATT TAT A - 3') was injected at same amount as the AtgMO and SpMO.

e. Staining methods

i. Embryos fixation

For *in situ* hybridization procedure, embryos at the required stage were fixed in 4% PFA for 2 to 4 hours at room temperature or over night at 4°C and transferred subsequently into 25% (vol/vol), 50% (vol/vol), 75% (vol/vol) methanol in PBS and 100% methanol. Fixed embryos were kept at -20°C until the start of the *in situ* experiment.

For immunohistochemical labeling, embryos were fixed in 4% PFA for 2 hours at room temperature or over night at 4°C, washed three times for 5 minutes in PTW (PBS 1x + Tween 20 0.1%) and kept in PTW at 4°C for up to 10 days.

ii. Double fluorescent *in situ* hybridization

A series of subsequent rehydration step was done: 75% (vol/vol), 50% (vol/vol), 25% (vol/vol) methanol in PBS and finally 100% PTW. Permeabilization was achieved using age-dependent concentrations of proteinase K (final concentration 10 µg.mL-1 diluted in PTW) at room temperature, followed by post-fixation in 4% PFA in PBS for 20 minutes.

Developmental stage	Proteinase K treatment duration
28 – 30 hpf	2 – 3 minutes
30 – 35 hpf	5 – 7 minutes
35 – 40 hpf	20 minutes
40 – 50 hpf	25 minutes
50 – 65 hpf	30 – 35 minutes
65 – 5 dpf	40 – 50 minutes

After 5 washings in PTW for 5 minutes each, to remove all residual PFA, embryos were transferred in 2 mL Eppendorf tubes containing pre-warmed hybridization mix for a minimum of 2 hours at 68°C. Both digoxigenin-UTP and fluorescein-UTP -labeled riboprobes (previously denaturated 5 minutes at 80°C) were mixed with the hybridization mix and added to the prehybridized embryos and incubated over night at 68°C. After recovery of the riboprobes, embryos were washed 2 times 30 minutes in 50% formamide diluted in 2xSSCT. Embryos were next transferred in 2x SSCT for

15 minutes at 68°C, which was then replaced by 0.2% SSCT 2 times for 30 minutes at 68°C. Successive TNT (0.1 M Tris, pH 7.5, 0.15 M NaCl, 0.1% Tween-20) washes at room temperature were done and embryos were blocked for 2 hours in TNB solution (containing 2% DIGBlock [Roche] diluted in TNT). Anti-fluorescein-POD (Fab fragments, Roche) antibody diluted 1:50 in TNB was then added to the blocked embryos and incubated over night at 4°C. The following day, the antibody was recovered and embryos were washed several times 10 minutes with TNT solution at room temperature. All steps were then done in the dark. For the detection step, embryos were rinsed with TSA (Perkin Elmer) solution and the riboprobe signal was detected using 1:50 TSA-diluted fluorescein-tyramide substrate (FITC, PerkinElmer). *Cxcr4b* riboprobe was detected after 20 minutes and *atoh7* after 40 minutes. The excess of substrate was washed out with several washes of TNT and embryos were incubated in 1% H_2O_2 in TNT for 20 minutes in order to eliminate residual activity of peroxidase. A short blocking step of 1 hour was done with TNB and embryos were then incubated in anti-digoxigenin-POD (Fab fragments, Roche) antibody diluted 1:100 in TNB for one over night. After recovering the antibody and washing the embryos several times with TNT, TSA solution was used to rise out the TNT. Cyanine3-tyramide (Cy3, PerkinElmer) substrate diluted in TSA (1:50) was used for the revelation of the second riboprobe similarly to the revelation of the FITC-UTP-labeled riboprobe. *Anillin* riboprobe was detected after 45 minutes. TNT washed embryos were finally incubated in with 4',6-diamidino-2-phenylindole (DAPI, diluted in TNT) over night at 4°C. After washing out the DAPI with TNT, the stained embryos were used for imaging or kept in the dark at 4°C until imaging.

iii. Immunohistochemical stainings

For Immunohistochemistry on section (Zn5 staining), embryos were rinsed and cryo-protected in 30% sucrose, embedded and mounted in tissue freezing medium (OCT, Jung – Leica Microsystems Nussloch GmbH), frozen in liquid nitrogen and cryosectioned at 16 µm thickness. Sections were recovered on SuperFrost Plus microscope slides (Menzel-Gläser) and left to

dry for 4 hours at room temperature or over night at 4°C. All sections were incubated in 10% blocking solution (10% heat-inactivated goat serum, 1% bovine serum albumin, 0.2% Triton X-100 in PBS) for 1 hour and 30 minutes at room temperature. Sections were incubated in Zn5 antibody diluted 1:300 in 1% blocking serum (1% heat-inactivated goat serum, 1% bovine serum albumin, 0.2% Triton X-100 in PBS) over night. After several washes in PTW, the sections were treated with Alexa Fluor 546 secondary antibody diluted 1:500 in 1% blocking serum for 2 hours at room temperature. Several 15 minutes washes in PTW were done after what nuclei were counterstained with DAPI diluted in PTW for 10 minutes and washed off with additional washes in PTW. Sections were mounted with 60% glycerol covered with a 24x60 mm coverslip (Roth Carl Karlsruhe) and sealed with nail polish. Until imaging, stained and sealed sections were kept in dark at 4°C.

For whole mount antibody staining, embryos were incubated in blocking solution (10% heat-inactivated goat serum, 1% bovine serum albumin, 0.2% Triton X-100 in PBS) for 60 minutes. For 30 hpf embryos, no permeabilization treatment with Tripsin-EDTA 0.25% were needed Embryos were incubated one overnight in the primary antibody (rabbit anti-PhosphoHistone3 [Millipore, 1:300] or mouse anti-Caspase 3 [abcam, 1:300]) and one overnight in the secondary antibody (goat anti-rabbit IgG [H+L] conjugated to Cy5 fluorophore [Amersham, 1:500] or donkey anti-mouse IgG conjugated with Alexa-Fluor 647 [Invitrogen, 1:500] . Nuclei were counterstained with DAPI and embryos were kept in dark at 4°C until imaging.

Abbreviations

Abbreviation	Stands for
3D	3 Dimensions
4D	4 Dimensions
Ac, ACs	Amacrine cell(s)
Amp	Ampicillin
Anln	Anillin
AnlnMO	Anillin morpholino injected embryos
APCCdh1	Anaphase-promoting complex activator protein CDH1
BAC	Bacterial Artificial Chromosome
bHLH	basic Helix Loop Helix
Bp	Bipolar cell
BSA	Bovine Serum Albumine
CCD	Charge-Coupled Device
CD2AP	CD2-Associated Protein
cDNA	complementary DeoxyriboNucleic Acid
Cm	Chloramphenicol
CNS	Central Nervous System
cPh	cone Photoreceptor
Ctr	Control
Cy3, Cy5	Cyanine3, Cyanine5
ddH_2O	double-distilled water
Dig-UTP	Digoxigenin-Uridine TriPhosphate
DMSO	DiMethyl SulfOxide
DNA	DeoxyriboNucleic Acid
dNTP	DeoxyriboNucleotide TriPhosphate
DsRed	*Discosoma sp.* Red
Ect2	Epithelial cell transforming sequence 2
F-actin	Filamentous actin
FITC	Fluorescein IsoThioCyanate
G1	Gap1
G2	Gap2

GCL	Ganglion Cell Layer
GFP	Green Fluorescent Protein
GTPase	Guanosine TriPhosphate hydrolase
H2B	Histone 2B
Hc, HCs	Horizontal cell(s)
hpf	hours post-fertilization
INM	Interkinetic Nuclear Migration
Kan	Kanamycin
Lak	*Lakritz*
LB	Lysogeny Broth
µ	micro
M	Mitosis
Mc	Müller Glia cell
Mklp1	Mitotic kinesin-like protein
mRNA	messenger RiboNucleic Acid
NA	Numerical Aperture
NPC	Nuclear Pore Complex
PBS	Phosphate Buffered Saline
PCR	Polymerase Chain Reaction
Pen/Strep	Penicillin/Streptomycin
PFA	ParaFormAldehyde
PH3	Phospho histone H3
POD	Peroxidase
PTU	Phenylthiourea
PTW	Phosphate buffered saline TWeen 20
RFP	Red Fluorescent Protein
RGC, RGCs	Retinal Ganglion Cell(s)
RNA	RiboNucleic Acid
RPC, RPCs	Retinal Progenitor Cell(s)
rPh	rod Photoreceptor
rpm	revolutions per minute
RT-PCR	Reverse Transcription Polymerase Chain

	Reaction
S	Synthesis
SEM	Standard Error of the Mean
SSCT	Saline-Sodium Citrate Tween 20
Tet	Tetracyclin
TNB	TrisNaCl-Blocking Buffer
TNT	TrisNaClTween
TSA	Tyramide Signal Amplification
UTP	Uridine TriPhosphate
vol	volume
UV	UltraViolet

References

Abe, G. et al., 2011. Transposon-mediated BAC transgenesis in zebrafish. *Nature Protocols*, 6(12), pp.1998–2021.

Agarwal, M. et al., 2010. Mid1p-dependent regulation of the M-G1 transcription wave in fission yeast. *Journal of Cell Science*, 123(24), pp.4366–4373.

Agathocleous, M. & Harris, W.A., 2009. From Progenitors to Differentiated Cells in the Vertebrate Retina. *Annual Review of Cell and Developmental Biology*, 25(1), pp.45–69.

Alexandre, P. et al., 2010. Neurons derive from the more apical daughter in asymmetric divisions in the zebrafish neural tube. *Nature Neuroscience*, 13(6), pp.673–679.

Almonacid, M. et al., 2009. Spatial Control of Cytokinesis by Cdr2 Kinase and Mid1/Anillin Nuclear Export. *Current Biology*, 19(11), pp.961–966.

Balciunas, D. et al., 2006. Harnessing a High Cargo-Capacity Transposon for Genetic Applications in Vertebrates. *PLoS Genetics*, 2(11), p.e169.

Bassett, E.A. & Wallace, V.A., 2012. Cell fate determination in the vertebrate retina. *Trends in Neurosciences*, pp.1–9.

Baye, L.M. & Link, B.A., 2007. Interkinetic Nuclear Migration and the Selection of Neurogenic Cell Divisions during Vertebrate Retinogenesis. *Journal of Neuroscience*, 27(38), pp.10143–10152.

Baye, L.M. & Link, B.A., 2008. Nuclear migration during retinal development. *Brain Research*, 1192, pp.29–36.

Bilitou, A. & Ohnuma, S.-I., 2010. The role of cell cycle in retinal development: Cyclin-dependent kinase inhibitors co-ordinate cell-cycle inhibition, cell-fate determination and differentiation in the developing retina. *Developmental Dynamics*, 239(3), pp.727–736.

Brown, N.L. et al., 2002. Molecular characterization and mapping of ATOH7,

a human atonal homolog with a predicted role in retinal ganglion cell development. *Mammalian genome : official journal of the International Mammalian Genome Society*, 13(2), pp.95–101.

Bultje, R.S. et al., 2009. Mammalian Par3 Regulates Progenitor Cell Asymmetric Division via Notch Signalingin the Developing Neocortex. *Neuron*, 63(2), pp.189–202.

Bussmann, J. & Schulte-Merker, S., 2011. Rapid BAC selection for tol2-mediated transgenesis in zebrafish. *Development*, 138(19), pp.4327–4332.

Calegari, F., 2003. An inhibition of cyclin-dependent kinases that lengthens, but does not arrest, neuroepithelial cell cycle induces premature neurogenesis. *Journal of Cell Science*, 116(24), pp.4947–4955.

Calegari, F., 2005. Selective Lengthening of the Cell Cycle in the Neurogenic Subpopulation of Neural Progenitor Cells during Mouse Brain Development. *Journal of Neuroscience*, 25(28), pp.6533–6538.

Cappello, S. et al., 2006. The Rho-GTPase cdc42 regulates neural progenitor fate at the apical surface. *Nature Neuroscience*, 9(9), pp.1099–1107.

Cayouette, M. et al., 2001. Asymmetric segregation of Numb in retinal development and the influence of the pigmented epithelium. *Journal of Neuroscience*, 21(15), pp.5643–5651.

Cayouette, M., Poggi, L. & Harris, W.A., 2006. Lineage in the vertebrate retina. *Trends in Neurosciences*, 29(10), pp.563–570.

Cepko, C.L. et al., 1996. Cell fate determination in the vertebrate retina. *Proceedings of the National Academy of Sciences*, 93(2), pp.589–595.

Chen, C.-T. et al., 2013. Resurrecting remnants: the lives of post-mitotic midbodies. *Trends in Cell Biology*, 23(3), pp.118–128.

Chiodini, F. et al., 2013. A Positive Feedback Loop between ATOH7 and a

Notch Effector Regulates Cell-Cycle Progression and Neurogenesis in the Retina. *CellReports*, pp.1–12.

Chong, S.W. et al., 2001. Expression pattern of two zebrafish genes, cxcr4a and cxcr4b. *Mechanisms of Development*, 109(2), pp.347–354.

Clark, B.S. et al., 2012. Loss of Llgl1 in retinal neuroepithelia reveals links between apical domain size, Notch activity and neurogenesis. *Development*, 139(9), pp.1599–1610.

Couturier, L., Mazouni, K. & Schweisguth, F., 2013. Numb Localizes at Endosomes and Controls the Endosomal Sorting of Notch after Asymmetric Division in Drosophila. *Current Biology*, 23(7), pp.588–593.

Das, R.M. & Storey, K.G., 2012. Mitotic spindle orientation can direct cell fate and bias Notch activity in chick neural tube. *EMBO reports*, 13(5), pp.448–454.

Das, T. et al., 2003. In vivo time-lapse imaging of cell divisions during neurogenesis in the developing zebrafish retina. *Neuron*, 37(4), pp.597–609.

Del Bene, F., 2011. Interkinetic nuclear migration: cell cycle on the move. *The EMBO Journal*, 30(9), pp.1676–1677.

Del Bene, F. et al., 2007. In Vivo Validation of a Computationally Predicted Conserved Ath5 Target Gene Set. *PLoS Genetics*, 3(9), p.e159.

Del Bene, F. et al., 2008. Regulation of Neurogenesis by Interkinetic Nuclear Migration through an Apical-Basal Notch Gradient. *Cell*, 134(6), pp.1055–1065.

Dong, Z. et al., 2012. Intralineage Directional Notch Signaling Regulates Self-Renewal and Differentiation of Asymmetrically Dividing Radial Glia. *Neuron*, 74(1), pp.65–78.

Dubreuil, V. et al., 2007. Midbody and primary cilium of neural progenitors

release extracellular membrane particles enriched in the stem cell marker prominin-1. *The Journal of Cell Biology*, 176(4), pp.483–495.

Ettinger, A.W. et al., 2011. Proliferating versus differentiating stem and cancer cells exhibit distinct midbody-release behaviour. *Nature Communications*, 2, p.503.

Field, C.M. & Alberts, B.M., 1995. Anillin, a contractile ring protein that cycles from the nucleus to the cell cortex. *The Journal of Cell Biology*, 131(1), pp.165–178.

Fish, J.L. et al., 2008. Making bigger brains-the evolution of neural-progenitor-cell division. *Journal of Cell Science*, 121(17), pp.2783–2793.

Gai, M. et al., 2011. Citron kinase controls abscission through RhoA and anillin. *Molecular biology of the cell*, 22(20), pp.3768–3778.

Galli-Resta, L. et al., 2008. The genesis of retinal architecture: An emerging role for mechanical interactions? *Progress in Retinal and Eye Research*, 27(3), pp.260–283.

Galvagni, F. et al., 2012. An apical actin-rich domain drives the establishment of cell polarity during cell adhesion. *Histochemistry and Cell Biology*, 138(3), pp.419–433.

Gambello, M.J. et al., 2003. Multiple dose-dependent effects of Lis1 on cerebral cortical development. *Journal of Neuroscience*, 23(5), pp.1719–1729.

Ge, X. et al., 2010. Hook3 Interacts with PCM1 to Regulate Pericentriolar Material Assembly and the Timing of Neurogenesis. *Neuron*, 65(2), pp.191–203.

Glotzer, M., 2009. The 3Ms of central spindle assembly: microtubules, motors and MAPs. *Nature Reviews Molecular Cell Biology*, 10(1), pp.9–20.

Goldbach, P. et al., 2010. Stabilization of the actomyosin ring enables

spermatocyte cytokinesis in Drosophila. *Molecular biology of the cell*, 21(9), pp.1482–1493.

Gregory, S.L. et al., 2008. Cell Division Requires a Direct Link between Microtubule-Bound RacGAP and Anillin in the Contractile Ring. *Current Biology*, 18(1), pp.25–29.

Guillot, C. & Lecuit, T., 2013. Adhesion Disengagement Uncouples Intrinsic and Extrinsic Forces to Drive Cytokinesis in Epithelial Tissues. *Developmental Cell*, 24(3), pp.227–241.

Hall, P.A., 2005. The Septin-Binding Protein Anillin Is Overexpressed in Diverse Human Tumors. *Clinical Cancer Research*, 11(19), pp.6780–6786.

He, J. et al., 2012. How Variable Clones Build an Invariant Retina. *Neuron*, 75(5), pp.786–798.

Hergovich, A. & Hemmings, B.A., 2012. Hippo signalling in the G2/M cell cycle phase: Lessons learned from the yeast MEN and SIN pathways. *Seminars in Cell & Developmental Biology*, 23(7), pp.794–802.

Herszterg, S. et al., 2013. Interplay between the Dividing Cell and Its Neighbors Regulates Adherens Junction Formation during Cytokinesis in Epithelial Tissue. *Developmental Cell*, 24(3), pp.256–270.

Hesse, M. et al., 2012. Direct visualization of cell division using high-resolution imaging of M-phase of the cell cycle. *Nature Communications*, 3, pp.1076–12.

Hickson, G.R.X. & O'Farrell, P.H., 2008. Anillin: a pivotal organizer of the cytokinetic machinery. *Biochemical Society Transactions*, 36(3), p.439.

Holt, C.E. et al., 1988. Cellular determination in the Xenopus retina is independent of lineage and birth date. *Neuron*, 1(1), pp.15–26.

Hu, C.K., Coughlin, M. & Mitchison, T.J., 2012. Midbody assembly and its

regulation during cytokinesis. *Molecular biology of the cell*, 23(6), pp.1024–1034.

Itoh, M. et al., 2003. Mind bomb is a ubiquitin ligase that is essential for efficient activation of Notch signaling by Delta. *Developmental Cell*, 4(1), pp.67–82.

Janetopoulos, C. & Devreotes, P., 2006. Phosphoinositide signaling plays a key role in cytokinesis. *The Journal of Cell Biology*, 174(4), pp.485–490.

Jusuf, P.R. et al., 2013. Imaging retinal progenitor lineages in developing zebrafish embryos. *Cold Spring Harb Protoc*.

Jusuf, P.R. et al., 2012. Biasing Amacrine Subtypes in the Atoh7 Lineage through Expression of Barhl2. *J Neurosci*, 32(40), pp.13929–44.

Jusuf, P.R. et al., 2011. Origin and determination of inhibitory cell lineages in the vertebrate retina. *Journal of Neuroscience*, 31(7), pp.2549–2562.

Karfunkel, P., 1972. The activity of microtubules and microfilaments in neurulation in the chick. *Journal of Experimental Zoology*, 181(3), pp.289-301

Kawakami, K. 2004. Transgenesis and gene trap methods in zebrafish by using the Tol2 transposable element. *Methods in Cell Biology*, 77: 201–222.

Kay, J.N. et al., 2001. Retinal ganglion cell genesis requires lakritz, a Zebrafish atonal Homolog. *Neuron*, 30(3), pp.725–736.

Kechad, A. et al., 2012. Anillin Acts as a Bifunctional Linker Coordinating Midbody Ring Biogenesis during Cytokinesis. *Current Biology*, 22(3), pp.197–203.

Kimmel, C.B. et al., 1995. Stages of embryonic development of the zebrafish. *Developmental Dynamics*, 203(3), pp.253–310.

Kimura, Y., 2006. alx, a Zebrafish Homolog of Chx10, Marks Ipsilateral

Descending Excitatory Interneurons That Participate in the Regulation of Spinal Locomotor Circuits. *Journal of Neuroscience*, 26(21), pp.5684–5697.

Kinoshita, M. et al., 2002. Self- and actin-templated assembly of Mammalian septins. *Developmental Cell*, 3(6), pp.791–802.

Knoblich, J.A., 2008. Mechanisms of Asymmetric Stem Cell Division. *Cell*, 132(4), pp.583–597.

Kosodo, Y. & Huttner, W.B., 2009. Basal process and cell divisions of neural progenitors in the developing brain. *Development, Growth & Differentiation*, 51(3), pp.251–261.

Kosodo, Y. et al., 2004. Asymmetric distribution of the apical plasma membrane during neurogenic divisions of mammalian neuroepithelial cells. *The EMBO Journal*, 23(11), pp.2314–2324.

Kosodo, Y. et al., 2008. Cytokinesis of neuroepithelial cells can divide their basal process before anaphase. *The EMBO Journal*, 27(23), pp.3151–3163.

Köster, R.W. & Fraser, S.E., 2001. Tracing Transgene Expression in Living Zebrafish Embryos. *Developmental Biology*, 233(2), pp.329–346.

Lancaster, M.A. & Knoblich, J.A., 2012. Spindle orientation in mammalian cerebral cortical development. *Current Opinion in Neurobiology*, 22(5), pp.737–746.

Latasa, M.J., Cisneros, E. & Frade, J.M., 2009. Cell cycle control of Notch signaling and the functional regionalization of the neuroepithelium during vertebrate neurogenesis. *The International Journal of Developmental Biology*, 53(7), pp.895–908.

Lee, H.O. & Norden, C., 2013. Mechanisms controlling arrangements and movements of nuclei in pseudostratified epithelia. *Trends in Cell Biology*, 23(3), pp.141–150.

Leung, L. et al., 2011. Apical migration of nuclei during G2 is a prerequisite for all nuclear motion in zebrafish neuroepithelia. *Development*, 138(22), pp.5003–5013.

Liu, H. et al., 2003. Characterization of Wnt signaling components and activation of the Wnt canonical pathway in the murine retina. *Developmental Dynamics*, 227(3), pp.323–334.

Liu, W., Mo, Z. & Xiang, M., 2001. The Ath5 proneural genes function upstream of Brn3 POU domain transcription factor genes to promote retinal ganglion cell development. *Proceedings of the National Academy of Sciences*, 98(4), pp.1649–1654.

Lyons, D.A., 2003. Monitoring neural progenitor fate through multiple rounds of division in an intact vertebrate brain. *Development*, 130(15), pp.3427–3436.

Madaule, P. et al., 1998. Role of citron kinase as a target of the small GTPase Rho in cytokinesis. *Nature*, 394(6692), pp.491–494.

Maddox, A.S., 2005. Distinct roles for two C. elegans anillins in the gonad and early embryo. *Development*, 132(12), pp.2837–2848.

Marthiens, V.E.R. & ffrench-Constant, C., 2009. scientific report. pp.1–6.

Martinez-Morales, J.-R. et al., 2005. Differentiation of the Vertebrate Retina Is Coordinated by an FGF Signaling Center. *Developmental Cell*, 8(4), pp.565–574.

Masai, I., 2003. N-cadherin mediates retinal lamination, maintenance of forebrain compartments and patterning of retinal neurites. *Development*, 130(11), pp.2479–2494.

Masai, I., 2005. The hedgehog-PKA pathway regulates two distinct steps of the differentiation of retinal ganglion cells: the cell-cycle exit of retinoblasts and their neuronal maturation. *Development*, 132(7), pp.1539–1553.

Matter-Sadzinski, L., 2005. A bHLH transcriptional network regulating the specification of retinal ganglion cells. *Development*, 132(17), pp.3907–3921.

Messier, P.E., 1978. Microtubules, interkinetic nuclear migration and neurulation. *Experientia*, 34(3), pp.289–296.

Meyer, E.J., Ikmi, A. & Gibson, M.C., 2011. Interkinetic Nuclear Migration Is a Broadly Conserved Feature of Cell Division in Pseudostratified Epithelia. *Current Biology*, 21(6), pp.485–491.

Monzo, P. et al., 2005. Clues to CD2-associated protein involvement in cytokinesis. *Molecular biology of the cell*, 16(6), pp.2891–2902.

Morais-de-Sá, E. & Sunkel, C., 2013. Adherens junctions determine the apical position of the midbody during follicular epithelial cell division. *EMBO reports*, 14(8), pp.696–703.

Morin, X. & Bellaïche, Y., 2011. Mitotic Spindle Orientation in Asymmetric and Symmetric Cell Divisions during Animal Development. *Developmental Cell*, 21(1), pp.102–119.

Mullins, J.M. & Biesele, J.J., 1977. Terminal phase of cytokinesis in D-98s cells. *The Journal of Cell Biology*, 73(3), pp.672–684.

Mullins, J.M. & McIntosh, J.R., 1982. Isolation and initial characterization of the mammalian midbody. *The Journal of Cell Biology*, 94(3), pp.654–661.

Murciano, A. et al., 2002. Interkinetic nuclear movement may provide spatial clues to the regulation of neurogenesis. *Molecular and Cellular Neuroscience*, 21(2), pp.285–300.

Neumuller, R.A. & Knoblich, J.A., 2009. Dividing cellular asymmetry: asymmetric cell division and its implications for stem cells and cancer. *Genes & Development*, 23(23), pp.2675–2699.

Norden, C. et al., 2009. Actomyosin Is the Main Driver of Interkinetic Nuclear

Migration in the Retina. *Cell*, 138(6), pp.1195–1208.

Oegema, K. et al., 2000. Functional analysis of a human homologue of the Drosophila actin binding protein anillin suggests a role in cytokinesis. *The Journal of Cell Biology*, 150(3), pp.539–552.

Ohata, S. et al., 2011. Dual Roles of Notch in Regulation of Apically Restricted Mitosis and Apicobasal Polarity of Neuroepithelial Cells. *Neuron*, 69(2), pp.215–230.

O'Farrell, F. & Kylsten, P., 2008. Drosophila Anillin is unequally required during asymmetric cell divisions of the PNS. *Biochemical and Biophysical Research Communications*, 369(2), pp.407–413.

Paoletti, A. & Chang, F., 2000. Analysis of mid1p, a protein required for placement of the cell division site, reveals a link between the nucleus and the cell surface in fission yeast. *Molecular biology of the cell*, 11(8), pp.2757–2773.

Piekny, A., Werner, M. & Glotzer, M., 2005. Cytokinesis: welcome to the Rho zone. *Trends in Cell Biology*, 15(12), pp.651–658.

Piekny, A.J. & Glotzer, M., 2008. Anillin is a scaffold protein that links RhoA, actin, and myosin during cytokinesis. *Current Biology*, 18(1), pp.30–36.

Piekny, A.J. & Maddox, A.S., 2010. The myriad roles of Anillin during cytokinesis. *Seminars in Cell & Developmental Biology*, 21(9), pp.881–891.

Poggi, L. et al., 2005. Influences on neural lineage and mode of division in the zebrafish retina in vivo. *The Journal of Cell Biology*, 171(6), pp.991–999.

Pollarolo, G. et al., 2011. Cytokinesis remnants define first neuronal asymmetry in vivo. *Nature Neuroscience*, 14(12), pp.1525–1533.

Riedl, J. et al., 2008. Lifeact: a versatile marker to visualize F-actin. *Nature Methods*, 5(7), pp.605–607.

Roszko, I. et al., 2006. Key role played by RhoA in the balance between planar and apico-basal cell divisions in the chick neuroepithelium. *Developmental Biology*, 298(1), pp.212–224.

Sagona, A.P. & Stenmark, H., 2010. Cytokinesis and cancer. *FEBS Letters*, 584(12), pp.2652–2661.

Sambrook, J. et al., 1989. Molecular cloning: a laboratory Manual, vol. 3. *Cold Spring Harbor Laboratory Press*, Cold Spring Harbor, N.Y.

Sauer, F.C., 1935. Mitosis in the neural tube. *The Journal of Comparative Neurology*, 62(2), pp.377–405.

Schenk, J. et al., 2009. Myosin II is required for interkinetic nuclear migration of neural progenitors. *Proceedings of the National Academy of Sciences*, 106(38), pp.16487–16492.

Siller, K.H. & Doe, C.Q., 2009. Spindle orientation during asymmetric cell division. *Nature cell biology*, 11(4), pp.365–374.

Singh, D. & Pohl, C., 2014. Coupling of Rotational Cortical Flow, Asymmetric Midbody Positioning, and Spindle Rotation Mediates Dorsoventral Axis Formation in C. elegans. *Developmental Cell*, 28(3), pp.253–267.

Skop, A.R. et al., 2004. Dissection of the mammalian midbody proteome reveals conserved cytokinesis mechanisms. *Science*, 305(5680), pp.61–66.

Steigemann, P. & Gerlich, D.W., 2009. Cytokinetic abscission: cellular dynamics at the midbody. *Trends in Cell Biology*, 19(11), pp.606–616.

Straight, A.F., Field, C.M. & Mitchison, T.J., 2005. Anillin binds nonmuscle myosin II and regulates the contractile ring. *Molecular biology of the cell*, 16(1), pp.193–201.

Sun, Y. et al., 2003. Conserved and divergent functions of Drosophila atonal,

amphibian, and mammalian Ath5 genes. *Evolution & development*, 5(5), pp.532–541.

Suzuki, C. et al., 2005. ANLN plays a critical role in human lung carcinogenesis through the activation of RHOA and by involvement in the phosphoinositide 3-kinase/AKT pathway. *Cancer research*, 65(24), pp.11314–11325.

Takahashi, T., Nowakowski, R.S. & Caviness, V.S., 1995. The cell cycle of the pseudostratified ventricular epithelium of the embryonic murine cerebral wall. *J Neurosci*, 15(9), pp.6046–6057.

Taverna, E. & Huttner, W.B., 2010. Neural Progenitor Nuclei IN Motion. *Neuron*, 67(6), pp.906–914.

Ueno, M. et al., 2006. Cell cycle progression is required for nuclear migration of neural progenitor cells. *Brain Research*, 1088(1), pp.57–67.

Vitorino, M. et al., 2009. Vsx2 in the zebrafish retina: restricted lineages through derepression. *Neural Development*, 4(1), p.14.

Webster, W. & Langman, J., 1978. The effect of cytochalasin B on the neuroepithelial cells of the mouse embryo. *American Journal of Anatomy*, 152(2), pp.209-21.

Werner, A. et al., 2013. SCFF^bxw5 mediates transient degradation of actin remodeller Eps8 to allow proper mitotic progression. pp.1–11.

Wilcock, A.C., Swedlow, J.R. & Storey, K.G., 2007. Mitotic spindle orientation distinguishes stem cell and terminal modes of neuron production in the early spinal cord. *Development*, 134(10), pp.1943–1954.

Willardsen, M.I. & Link, B.A., 2011. Cell biological regulation of division fate in vertebrate neuroepithelial cells. *Developmental Dynamics*, 240(8), pp.1865–1879.

Woo, K. & Fraser, S.E., 1995. Order and coherence in the fate map of the

zebrafish nervous system. *Development*, 121(8), pp.2595–2609.

Xie, Y. et al., 2013. The Phosphatase PP4c Controls Spindle Orientation to Maintain Proliferative Symmetric Divisionsin the Developing Neocortex. *Neuron*, 79(2), pp.254–265.

Xie, Z. et al., 2007. Cep120 and TACCs Control Interkinetic Nuclear Migration and the Neural Progenitor Pool. *Neuron*, 56(1), pp.79–93.

Yang, Y.-T., Wang, C.-L. & Van Aelst, L., 2012. DOCK7 interacts with TACC3 to regulate interkinetic nuclear migration and cortical neurogenesis. *Nature Neuroscience*, pp.1–12.

Yang, Z. et al., 2003. Math5 determines the competence state of retinal ganglion cell progenitors. *Developmental Biology*, 264(1), pp.240–254.

Zhao, W. & Fang, G., 2005. Anillin is a substrate of anaphase-promoting complex/cyclosome (APC/C) that controls spatial contractility of myosin during late cytokinesis. *Journal of Biological Chemistry*, 280(39), pp.33516–33524.

Žigman, M. et al., 2005. Mammalian inscuteable regulates spindle orientation and cell fate in the developing retina. *Neuron*, 48(4), pp.539–545.

Zolessi, F.R. et al., 2006. Polarization and orientation of retinal ganglion cells in vivo. *Neural Development*, 1, p.2.

Publications

Related to this thesis:

Paolini, A. et al., 2014. Anillin links cytokinesis to asymmetric inheritance and mode of cell division in the retinal neuroepithelium. *Under revision*

From other work:

Jusuf, P.R. et al., 2012. Biasing Amacrine Subtypes in the Atoh7 Lineage through Expression of Barhl2. *J Neurosci*, 32(40), pp.13929–44.

Mwafi, N. et al., 2014. Divergent Wnt8a Gene Expression in Teleosts S. D. Fugmann, ed. *PLoS ONE*, 9(1), p.e85303.